Final Report

IONOSPHERIC SCINTILLATION STUDIES

By: C. L. RINO E. J. FREMOUW

Prepared for:

NATIONAL AERONAUTICS AND SPACE ADMINISTRATION
GODDARD SPACE FLIGHT CENTER
GREENBELT, MARYLAND 20071

CONTRACT NAS5-21891

SRI Project 2273

STANFORD RESEARCH INSTITUTE
Menlo Park, California 94025 · U.S.A.

STANFORD RESEARCH INSTITUTE
Menlo Park, California 94025 · U.S.A.

Final Report *November 1973*

IONOSPHERIC SCINTILLATION STUDIES

By: C. L. RINO E. J. FREMOUW

Prepared for:

NATIONAL AERONAUTICS AND SPACE ADMINISTRATION
GODDARD SPACE FLIGHT CENTER
GREENBELT, MARYLAND 20071

CONTRACT NAS5-21891
Contract Period: 10 November 1972 through 10 November 1973
Principal Investigator: C. L. Rino
(415) 326-6200 Ext. 2165
Technical Officer: T. S. Golden
(301) 982-4297

SRI Project 2273

Approved by:

DAVID A. JOHNSON, *Director*
Radio Physics Laboratory

RAY L. LEADABRAND, *Executive Director*
Electronics and Radio Sciences Division

Copy No. 68

ABSTRACT

Ionosphere-induced scintillation effects have been studied for many years. Only recently, however, have communications engineers begun to consider the detailed nature of the signal perturbation. Scintillation activity was first characterized by a scintillation index and later by its first-order amplitude statistics. This gives sufficient information to determine the probability of occurrence of deep fades.

However, if one considers the problem of optimizing receiver and signal design for combating scintillation effects, or of even evaluating them in a given system, it becomes clear that a much more detailed description of ionospheric scintillation is necessary. Ideally, one would develop a channel model that describes the scintillation effects for an elementary waveform. Fourier techniques could then be used to analyze more complicated waveforms.

The research reported herein provides a basis for developing such a channel model. The model would proceed from a parameterized functional description of the ionospheric spectral-density function. We have employed a power-law form with irregularity elongation along the direction of the geomagnetic field, but no attempt was made to determine the parameter dependence on geophysical variables.

We have characterized the diffracted field of a monochromatic plane wave by two complex correlation functions. For a gaussian complex field, these quantities suffice to completely define the statistics of the field. Thus, one can in principle calculate the statistics of any measurable quantity in terms of the model parameters.

The question of the validity of hypothesizing gaussian statistics for the complex field is an important one. At best, gaussian statistics are a limiting form. Moreover, a considerable body of literature exists that questions the validity of this hypothesis. We therefore carefully analyzed the structure of the intensity statistics of several selected data sets for ionospheric and interplanetary scintillation.

Our results show that the best data fits are achieved for intensity statistics derived under the gaussian-statistics hypothesis. The signal structure that achieves the best fit is nearly invariant with scintillation level and irregularity source (ionosphere or solar wind). It is characterized by the fact that more than 80% of the scattered signal power is in phase quadrature with the undeviated or coherent signal component. Thus, the gaussian-statistics hypothesis is both convenient and accurate for channel-modeling work.

To illustrate the technique of applying the channel model and the gaussian signal structure, we have computed the two-frequency correlation function for the complex field and its intensity as well as the wavelength dependence of the normalized rms intensity scintillation index S_4. The results are in agreement with reported UHF data, but they evidently cannot be extrapolated to L-band and higher frequencies on the basis of a simple power-law SDF.

The technique of calculating phase statistics and the nature of the limitation imposed by the implicit first Born approximation in our diffraction calculations are also discussed in this report.

CONTENTS

ABSTRACT iii

LIST OF ILLUSTRATIONS ix

LIST OF TABLES xi

ACKNOWLEDGMENTS xiii

I INTRODUCTION 1

A. Background 1

B. Objectives 3

1. Gaussian Signal-Statistics Hypothesis Test 4
2. Computation of Ionospheric Time-Variant Transfer Function 4

C. Organization of Report 5

II SIGNAL STATISTICS 7

A. The Log-Normal Hypothesis 8

B. The Gaussian-Statistics Hypothesis 9

III DATA REDUCTION AND ANALYSIS FOR SIGNAL STATISTICS 13

A. Histogram Computation 14

B. Goodness-of-Fit Tests 15

C. Computation of Theoretical Gaussian PDFs 16

D. Data Analysis 19

1. NASA OAO-2 Data 19
2. NASA ATS-5 Data 28
3. AFCRL ATS-5 Data 35
4. UCSD Interplanetary Scintillation Data 41

E. Summary and Conclusions 42

IV THEORETICAL BASIS FOR CHANNEL MODELING 47

A. Introduction 47

B. The Transfer Function for a Weakly Scattering Irregularity Layer 52

C. The Special Case of a Power-Law Spectral-Density Function 58

D. Effects of Time-Varying Media 65

E. Method of Numerical Computation 67

F. Discussion and Examples 70

1. Normal-Incidence Computations with $\Delta f = 0$ 72
2. Coherence Bandwidth 73

V APPLICATIONS 77

A. Intensity Statistics for Gaussian Fields 77

1. The Wavelength (Frequency) Dependence of S_4 79
2. Two-Frequency Correlation Function for Intensity 82

B. The Method of Computing Phase Statistics 82

VI SUMMARY, DISCUSSION, AND RECOMMENDATIONS 85

A. Gaussian Signal Statistics 85

B. The Nakagami Distribution 87

C. Complex Second Moments for Ionospheric-Transfer-Function Characterization 88

D. Consequences of the Weak-Scattering Restriction 91

E. Data Restrictions 93

APPENDICES

A THE SPECTRAL REPRESENTATION OF HOMOGENEOUS COMPLEX RANDOM FIELDS WITH APPLICATIONS TO FREE-SPACE PROPAGATION 95

B THE TEMPORAL STRUCTURE OF THE SCATTERED FIELD 103

C POWER-LAW SPECTRAL-DENSITY-FUNCTION FORMULAS FOR NORMAL INCIDENCE 107

D SPECTRAL-DENSITY FUNCTIONS FOR "SIMPLY" ANISOTROPIC MEDIA 113

E INTENSITY CORRELATIONS FOR COMPLEX GAUSSIAN FIELDS . . . 119

REFERENCES 125

ILLUSTRATIONS

III-1	Family of Gaussian PDFs Parameterized by Z Compared with the Corresponding Nakagami and Log-Normal PDFs. For large Z, the gaussian PDF is very nearly Rician . .	20
III-2	Log-Normal and Best-Fit Gaussian PDFs for NASA 136-MHz OAO-2 Data--Antennas Horizontally Polarized . .	26
III-3	Log-Normal and Best-Fit Gaussian PDFs for NASA 136-MHz OAO-2 Data--Antennas Vertically Polarized . . .	27
III-4	Log-Normal PDFs for NASA 136-MHz ATS-5 Data	30
III-5	Best-Fit Gaussian PDF for NASA 136-MHz ATS-5 Data--Channel 1	31
III-6	Best-Fit Gaussian PDF for NASA 136-MHz ATS-5 Data--Channel 2	32
III-7	Intensity Power Spectrum for NASA ATS-5. Arrows point to satellite spin lines. Solid curves are for power-law analytic forms.	34
III-8	Best-Fit Gaussian and Log-Normal PDFs for AFCRL Data--Set 1	38
III-9	Best-Fit Gaussian and Log-Normal PDFs for AFCRL Data--Set 5	39
III-10	Best-Fit Gaussian and Log-Normal PDFs for AFCRL Data--Set 3	40
III-11	Best-Fit Gaussian and Log-Normal PDFs for UCSD Interplanetary Scintillation Data	43
III-12	Fade-Margin Comparison for Gaussian, Log-Normal, and Nakagami PDFs	44
IV-1	Functional Block Diagram of Satellite-Earth Communication System	47
IV-2	Geometry for Layered-Medium Scattering Calculations . .	57

IV-3 Spectral-Density-Function Cross-Section Plots Showing the Effect of H^*_ρ Terms in Eq. (40) 64

IV-4 Plots of σ_x^2 and C_{xy} Showing Effect of Finite Layer Thickness 73

IV-5 Family of σ_x^2 vs. Z Curves Showing Effect of Anisotropy 74

IV-6 Family of σ_x^2 vs. Z Curves Showing Effect of Power-Law Spectral Index 74

IV-7 Coherence Bandwidth Curves for Complex-Field Random Component 76

V-1 Wavelength Dependence of S_4 Scintillation Index 81

V-2 Two-Frequency Correlation Function for Intensity 83

TABLES

III-1	NASA OAO-2 Digital-Data Tapes	21
III-2	S_4^2 Values for OAO-2 Fall Equinox Data	22
III-3	NASA ATS-5 Data	28
III-4	Parameters for NASA ATS-5 Data	33
III-5	Summary of AFCRL ATS-5 Data	36
III-6	Parameters for VHF Data	36
III-7	Parameters for UHF Data	41
IV-1	Parameters for Complex-Correlation-Function Formulas	62
VI-1	Parameters for Machine Computation	90

ACKNOWLEDGMENTS

The data-reduction and computer-analysis technique employed in this research was developed by Mr. Gary Bream. The analysis presented in Appendix C was performed by Mr. Howard Singhaus who, regrettably, died suddenly before that work was complete.

The ATS-5 midlatitude data reported in Section III-D-3 was kindly provided by Dr. Jules Aarons and Hubert Whitney of the Air Force Cambridge Research Laboratory. The interplanetary scintillation data reported in Section III-D-4 was made available by Dr. William Coles of the University of California, San Diego Department of Applied Physics and Information Science.

PRECEDING PAGE BLANK NOT FILMED

I INTRODUCTION

Ionosphere-induced scintillation effects are the main cause of signal degradation on satellite-to-earth radio transmissions at UHF and higher frequencies. In the report by Golden and Wolf (1973)*, a need for a scintillation-effects channel model was clearly established. The research that is reported herein provides a basis for developing such a model.

Channel modeling involves three tasks. Firstly, the ionospheric-irregularity structure must be determined. Secondly, a diffraction calculation must be performed to describe the electromagnetic-wave interaction with the scattering medium. Finally, the dependences of the model parameters on geophysical variables must be established.

This work evolved from our efforts to extend and improve an existing scintillation model that we shall presently describe. Briefly, we have reformulated the diffraction theory so that it is more relevant to systems analysis, and we have attempted to validate a gaussian signal-statistics hypothesis that greatly extends the usefulness of the theory.

A. Background

Scintillation activity is most commonly characterized by an amplitude (or intensity) scintillation index. Briggs and Parkin (1963) proposed four indices (S_1, S_2, S_3, and S_4) and pointed out that the interrelations among them could be determined if the amplitude statistics were known. Their index S_4 is the standard deviation of intensity normalized to the average intensity, and it is most convenient for theoretical

*References are listed at the end of the report.

computations. Briggs and Parkin (1963) performed a diffraction calculation that relates S_4 to ionospheric and geometrical parameters.

Bischoff and Chytil (1969) used the Nakagami distribution (Section II), which depends only on a parameter $m = S_4^{-2}$, to calculate Briggs and Parkin's indices S_1, S_2, and S_3 as functions of S_4. At the same time, because a large body of scintillation data existed on strip charts, Whitney, Aarons, and Malik (1969) devised a scintillation index that could be determined from amplitude peaks. They showed empirically that their index was linearily related to S_3.

Thus, a means existed for standardizing the various reported scintillation indices to S_4, which could then be related to ionospheric parameters. In the Briggs and Parkin theory a random phase-changing screen with a gaussian autocorrelation function was postulated. The ionospheric parameters consist of an axial ratio, a transverse scale size, and an rms phase variation. The rms phase variation is proportional to the ionospheric rms electron-density variation.

In addition to these theoretical results, there existed a large body of published scintillation data. Hence, on 3 February 1971, NASA awarded a contract to SRI to develop a worldwide model for F-layer-produced scintillation (Fremouw and Rino, 1971, 1972). The model was based on a detailed empirical formula for the ionospheric rms electron-density variation. Model constants were determined by using the Briggs and Parkin theory to fit carefully selected data sets.

The scintillation model predicts an average scintillation index as a function of geomagnetic latitude, local time, season, and sunspot number. However, it was recognized that a scintillation index alone is insufficient for systems evaluation. At the very least, one needs the probability of occurrence of signal fades below a specified level (Whitney, Aarons, Allen, and Seemann, 1972). Hence a corollary study of amplitude statistics was conducted (Rino and Fremouw, 1973).

Our approach was to hypothesize gaussian statistics for the complex field and then calculate the amplitude probability-density function (PDF). The main difficulty lies with the fact that amplitude moments do not uniquely determine the general gaussian PDF. The Rice, Rayleigh, and Nakagami PDFs are special cases that circumvent this problem. However, our initial calculations showed that none of these PDFs was accurate, although for some applications they would be usable.

More disturbing was the fact that researchers in optics and radio astronomy had rejected the gaussian hypothesis altogether. They presented both theory and data that showed the logarithm of amplitude to be normally distributed. When gaussian statistics cannot be hypothesized, the channel-modeling problem is considerably more difficult. Hence, our first concern was to determine to what extent gaussian statistics were accurate.

We also recognized a need for extending the diffraction theory so that the full temporal and spatial structure of the field could be determined. Ideally, the problem should be formulated within the framework of engineering systems analysis. This would make the results the kernel for the analysis of a broad spectrum of scintillation effects.

On 11 November 1972, SRI received a second contract from NASA to carry out this work. The detailed objectives are summarized below. The results of the research are presented and discussed in Sections III through VI of this report.

B. Objectives

The objectives of this research were twofold. The first was to evaluate the gaussian hypothesis. The technique to be employed is described below. The second objective involved a purely theoretical effort also described below. The objectives were to be pursued simultaneously with the hope that the results would be complementary.

1. Gaussian Signal-Statistics Hypothesis Test

In an earlier document (Rino and Fremouw, 1973) we proposed a scheme for obtaining a family of general gaussian PDFs all with the same scintillation index S_4. The PDF family is parameterized by the ratio of the Fresnel-zone area to the square of the transverse scale size for a given effective axial ratio and incidence direction. Each PDF corresponds effectively to a different ionospheric rms electron-density value.

Our first objective was to obtain a large body of data, compute histograms for each suitably stationary data segment, and obtain a best fit from the aforementioned PDF family for the measured S_4 scintillation index. We then compared the fit to the corresponding log-normal PDF to determine which hypothesis (gaussian vs. log-normal) is more nearly correct, and to what extent.

2. Computation of the Ionospheric Time-Variant Transfer Function

In general, a system transfer function is the response (output) to a sinusoidal excitation (input). The ionosphere can be modeled with a suitable stochastic transfer function. Once the transfer function is determined, Fourier techniques can be used to determine the response to an arbitrary input.

Thus, our second objective was to calculate the time-variant transfer function for a scattering layer that would provide a reasonably accurate representation of the ionosphere. The initial formulation was to be completely general and then specialized to a power-law spectral-density function. We proposed to make as few a-priori approximations as possible in order to test the various assumptions that are typically made.

The theoretical calculations given define two complex correlation functions that suffice to completely specify the statistics of a complex

gaussian field. Thus, in principle, one could calculate the statistics of any measurable quantity in terms of the model parameters.

C. Organization of Report

Because of the conflicting theories on signal statistics, we have devoted Section II of this report to briefly reviewing this subject, and to a discussion of the problem of testing the gaussian-statistics hypothesis from amplitude data alone.

In Section III we describe in detail our data-reduction procedure and present the results of the data that we have analyzed to date. In Sections III-A and III-B we review the theoretical basis for analyzing histograms and applying goodness-of-fit tests. In Section III-C we review our method of obtaining a family of gaussian PDFs each with the same first and second moments of intensity.

In Section III-D we present the results of applying these procedures to ionospheric and interplanetary scintillation data. The results, which are discussed in Section III-E, support the conclusion that the gaussian-statistics hypothesis is more nearly correct than the log-normal hypothesis.

In Section IV we attack the general problem of channel modeling. In Section IV-A we discuss the philosophy of channel modeling and identify the quantities that must be computed. We then make a general computation for an arbitrary spectral-density function (Section IV-B). This is followed by a specialization of the results for a power-law spectral-density function that admits a simple anisotropy (Section IV-C).

In Section IV-D we consider the effects of relative observer medium motion, which is the main source of the observed signal temporal fluctuations. In Section IV-E we discuss the method of evaluating the resulting integrals, and in the Section IV-F we characterize the general

properties of the transionospheric channel and demonstrate them with some examples calculated by numerically integrating the power-law formulas.

Section V can be considered a synthesis of Sections III and IV. In that section we apply the gaussian-statistics hypothesis to extend the complex correlations functions computed in Section IV to include intensity statistics. As examples we have computed the wavelength dependence of the S_4 scintillation index and the two-frequency intensity correlation function. The results are in general agreement with published data. We have concluded the section with an outline of the method of making similar computations for phase statistics.

In Section VI we have summarized the complete report and discussed its implications. We also consider the nature of the limitations imposed by the first Born approximation and a method that we believe could be employed to extend our results to allow for the effects of multiple scattering.

II SIGNAL STATISTICS

Ratcliffe was among the first researchers to suggest that radio-wave fading is caused by diffraction from ionospheric irregularities (Ratcliffe and Pawsey, 1933). By 1950, the theoretical basis for explaining the phenomenon was well developed (Booker, Ratcliffe, and Shinn, 1950; Briggs and Phillips, 1950; Hewish, 1952). The theory was restricted to single scattering, but Fejer (1953) had extended some results to include multiple-scattering effects.

In the diffraction theories, the complex field is given as an integral over a random function that represents the scattering medium. Hence, by applying the central-limit theorem one can deduce limiting gaussian statistics for the complex field. However, evidently because of the influence of Rice's (1945) work, the additional assumption of random phase was usually made. This is well illustrated in Section 8.2 of the popular survey paper by Ratcliffe (1956).

Of course, other analytic techniques were exploited to analyze scintillation effects. Chandrasekhar (1952) used geometrical optics to calculate amplitude and phase scintillation for starlight. In 1960 and 1961, however, English translations of the Russian monographs by Chernov (1960) and Tatarski (1961) became available. These were essentially complete treatments of wave propagation in random media. Their influence on the theoretical work that followed was considerable.

In the Russian works the Rytov solution to the wave equation was introduced. It predicts gaussian statistics for the logarithm of the complex field rather than for the complex field itself. Moreover, it was originally thought to have a broader range of validity than the

first Born approximation, which is implicit in the diffraction theories. However, this was later shown to be incorrect. What seems to be the current most widely accepted view is summarized in Barabanenkov et al. (1971).

Our own results inject new evidence that favors the gaussian hypothesis over the log-normal hypothesis. Because this is a fundamental question we have summarized the earlier arguments and the supporting evidence below.

A. The Log-Normal Hypothesis

The theoretical basis for the log-normal hypothesis is the Rytov solution to the wave equation. It gives the diffracted field E as $E/E_{inc} = e^{\psi}$, where E_{inc} is the incident field and ψ is an integral over a random function that represents the medium. Hence, an application of the central-limit theorem leads to the conclusion that $\log E/E_{inc}$ has gaussian statistics.

We note, however, that when $|\psi| << 1$, $E/E_{inc} \cong 1 + \psi$, which is identical to the diffraction-theory solution. Hence, the Rytov solution appears to be more general. However, it has been more recently demonstrated that the condition $|\psi| << 1$ is actually necessary for the validity of the Rytov solution (Brown, 1966). Nonetheless, the calculations require many approximations, and they are subject to some question. In view of this, theorists have considered the available data to help resolve the question.

Most often cited are the optics data of Ochs and Lawrence (1969). Their plots of the logarithm of intensity versus cumulative gaussian probability show near linearity over three decades of intensity. Moreover, their data fits for Rayleigh statistics are very poor by comparison. Nonetheless, their method of presenting the data tends to obscure small discrepancies.

More recently, Armstrong, Coles, and Rickett (1972) have analyzed radio-star intensity statistics for interplanetary scintillation data. Their data show clearly that log-normal statistics give substantially better fits than do the corresponding Rician statistics. However, they do note statistically significant departures of their measured histograms from the corresponding log-normal PDF. Thus, while their data are sufficient to reject the Rician-statistics hypothesis, they do not necessarily exclude the general gaussian-statistics hypothesis.

In Barabanenkov et al. (1971) additional theoretical support for the log-normal hypothesis is given, however. By making a Markov approximation for the wave-medium interaction, it is possible to obtain an exact wave-equation solution for narrow-angle scattering. The calculated second moments evidently agree with the Rytov solution. Moreover, the calculated odd moments are finite. For gaussian statistics to be strictly applicable the odd moments must be zero.

Even so, there have been no reported tests of the general gaussian hypothesis, for reasons discussed below. The difficulty lies with the fact that the gaussian hypothesis cannot be tested with intensity or amplitude data alone.

B. The Gaussian-Statistics Hypothesis

Our approach has been to hypothesize general gaussian statistics. The joint probability-density function of the real and imaginary parts of the complex field--say X and Y respectively--depends explicitly on five parameters. These are the variances and means of X and Y, σ_x^2, σ_y^2, η_x, η_y and their covariance C_{xy}. None of these parameters can be determined from intensity or amplitude data. However, in most experiments the undeviated component is effectively the phase reference, so that $\eta_y = 0$.

For Rayleigh statistics $\sigma_x^2 = \sigma_y^2$, and $C_{xy} = \eta_x = \eta_y = 0$. Rician statistics permit a finite coherent component η_x. For these special PDFs, the moments of intensity uniquely determine the corresponding PDF. Hence, they are easily tested. The Nakagami PDF, which has been used extensively for ionospheric scintillation, has the same property. It depends on the parameter $m = S_4^{-2}$. Moreover, in some sense it is an approximation of the general gaussian amplitude PDF.

However, as discussed in Rino and Fremouw (1973), the precise relationship of m to σ_x^2, σ_y^2, C_{xy}, and η_x is not specified. When S_4 is sufficiently small the Nakagami PDF is close to the Rician PDF. As S_4 approaches unity, the Nakagami PDF approaches the Rayleigh PDF. Between these extremes the Nakagami distribution differs substantially from the Rice distribution. Even so, we had no theoretical basis for expecting the Nakagami distribution to provide a better data fit than the log-normal PDF.

In Rino and Fremouw (1973), we showed that by using a simple diffraction-theory computation for σ_x^2, σ_y^2, and C_{xy}, and choosing η_x such that $\sigma_x^2 + \sigma_y^2 + \eta_x^2 = \langle |E_{inc}|^2 \rangle$ --that is, to ensure energy conservation--we could obtain a family of gaussian PDFs all with the same first and second moments of intensity. Our initial results showed that the best data fit among the members of this family appeared to be as good as the log-normal PDF. The best-fit general gaussian PDF is distinguished by the fact that $\sigma_y^2 >> \sigma_x^2$, thus explaining why the fits for Rayleigh and Rician statistics $\left(\sigma_x^2 = \sigma_y^2\right)$ are poor. Moreover, the condition $\sigma_y^2 >> \sigma_x^2$ occurs when large-scale structure dominates the diffraction. Stated another way, we are observing a manifestation of the fact that the apparent scale size (squared) that produces amplitude scintillation is roughly equal to the Fresnel-zone area.

The idea of using general gaussian statistics to fit amplitude-scintillation data is not new. It is discussed in Wernik and Liszka (1969). Also, Bischoff and Chytil (1969) discussed the possible effects of C_{xy} on amplitude statistics. However, evidently the idea had not been previously tested, even though Bowhill's (1961) calculations were directly applicable.

In Section III we describe our data-reduction procedure and present our results, which show that general gaussian statistics as described give a data fit that is at least as good as, and generally better than, the corresponding log-normal statistics.

III DATA REDUCTION AND ANALYSIS FOR SIGNAL STATISTICS

In this section we shall make some general comments about histograms and goodness-of-fit tests. We shall then describe the theoretical basis for our data-reduction procedure and present our results.

The data that we have processed consist of digitized scintillation records. The calibrated data samples constitute an instantaneous-power time series $\{P_k\}$ for some period of time--say, T. The data are segmented into blocks of some convenient size for machine processing. For each data block an estimate of the average power $\langle P \rangle$ and the second moment of power $\langle P^2 \rangle$ is made.

Generally, there are slow variations in the mean power level that can be compensated by renormalizing the data blocks to some convenient level. Once this is done, the data blocks are grouped into quasi-stationary periods. The stationarity is subjectively evaluated by observing changes in $\langle P^2 \rangle$ and carefully evaluating strip-chart recordings. It is important for our analysis that genuine changes in the statistics do not get averaged out.

Finally, we generate histograms for each quasistationary data period and estimate the S_4 scintillation index and, when enough data blocks are available, its standard deviation. The histograms are recorded on digital tape for comparison to various theoretical PDFs. Our main interest is in the best fit for the family of general gaussian PDFs that have the same first and second moments of intensity or power.

A. Histogram Computation

Histograms are computed by dividing the power range into small intervals $(P_i, P_i + \Delta P_i)$, and counting the number of samples that fall into each interval. If the true PDF, f(P), is known, one can calculate the probability P_{r_i} of one sample falling into the i^{th} interval. For small ΔP_i, $P_{r_i} \cong f(P_i + \Delta P_i/2)\, \Delta P_i$. From P_{r_i}, one can calculate the histogram statistics.

Indeed, for independent samples the number of samples that fall in the i^{th} interval (say, O_i) is governed by the binomial probability law

$$P[O_i = k] = \binom{N}{k} P_{r_i}^{k} \left(1 - P_{r_i}\right)^{N - k} \qquad \text{(III-1)}$$

It follows that

$$\langle O_i \rangle = N P_{r_i} \qquad \text{(III-2)}$$

and

$$\langle O_i^2 \rangle - \langle O_i \rangle^2 = N P_{r_i} \left(1 - P_{r_i}\right) . \qquad \text{(III-3)}$$

Hence, the standard deviation of O_i is given as $(1-P_{r_i})/(N P_{r_i})$. Clearly the uncertainty increases as P_{r_i} becomes small, so that one must make the usual compromise between resolution and precision.

For convenience we have employed uniform increments. One would like at least five samples in the least significant interval to obtain good accuracy. However, this is not always possible for small N. A procedure for calculating confidence limits is given in Introduction to the Theory of Statistics by Mood (1950, pp. 233-235), when it is important to evaluate the significance of some segment of the histogram such as the tail.

In our analysis, however, we have used a single measure of the overall fit, as described below.

B. Goodness-of-Fit Tests

Goodness-of-fit tests are developed by devising a test statistic--that is, a measure of the discrepancy between the histogram (or some other quantity derived from the sample population) and the hypothesized probability law. Ideally, one would calculate the probability of the test statistic achieving a given level when the hypothesized probability law is correct.

If the test is a good one, the test statistic will achieve a high confidence level only for sample populations that closely follow the hypothesized probability law. However, developing good test procedures is an art. Moreover, it is usually possible to calculate the limiting cummulative distribution for the test statistics only as the number of samples approaches infinity.

We have investigated the Kolmogoroff-Smirnoff (K-S) and the chi-square goodness-of-fit tests. The test statistics for the K-S test is the absolute value of the maximum departure of the estimated cummulative-density function (CDF) from the hypothesized CDF. The limiting distribution for the test statistic has been determined. We found, however, that the K-S test is not sensitive to small parameter changes.

The test statistic for the chi-square test is derived directly from the histogram. It is given explicitly as

$$\chi^2 = \sum_{i=1}^{k} \frac{\left(o_i - \langle o_i \rangle\right)^2}{\langle o_i \rangle} \quad . \qquad \text{(III-4)}$$

Hence, except for the normalization, it is a mean-square-error measure. Moreover, the test statistic χ^2 has a limiting chi-square distribution with k degrees of freedom less one degree of freedom for each parameter

that must be estimated from the sample population (Bowker and Liberman, 1959, pp. 458-461).

We have found that Eq. (III-4) is very sensitive to changes in the gaussian parameters when they are varied as described below. Hence, we have used this test exclusively in our data analysis.

C. Computation of Theoretical Gaussian PDFs

The log-normal, Rayleigh, Rice, and Nakagami PDFs have the common property that they are completely specified by the moments $\langle P \rangle$ and $\langle P^2 \rangle$. By comparison, the general gaussian intensity PDF cannot be specified from intensity moments alone. One can show that for gaussian statistics,

$$\langle P \rangle = \sigma^2 + \eta_x^2 + \eta_y^2 \tag{III-5}$$

and

$$\langle P^2 \rangle - \langle P \rangle^2 = 2\sigma^2(\langle P \rangle - \sigma^2)\left[1 + \frac{|B|}{\sigma^2}\cos 2(\zeta - \phi)\right] + \sigma^4\left[1 + \frac{|B|^2}{\sigma^4}\right] \tag{III-6}$$

where

$$\sigma^2 = \sigma_x^2 + \sigma_y^2 \tag{III-7}$$

$$B = |B| \exp\{2i\zeta\} = \sigma_x^2 - \sigma_y^2 + 2i\, C_{xy} \tag{III-8}$$

and

$$\tan \phi = \frac{\eta_y}{\eta_x} \quad . \tag{III-9}$$

We emphasize that none of the parameters σ_x^2, σ_y^2, C_{xy}, η_x nor η_y, can be determined from amplitude or intensity data alone.

It follows from Eqs. (III-5) through (III-9) that there is an infinity of parameter combinations that give rise to the same moments $\langle P \rangle$

and $\langle P^2 \rangle$. To make the problem of testing the various possibilities tractable, we have used a diffraction-theory computation for B to derive equations for the necessary parameters. Suppose, for example, that $\eta_y = 0$, and B is known. From Eq. (III-6) it follows that S_4^2 can be written as

$$S_4^2 = 2\,\sigma^2 g_1 + \sigma^4\,(g_2 - 2g_1) \tag{III-10}$$

where

$$g_1 = 1 + \left(\frac{|B|}{\sigma^2}\right) \cos 2\,\zeta \tag{III-11}$$

and

$$g_2 = 1 + \frac{|B|^2}{\sigma^4} \quad . \tag{III-12}$$

Now, if we measure S_4^2, σ^2 can be determined from the formula

$$\sigma^2 = \langle P \rangle \left[-g_1 + \left[g_1^2 + (g_2 - 2g_1)\, S_4^2\right]^{1/2}\right] \Big/ \left[g_2 - 2g_1\right] \tag{III-13}$$

which gives the positive root of Eq. (III-10). Once σ^2 is determined, the gaussian parameters follow from Eqs. (III-5), (III-7), and (III-8) as

$$\eta_x = \left[\langle P \rangle - \sigma^2\right]^{1/2} \tag{III-14}$$

$$\sigma_x^2 = \frac{1}{2}\,\sigma^2 \left[1 + \frac{\mathrm{Re}\{B\}}{\sigma^2}\right] \tag{III-15}$$

$$\sigma_y^2 = \frac{1}{2}\sigma^2\left[1 - \frac{\mathrm{Re}\{B\}}{\sigma^2}\right] \qquad \text{(III-16)}$$

and

$$C_{xy} = \frac{1}{2}\sigma^2\left[\frac{\mathrm{Im}\{B\}}{\sigma^2}\right] . \qquad \text{(III-17)}$$

A simplified diffraction calculation with a gaussian autocorrelation function for the irregularity structure gives the result

$$B = -\sigma^2\left[\left(1-\tan U_1 \tan U_2 \sec^2\theta\right)^2 + \left(f_1 \tan U_1 + f_2 \tan U_2\right)^2\right]^{-1/4}$$

$$\times\left\{\exp\left[\frac{1}{2} i \tan^{-1}\left(\frac{f_1 \tan U_1 + f_2 \tan U_2}{1-\tan U_1 \tan U_2 \sec^2\theta}\right)\right]\right\} \qquad \text{(III-18)}$$

where

$$\tan U_1 = \frac{Z}{\beta^2} \qquad \text{(III-19)}$$

$$\tan U_2 = Z \qquad \text{(III-20)}$$

$$f_1 = 1 + \tan^2\theta \cos^2\varphi \qquad \text{(III-21)}$$

$$f_2 = 1 + \tan^2\theta \sin^2\varphi \quad . \qquad \text{(III-22)}$$

The parameter Z is the ratio of the Fresnel-zone area $\left(\frac{2\lambda z \sec\theta}{\pi}\right)$ to the transverse scale size squared. The parameter β is related to the axial ratio, a, and the geomagnetic dip angle, ψ, by the relation

$$\beta = \left(a^2 \cos \psi + \sin^2 \psi\right)^{1/2} \qquad \text{(III-23)}$$

The angles θ and φ are the incidence angles at the ionospheric penetration point (see Rino and Fremouw, 1973).

From Eq. (III-18) we see that as Z varies from zero to infinity, B varies from $-\sigma^2$ to zero. Hence, from Eqs. (III-15) and (III-16), we see that for small Z, $\sigma_y^2 >> \sigma_x^2$. Only in the limit as Z approaches infinity are Rician statistics $\left(\sigma_x^2 = \sigma_y^2 = \sigma^2/2\right)$ achieved. Hence, for a given value of S_4, we can change the form of the intensity PDF considerably by varying the single parameter Z. We must, of course, first fix the axial ratio a and determine the angles θ, φ, and ψ.

Examples of two families of curves obtained in this manner are shown in Figures III-1(a) and III-1(b). For comparison we also show the corresponding Nakagami and log-normal PDFs. One can see clearly that there are significant differences for small Z values, particularly for the larger scintillation-index curves. Hence, if the data show similar differences, they should be detected by careful processing. The question of the validity of Eq. (III-18) will be deferred until the results are presented.

D. Data Analysis

1. NASA OAO-2 Data

Simultaneous data at 136 and 400 MHz are transmitted by the OAO-2 satellite, which is in polar orbit. The purpose of the transmission is to telemeter data on the 400-MHz channel. The satellite was routinely observed at the NASA tracking at Quito, Ecuador during 1969 and 1970. Data were selected for scintillation analysis when operator logs indicated that difficulties were being encountered in applying normal operating procedures.

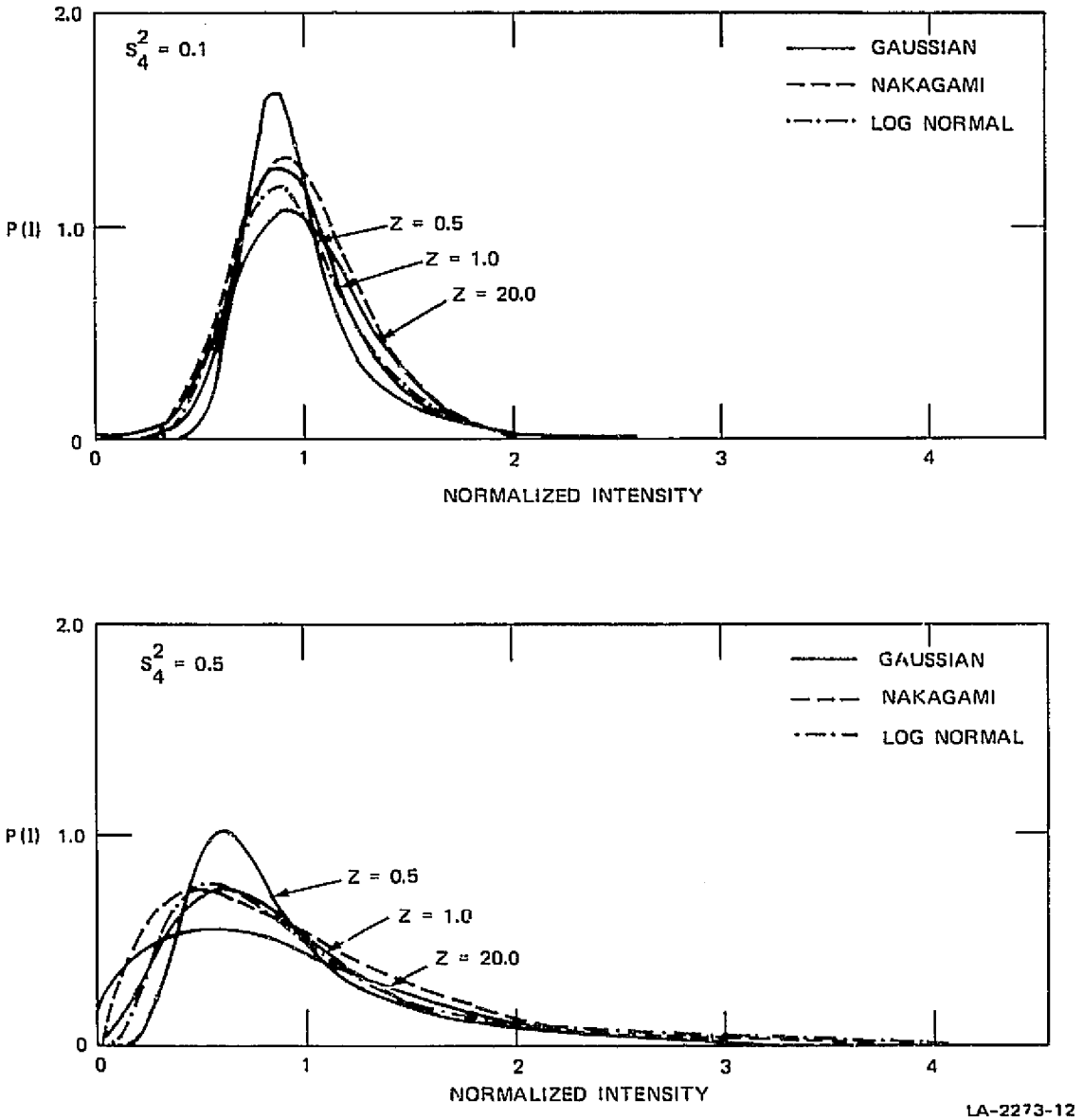

FIGURE III-1 FAMILY OF GAUSSIAN PDFs PARAMETERIZED BY Z COMPARED WITH THE CORRESPONDING NAKAGAMI AND LOG-NORMAL PDFs. For large Z, the gaussian PDF is very nearly Rician.

Data for eight representative passes, selected as described above, have been processed. Four data channels (numbered 1, 3, 5, and 7), consisting of horizontal and vertical polarizations at 136 and 400 MHz respectively, were recorded for each pass. The data base is summarized in Table III-1. The data were generally recorded at low elevation angles, and they were characterized by very intense scintillation. Indeed, the S_4 index was often greater than unity at 400 MHz.

Table III-1

NASA OAO-2 DIGITAL-DATA TAPES

	Analog Number	Date	GORF Tape Numbers		Time (UT)
			Channels 1-3, 1-5	Channels 3-7, 5-7	
Fall Equinox	1040	10/1/69	BW7975	BW9417	0951-1006
	1082	10/14/69	BW9421	BW9433	0314-0329
	1085	10/15/69	BW9419	BT4556	0235-0257
	1092	10/17/69	BT4578	BT4587	0304-0319
Spring Equinox	1489	03/3/70	BW9544	BX0487	0055-0110
	1556	03/28/70	BX0481	BW8890	0220-0233
	1660	03/30/70	BW9545		0233-0248
	1665	03/31/70	BX0239	BX0240	0340-0356

The measured S_4 scintillation indices for the fall equinox data are summarized in Table III-2. Each data block encompasses approximately 15 seconds of data. A most disturbing fact is that the statistics are dissimilar at the same frequency for different polarizations. The single exception is the 1 October 1969, 400-MHz data for Blocks 8, 9, and 10.

Table III-2

S_4^2 VALUES FOR OAO-2 FALL EQUINOX DATA

(a) 1 October 1969, 0959:15 UT

Block No.	BW 7975 File 1		BW 9417 File 2	
	136 MHz Horiz.	136 MHz Vert.	400 MHz Horiz.	400 MHz Vert.
1	1.1789	2.1233	0.4071	0.6052
2	1.2252	2.7863	0.7741	2.6971
3	1.0005	2.4049	0.6281	0.2355
4	0.9925	1.8213	0.7195	0.5011
5	1.1087	2.0123	0.1931	0.2767
6	1.3726	2.2537	0.4766	0.3655
7	1.05124	3.2596	0.5740	0.6639
8	1.5115	4.7579	0.9410	0.9278
9	1.5744	3.1266	0.7641	0.7553
10	0.7745	1.4798	0.2699	0.2757

Table III-2 (continued)

(b) 14 October 1969, 0316:04 UT

Block No.	BW 9421 File 1		BW 9433 File 2	
	136 MHz Horiz.	136 MHz Vert.	400 MHz Horiz.	400 MHz Vert.
1	0.9339	0.8759	0.8817	1.0477
2	1.9755	2.5796	0.7025	0.8122
3	1.8632	2.1910	0.8834	0.6527
4	2.7457	3.8259	0.9971	0.8230
5	1.3776	1.9358	0.9317	0.8113
6	2.4834	2.9448	1.9673	1.7433
7	2.2778	2.8537	1.5217	1.2464
8	1.9309	2.2038	1.0278	2.4421
9	2.0347	2.3987	3.6043	1.3116
10	1.7913	1.8859	1.5389	0.7388
11	2.7145	2.9625	0.7257	0.5043
12	1.9286	2.1612	0.5467	0.4050
13	1.8836	2.4187	0.2795	0.2372
14	1.3492	1.0591	0.6565	0.5001

Table III-2 (continued)

(c) 15 October 1969, 0244:03 UT

Block No.	BT 9419 File 1		BT 4556 File 2	
	136 MHz Horiz.	136 MHz Vert.	400 MHz Horiz.	400 MHz Vert.
1	2.8125	4.4357	1.0061	0.5967
2	1.1833	2.7865	1.0472	0.6532
3	2.2734	2.8146	0.7737	0.8753
4	2.0565	3.1683	1.5404	0.8502
5	1.9092	2.7466	1.0703	1.3409
6	1.8667	2.7279	1.2106	0.8164
7	1.9109	2.2961	0.8316	0.7684
8	1.6300	1.5960	0.5620	0.7638
9	1.6658	1.5764	1.0015	1.4876
10	1.7062	1.8075	0.3899	0.4950
11	2.0086	1.9361	0.2221	0.3846
12	1.5782	1.4455	0.2316	0.3820
13	1.5835	1.4111	0.3557	0.4869
14	1.9054	1.5007	0.3103	0.4052
15	1.9456	2.3084	0.3961	0.5007
16	2.1826	2.0509	0.5640	0.5809
17	1.8364	1.8634	1.0538	1.3310

Table III-2 (concluded)

(d) 17 October 1969, 0308:01 UT

Block No.	BT 4578 File 1		BT 4587 File 2	
	136 MHz Horiz.	136 MHz Vert.	400 MHz Horiz.	400 MHz Vert.
1	1.3234	1.1452	0.3656	0.3277
2	1.8886	1.4484	0.2815	0.3012
3	1.5665	1.2048	0.4251	0.4375
4	1.8715	1.2709	0.3925	0.4126
5	2.7674	2.8522	0.5915	0.7938
6	7.4664	5.0305	1.5980	1.0067
7	5.6374	4.3270	0.5403	1.7873
8	3.7195	2.9596	0.3623	0.5829
9	3.7616	3.0175	0.4199	0.5931
10	2.8402	2.9652	0.3279	0.3569
11	1.5799	2.1713	0.2110	0.0982
12	8.4029	1.2729	0.5618	0.1661
13	6.3948	17.7023	0.3794	0.3641
14	3.5439	3.9836	0.9426	1.0086
15	6.3153	1.0640	0.5162	0.4097
16	1.0136	1.6912	1.2929	0.8343
17	2.0756	2.3189	0.7393	0.7099
18	2.9416	3.4522	1.7486	0.9880
19	2.9619	3.9994	1.5129	0.9516
20	6.5558	7.9449	3.1781	2.9251
21	8.0384	1.8612	1.3810	1.5783
22	13.5004	7.7942	1.0309	1.0226
23	9.3590	5.6452	1.4560	1.1452
24	2.7745	3.2785	1.8369	1.5030
25	1.6137	1.7660	0.2078	0.2250
26	1.9871	1.8546	0.7048	0.4457
27	2.2410	1.7230	0.4764	0.5736
28	4.9856	2.5434	0.7316	0.9798
29	5.6505	3.0766	0.8343	1.2218
30	7.3730	3.2692	0.6834	0.9621

The above mentioned fact, coupled with the generally strong scattering conditions and the short stationary periods due to satellite motion, renders these data unusable for our purposes. We note that a gaussian field cannot produce an S_4 index greater than $\sqrt{2}$. Nonetheless, we have processed one data set to illustrate the difficulties.

For the 16 October 1969 data, only the first of the pair of digital tapes that constitute one pass was available. Hence, only the 136-MHz data were complete. Nonetheless, they display generally weaker scattering than for the data summarized in Table III-2. The processed data for the horizontally polarized antenna is shown in Figure III-2.

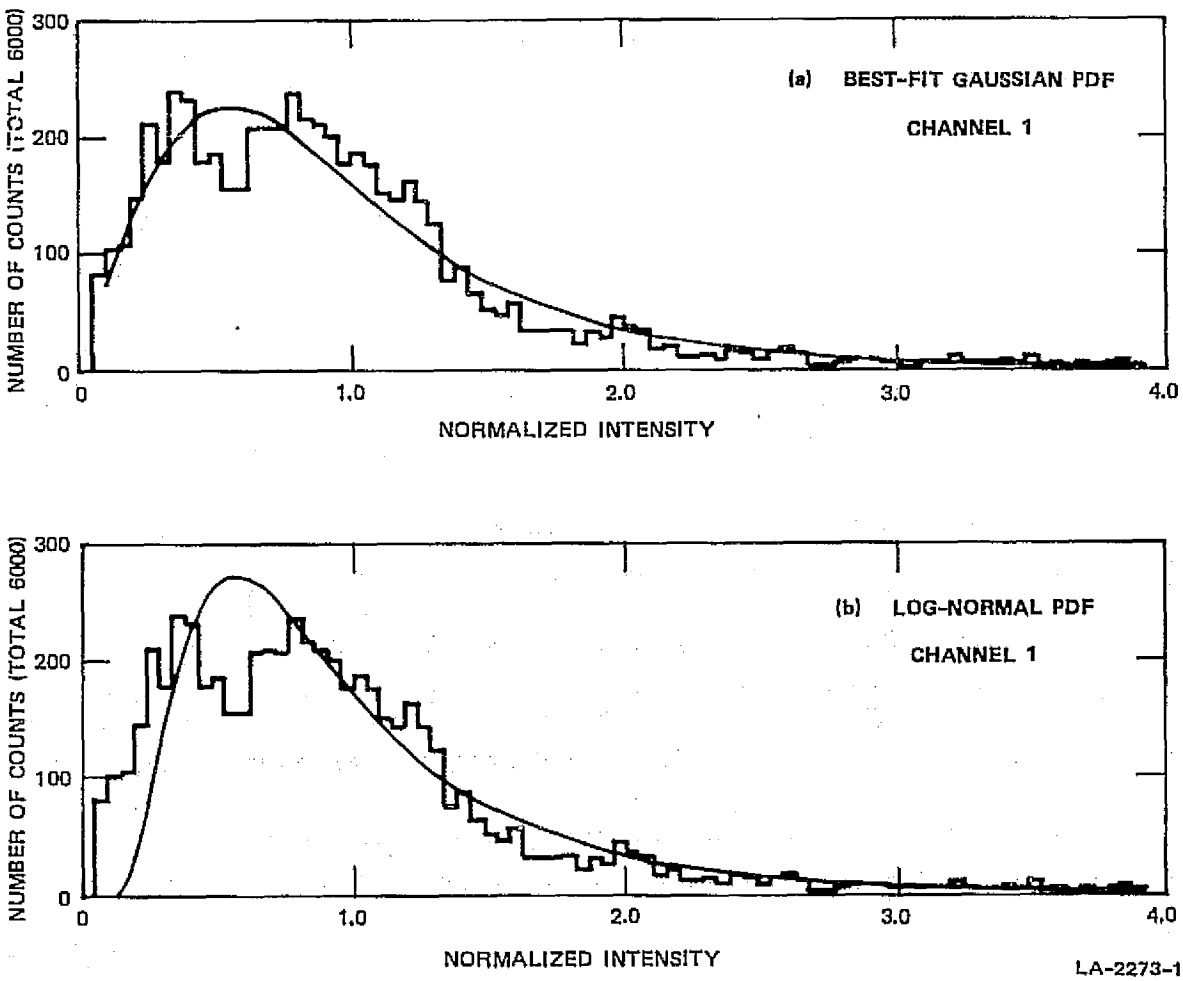

FIGURE III-2 LOG-NORMAL AND BEST-FIT GAUSSIAN PDFs FOR NASA 136-MHz OAO-2 DATA — ANTENNAS HORIZONTALLY POLARIZED

The best-fit gaussian PDF is clearly a better fit to the data than the corresponding log-normal PDF. However, for the corresponding vertically polarized data shown in Figure III-3, neither PDF provides a good fit.

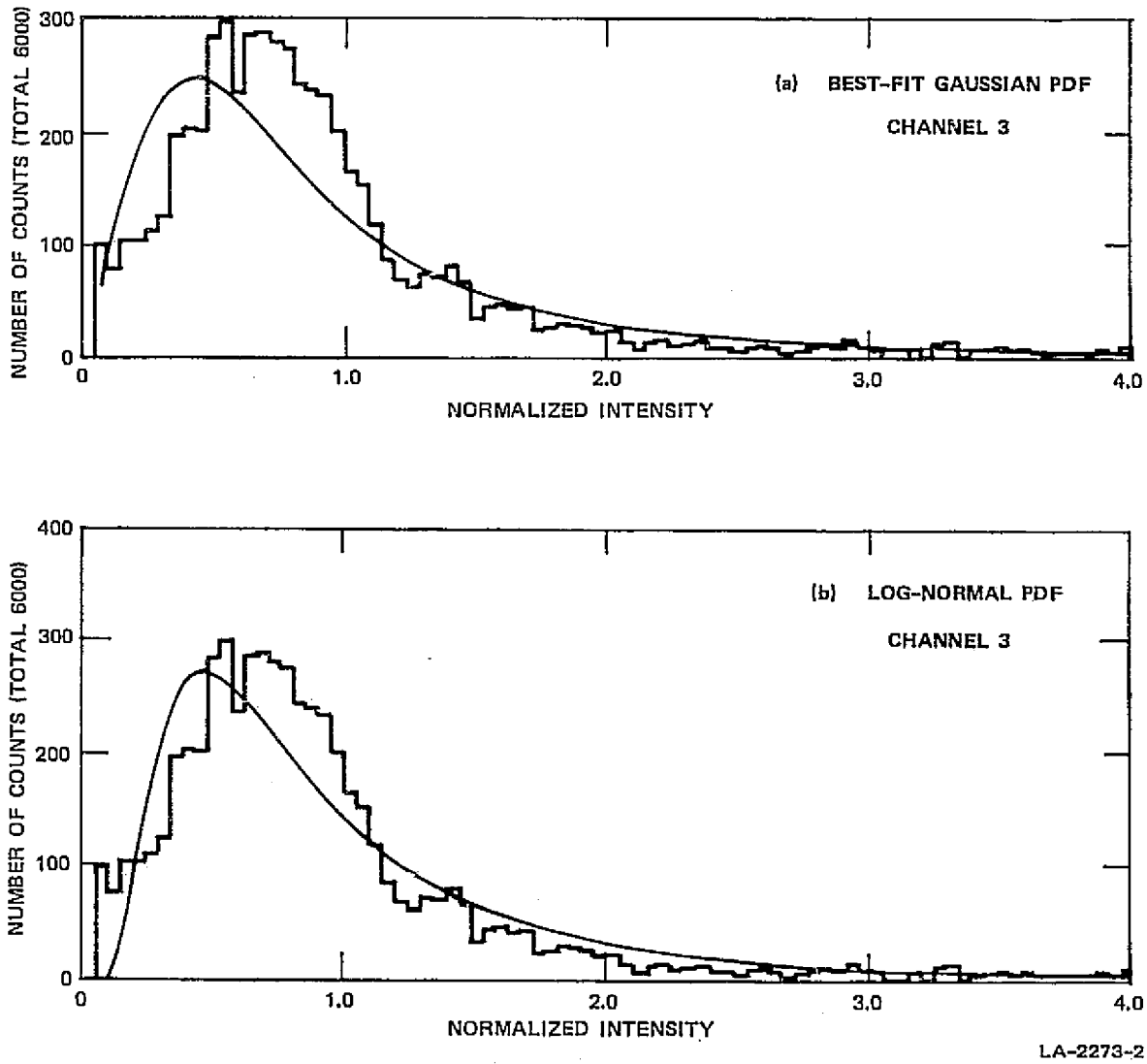

FIGURE III-3 LOG-NORMAL AND BEST-FIT GAUSSIAN PDFs FOR NASA 136-MHz OAO-2 DATA — ANTENNAS VERTICALLY POLARIZED

Because such behavior cannot be reconciled with any currently available weak or strong scatter theory, we did not pursue these data further. Rather, we have concentrated on synchronous-satellite data

taken under conditions of weaker scattering. However, the OAO-2 data are interesting in their own right. They have been analyzed (Blank and Golden, 1973) and the polarization effect noted.

2. NASA ATS-5 Data

Six data sets for the synchronous satellite ATS-5 recorded at Lima, Peru during November 1971 have been processed. Among the six data sets only one produced processable data. The data tapes and the difficulties encountered are summarized in Table III-3 below.

Table III-3

NASA ATS-5 DATA

GORF No.	Date	Comments
BO7445	11/17/71	Short record
BO5334	11/02/71	Bad tape
BO7830	11/11/71	Good data
BO7805	11/12/71	Bad calibration (possibly recoverable)
BO6819	11/08/71	Wrong format
BO6327	11/04/71	Wrong format

Two channels of data were recorded with spaced receivers separated by 1200 ft. along an east-west baseline. The receivers were located at Lima, Peru. These data are identical in format to those presented by Rino and Fremouw (1973). The two data channels should have nearly identical statistics. The data tapes BO6819 and BO6327 had very different data in the two recorded channels. Hence, we did not process these data further.

One complication with the ATS-5 data lies with the fact that the satellite is spin-stabilized. The antennas are not completely

despun, so that the data show a slight periodic modulation at approximately 0.16 Hz. The effect is to smear the histograms, since data from different parts of each cycle have different means. We did not attempt to correct the data for the satellite spin because of the increased complexity and cost.

In Figure III-4 we show the histograms for the 11 November 1971 data together with the corresponding log-normal PDFs. The measured S_4 indices were 0.37 and 0.34 for Channels 1 and 2, respectively. There is clearly a statistically significant difference between the measured histograms for the two channels. The near 10% difference in the S_4 indices is larger than their individual standard deviations of ~ 2%. Moreover, the respective χ^2 parameters differ by more than a factor of 4.

Evidently the two receiver characteristics are different. For example, the satellite spin is slightly more pronounced in the Channel-2 data. This was inferred by noting that the relative intensities of the spectral lines due to the satellite spin* are approximately 1 dB higher for the Channel-2 data.

The results of applying the curve-fitting procedure that we have described reflects the differences between the two channels. In Figures III-5 and III-6 we show the best-fit gaussian PDFs. For the Channel-1 data the improvement is considerable. We see that the "rise time" for the log-normal PDF is too slow. Moreover, it underestimates the peak of the histogram. The best-fit gaussian PDF completely corrects these discrepancies (cf. Figure III-4). The best-fit parameters are summarized in Table III-4. We see that for both channels, less than 20% of the scattered power is in-phase with the undeviated component.

---

* See Figure III-7.

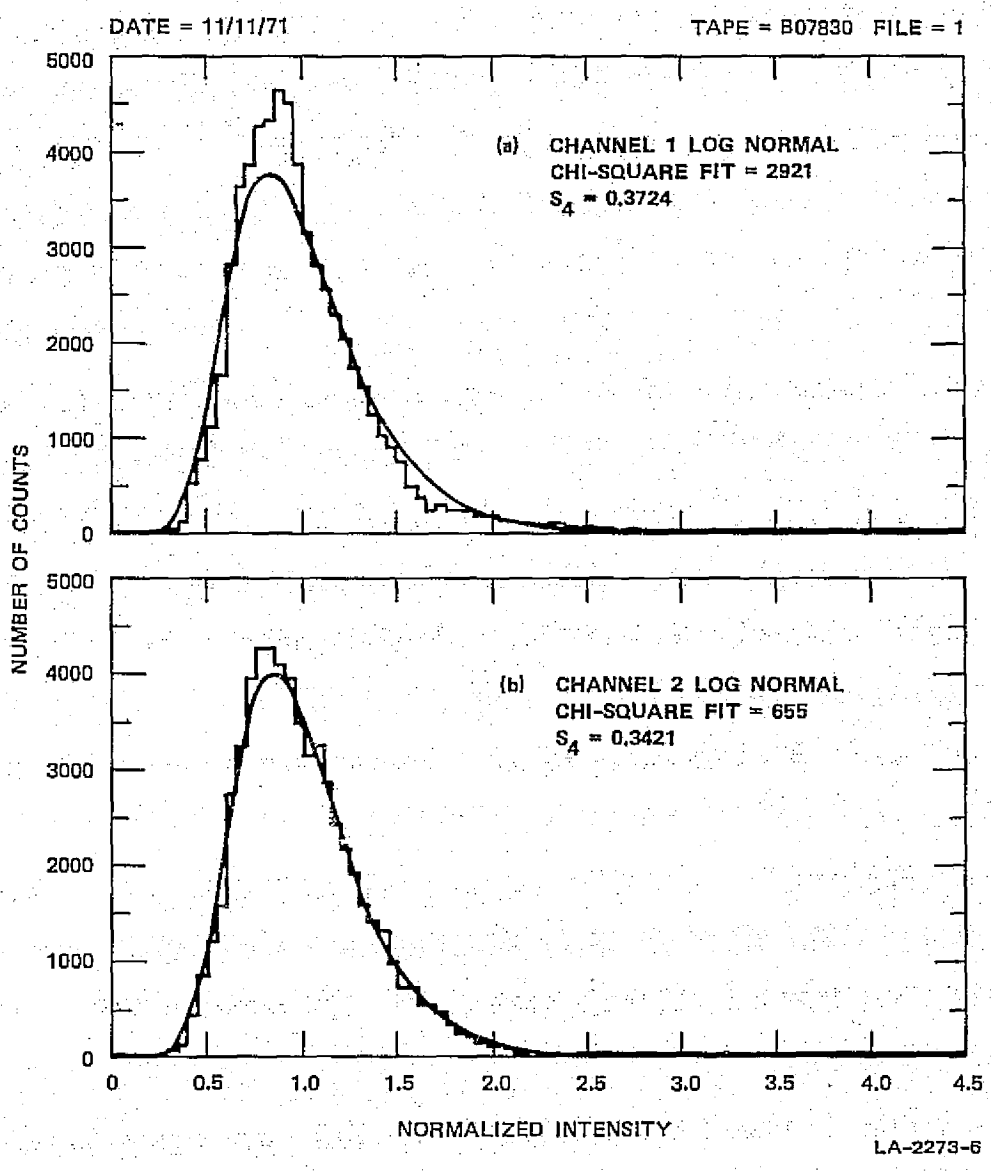

FIGURE III-4 LOG-NORMAL PDFs FOR NASA 134-MHz ATS-5 DATA

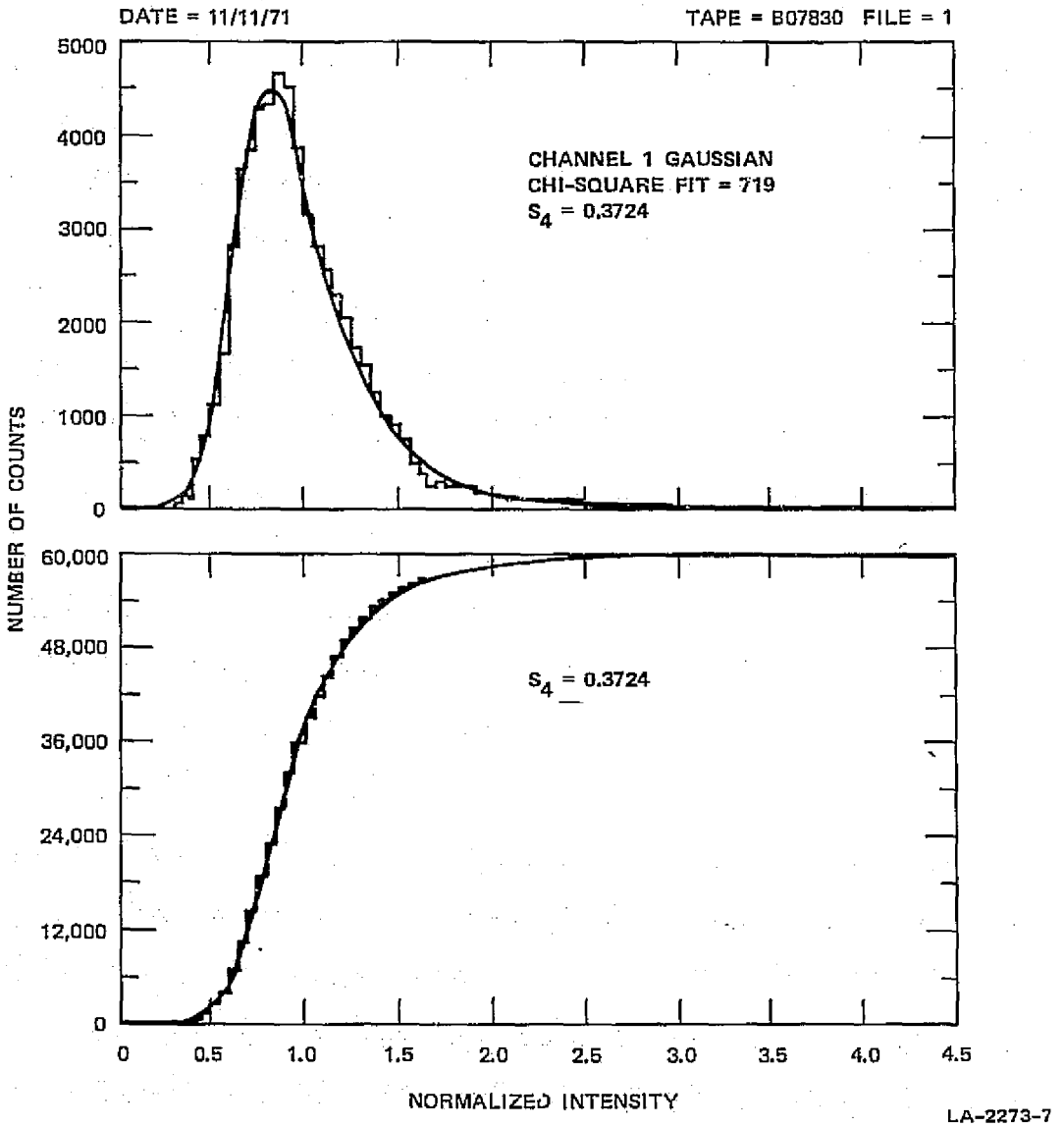

FIGURE III-5 BEST-FIT GAUSSIAN PDF FOR NASA 134-MHz ATS-5 DATA — CHANNEL 1

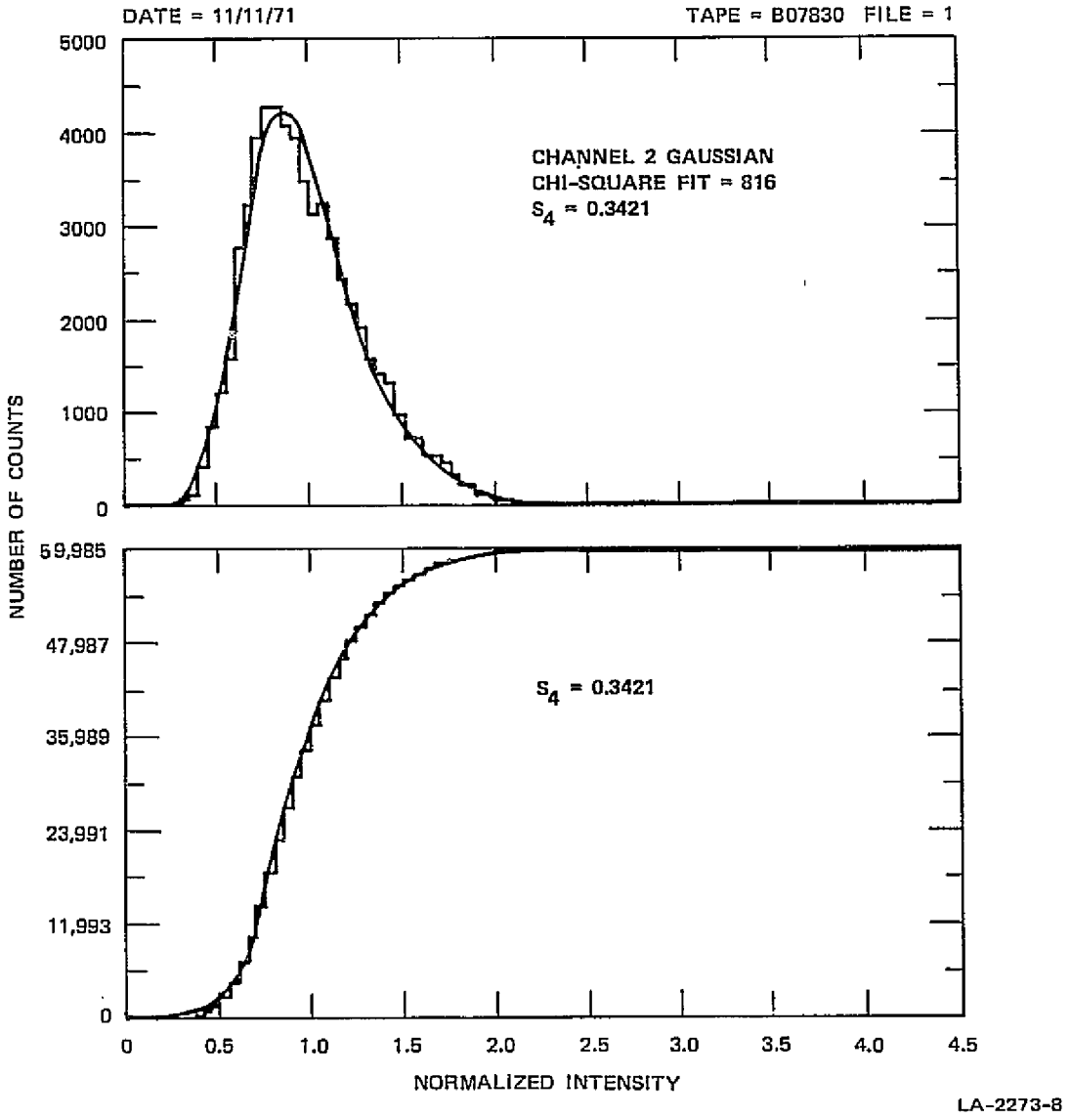

FIGURE III-6 BEST-FIT GAUSSIAN PDF FOR NASA 136-MHz ATS-5 DATA — CHANNEL 2

Table III-4

PARAMETERS FOR NASA ATS-5 DATA

(β = 5.0, θ = 31.04°, ϕ = 110.8°)

Parameter	Channel 1	Channel 2
S_4	0.3724	0.3421
χ^2	719.0	816.0
Z	0.590	0.880
σ^2	0.2162	0.1620
σ_x^{2*}	0.0811	0.1357
$\lvert B \rvert^*$	0.8892	0.8082
$\angle B$	19.60°	25.60°

*Normalized to incoherent component rms power.

For the Channel-2 data the log-normal PDF remained a slightly better fit than the best-fit gaussian PDF. Hence, the data are not mutually consistent. However, as noted above, the more pronounced spin effect may be cause for rejecting the Channel-2 data.

To complete analysis of the ATS-5 Lima data we have computed the power spectrum of the intensity fluctuations. The results are shown in Figure III-7 together with a family of power-law SDFs [Eq. (IV-27)] for different spectral indices γ. The γ = 1.5 curve, which is evidently the best fit, is close to the γ = 1.45 value inferred from satellite in-situ measurements (see Section V-D). However, the receiver noise tends to force this result, and a more careful analysis should be performed. The arrows point to the satellite spin lines.

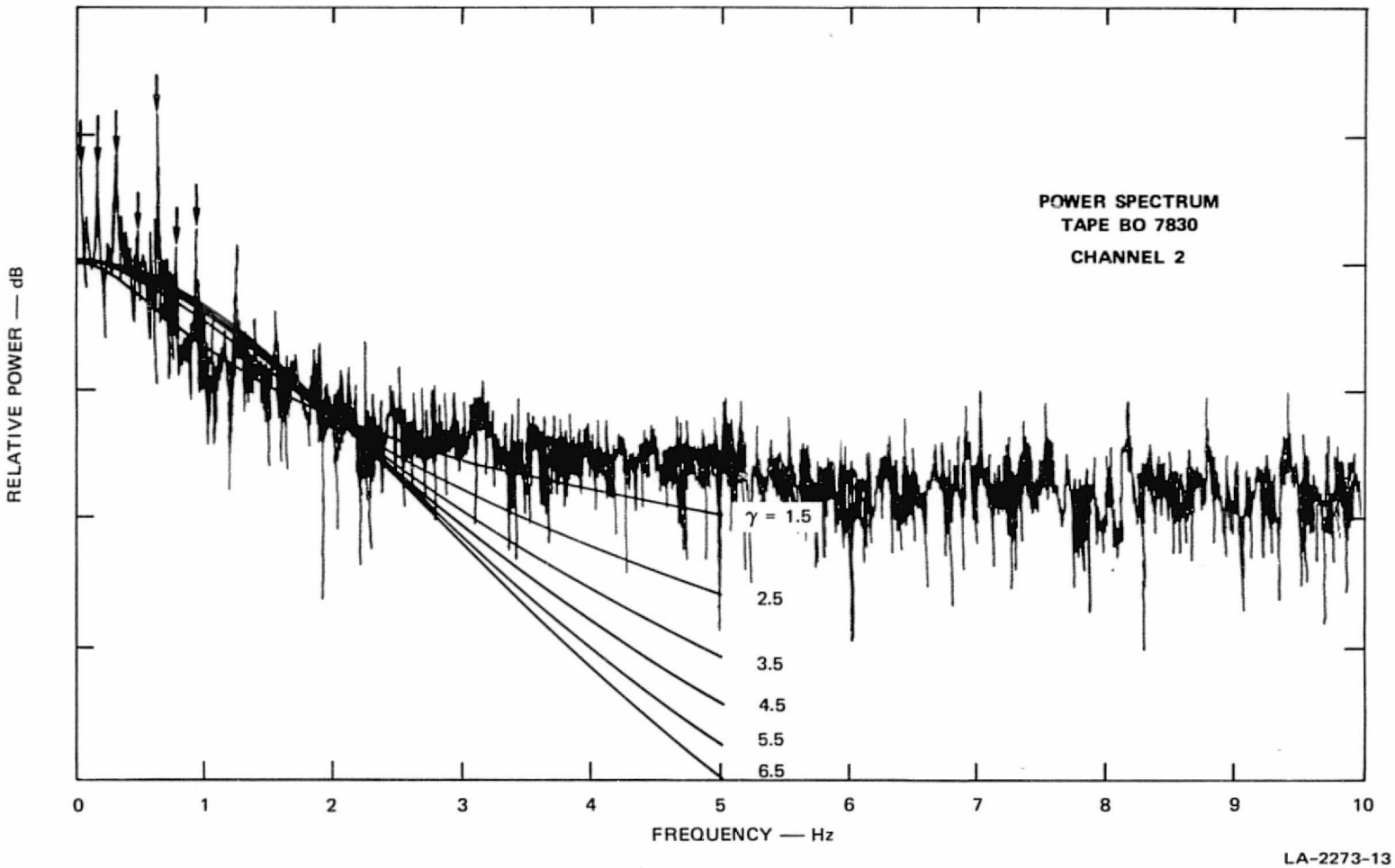

FIGURE III-7 INTENSITY POWER SPECTRUM FOR NASA ATS-5. Arrows point to satellite spin lines. Solid curves are for power-law analytic forms.

3. AFCRL ATS-5 Data

The Air Force Cambridge Research Laboratory has processed a large volume of scintillation data for amplitude statistics. Their primary interest was in characterizing the average statistics for relatively long periods of time. They found the Nakagami distribution to be well suited for that particular task (Whitney, Aarons, Allen, and Seemann, 1972).

Because of our mutual interest in intensity statistics, arrangements were made for SRI to obtain and process some representative samples of the AFCRL data. Our analysis of the data was complementary, in that we are interested in a precise computation of the statistics for short periods. In this subsection we summarize the results of processing sixteen hours of data recorded at Hamilton, Massachusetts during April and May of 1973. Both VHF and UHF signals were recorded, although the UHF scintillation was generally too low to be reliably processed.

The data are grouped into five quasistationary segments, as described in the introduction to this section. The data base is summarized in Table III-5. Data Sets 2 and 4 contain only 1000 samples each. Hence, their accuracy is generally poorer than for Data Sets 1, 3, and 5. For each data set we have obtained the best-fit gaussian and the corresponding log-normal PDFs.

The parameters for the VHF (136 MHz) data are summarized in Table III-6. We first note that for each data set the gaussian χ^2 value denoted as χ^2_{gauss} achieves a lower value than the corresponding log-normal χ^2 value denoted as χ^2_{LN}. Moreover, the difference is largest for Data Sets 1, 3, and 5, which are statistically most significant.

Table III-5

SUMMARY OF AFCRL ATS-5 DATA

Data Set	Date	No. of Hours	Sample Rate (Hz)	S_4(VHF)
1	4/12/73	2	0.14	0.5527
2	4/12/73	1	0.14	0.3442
3	4/15/73	3	0.14	0.2664
4	4/15/73	1	0.14	0.1356
5	5/18/73	4	0.31	0.2829

Table III-6

PARAMETERS FOR VHF DATA

(β = 3.2, θ = 55.20°, ϕ = 40.21°)

Data Set	S_4	χ^2_{LN}	χ^2_{gauss}	σ^2	σ^2_x	$\lvert B \rvert$	$\angle B$	Z
1	0.5527	175.4	166.5	0.3501	0.0971	0.8780	23.4°	0.4
2	0.3442	113.9	113.8	0.1494	0.1618	0.7879	31.1°	0.6
3	0.2664	86.5	56.67	0.1091	0.1307	0.8329	27.5°	0.5
4	0.1356	82.7	75.64	0.0145	0.3171	0.5481	48.1°	1.4
5	0.2829	169.5	107.2	0.1362	0.1005	0.8734	23.8°	0.41

We also note that for Data Sets 1, 3, 5, the Z parameter lies between 0.4 and 0.5. The corresponding σ_x^2 parameters show that less than 20% of the scattered power is in phase with the steady or undeviated signal components. The equiprobability ellipses for the joint PDF of X and Y are characterized by $|B|$ and $\angle B$. Indeed, one can show that the ratio of major to minor axes is given as $\frac{1 + |B|}{1 - |B|}$, and the orientation angle is $1/2\ \angle B$.

Hence, the best-fit gaussian PDF has an axial ratio greater than 10 (not to be confused with the irregularity axial ratio a) and it is within 10° of being perpendicular to the undeviated signal component. The strength of the scattered component is the main variable. We note that there is no obvious breakdown of the theory for σ^2 as large as 0.35. It is worth noting that while we have discounted the OAO-2 data, the PDF in Figure III-2(a) corresponds to a σ^2 parameter larger than 0.9.

In Figures III-8, III-9, and III-10 we show the log-normal PDF and the best-fit gaussian PDF for Data Sets 1, 3, and 5. We see in each case that the log-normal statistics achieve a slower rise time, and then underestimate the peak of the histogram. This pattern was previously observed in the NASA ATS-5 data at least for the Channel-1 data [cf. Figures III-4(a) and III-5(a)].

In Table III-7 we have summarized the UHF parameters for the three data sets that showed the strongest scintillation. The parameter η is the spectral index defined in Section V [Eq. (V-3)]. We first note that theory predicts $\sigma^2 \propto \lambda^2$. However, for Data Set 1, $\frac{\sigma^2_{VHF}}{\sigma^2_{UHF}} = 11.9$, whereas $\frac{\lambda^2_{VHF}}{\lambda^2_{UHF}} = 9.18$. We believe the discrepancy to be due to noise contamination of the VHF data. The spectral-index value is also somewhat smaller than we expect (see Section V-A-1).

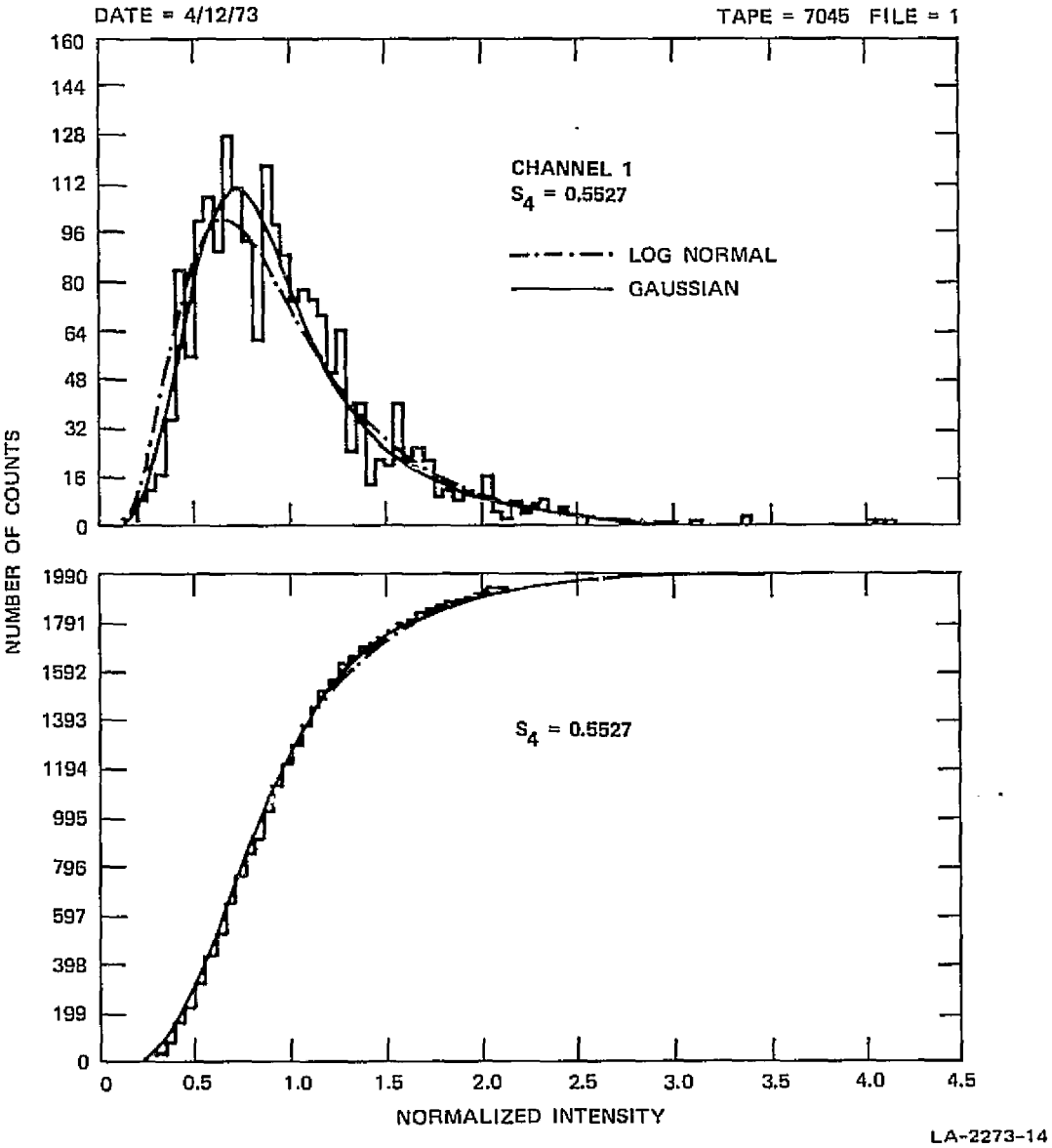

FIGURE III-8 BEST-FIT GAUSSIAN AND LOG-NORMAL PDFs FOR AFCRL DATA — SET 1

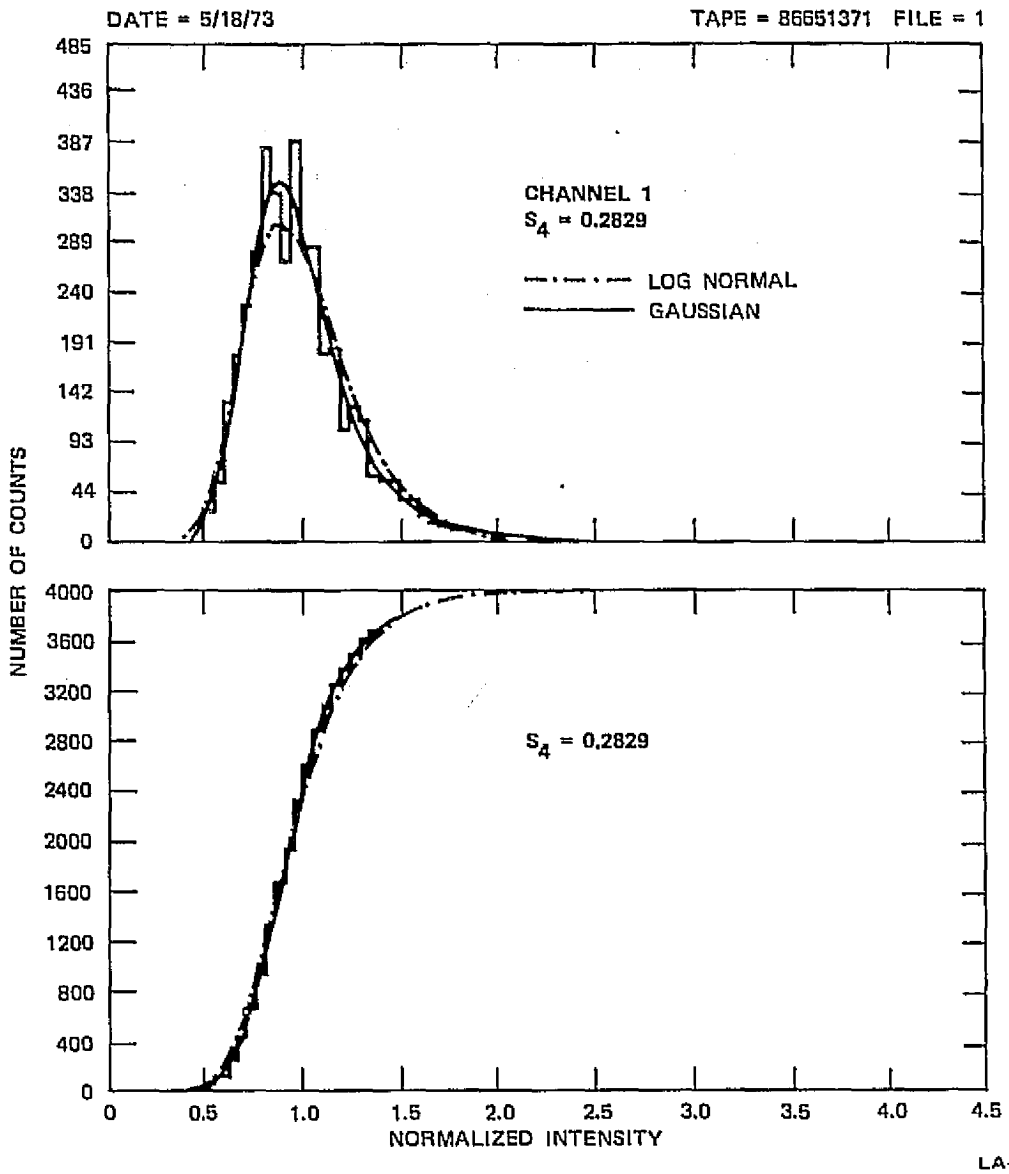

FIGURE III-9 BEST-FIT GAUSSIAN AND LOG-NORMAL PDFs FOR AFCRL DATA — SET 5

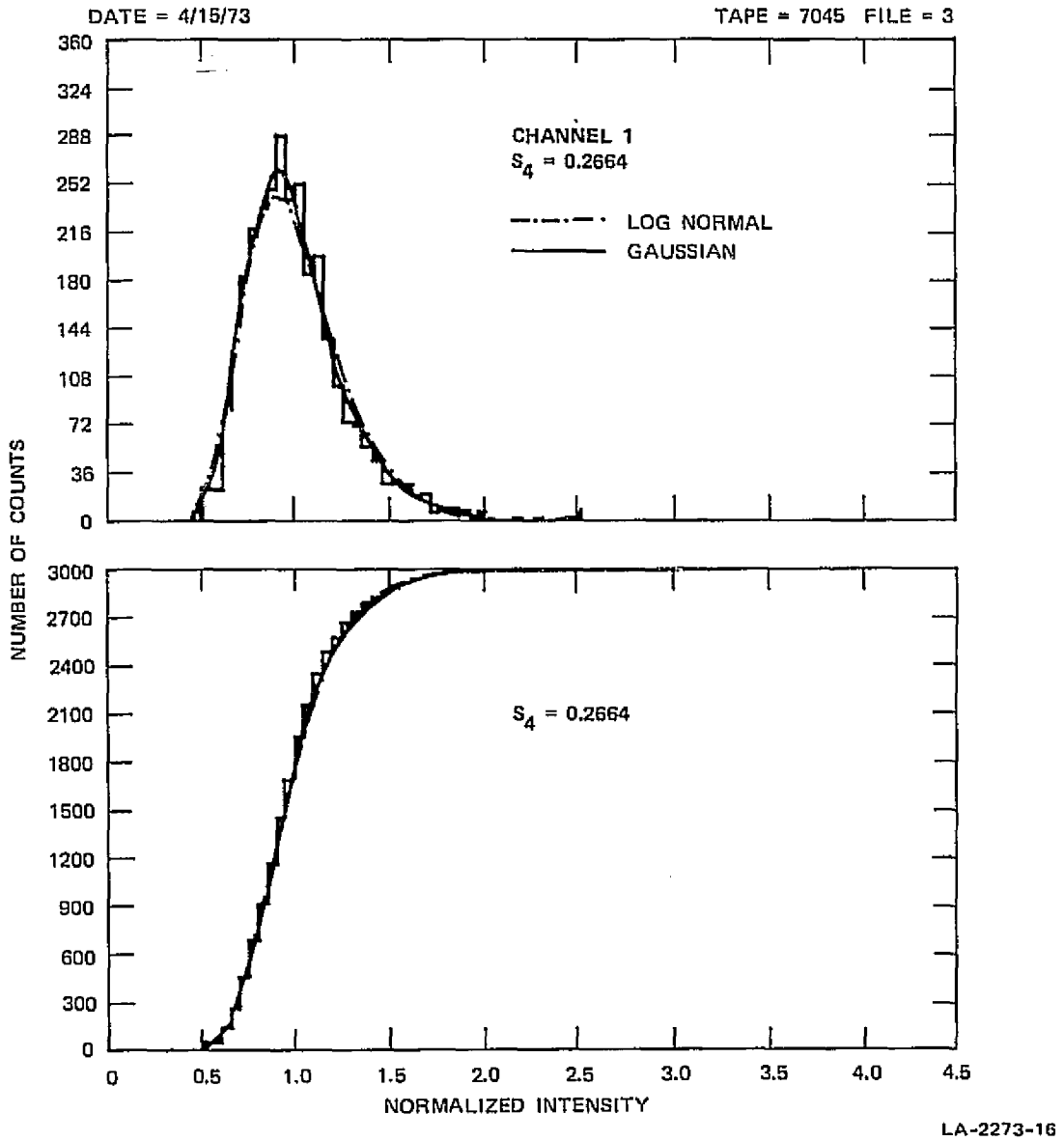

FIGURE III-10 BEST-FIT GAUSSIAN AND LOG-NORMAL PDFs FOR AFCRL DATA — SET 3

Table III-7

PARAMETERS FOR UHF DATA

($\beta = 2.1$, $\theta = 31.04^{\circ}$, $\phi = 10.8^{\circ}$)

Data Set	S_4	χ^2_{LN}	χ^2_{gauss}	σ^2	σ_x^2	$\lvert B \rvert$	$\angle B$	Z	η
1	0.0831	123.8	123.8	0.0293	0.0464	0.9431	15.9°	0.25	1.76
2	0.0714	61.87	61.87	0.0126	0.0971	0.8780	28.4°	0.4	1.46
5	0.0634	80.00	65.61	0.0023	0.43	0.32	65.4°	3.2	1.39

The discrepancies become larger as the UHF S_4 index becomes smaller. Moreover, we observe that the best-fit Z parameter steadily increases. That is, the statistics are tending to Rician as we would expect if the noise contribution were dominating the statistics. We do note, however, that for each data set the best-fit gaussian PDF achieves a lower χ^2 value than the corresponding log-normal χ^2 value.

4. UCSD Interplanetary Scintillation Data

As a final example we present some interplanetary radio-star scintillation data taken at the University of California Solar Observatory located near San Diego, California. The observations were made at 75 MHz. The UCSD data processing for amplitude statistics is discussed by Armstrong, Coles, and Rickett (1972), which we referred to in Section II-A.

Arrangements were made to apply our data-reduction procedure to some representative UCSD data. We assumed normal incidence and iostropic irregularities. In the data reduction we varied the transverse scale size rather than Z directly. The wavelength is known, and the mean distance between the earth and the sun was used for the distance parameter z.

Three typical results are shown in Figures III-11(a), (b), and (c). In all cases the best-fit gaussian PDF fit better than the corresponding log-normal PDF. The transverse-scale parameter varied between 800 and 1000, which is comparable to the square root of the Fresnel-zone area for 75 MHz at the distance of the sun. Thus, the best-fit Z-parameter value is near or less than unity just as it was for the ionospheric scintillation data. Indeed, the striking feature in these data is the similarity of the histograms to those obtained for the ionospheric scintillation data. We observe again that the discrepancy between the data and the log-normal PDF is systematic in that the log-normal PDF achieves too small a rise time, and then underestimates the peak of the histogram.

The similarities between the ionospheric and interplanetary scintillation strongly suggest that certain features of the scattering are universal. This possibility is discussed in the next subsection.

E. Summary and Conclusions

In this section we have described a procedure for obtaining a family of probability-density functions for intensity based on the assumption of gaussian statistics. Each member of the family has the same first and second moments of intensity. By comparison, the log-normal and Nakagami PDFs are uniquely determined by the first and second moments of intensity.

In Section III-D we applied the procedure to obtain a best fit to measured histograms from ionospheric and interplanetary scintillation data. The results support the general conclusion that the best data fit among the members of the gaussian family is significantly better than the corresponding log-normal PDF. The implication is that the diffracted field rather than its logarithm has gaussian statistics.

The best-fit gaussian PDFs display a considerable degree of similarity. We find that independent of the value of S_4, the magnitude

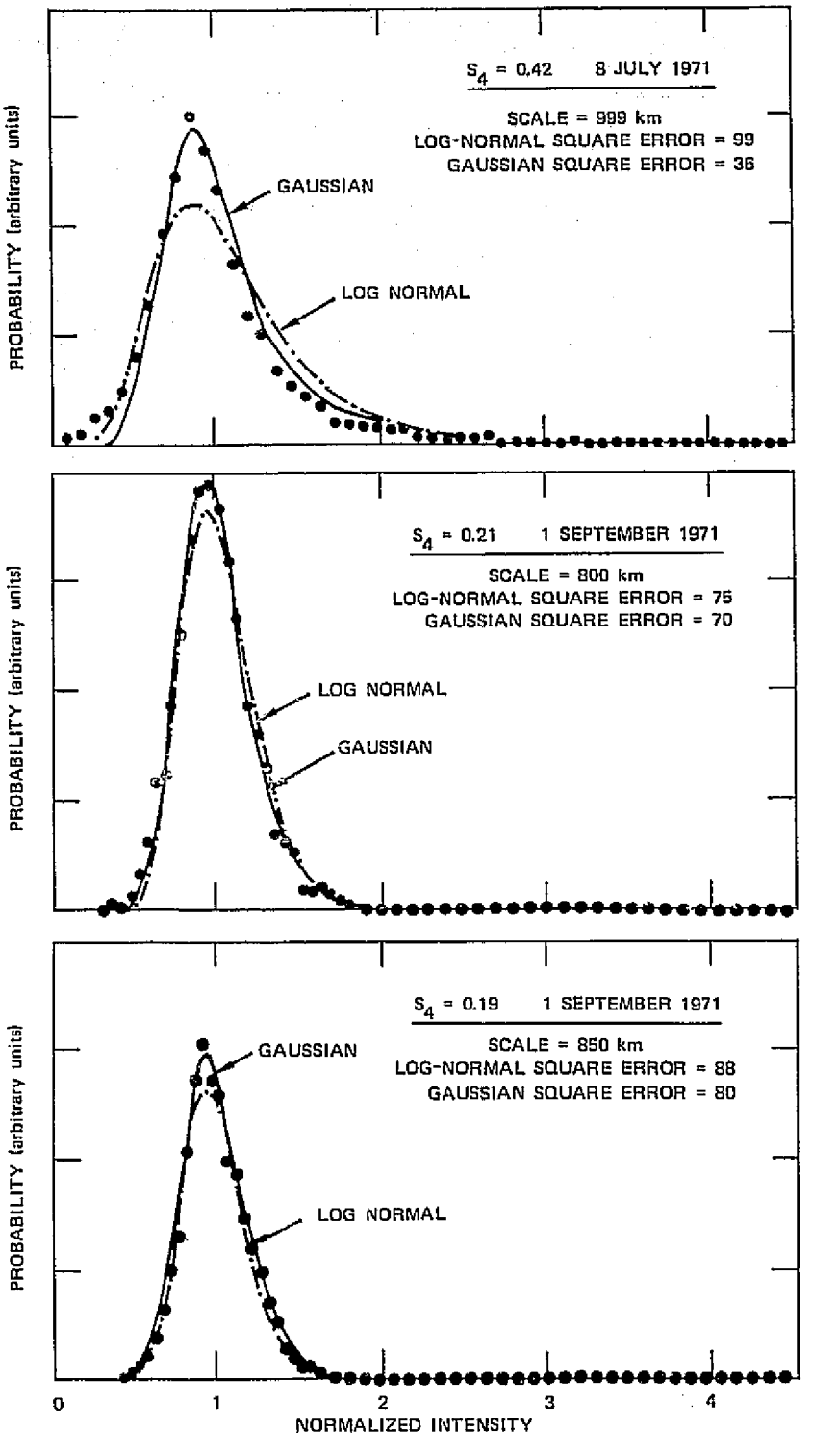

FIGURE III-11 BEST-FIT GAUSSIAN AND LOG-NORMAL PDFs FOR UCSD INTERPLANETARY SCINTILLATION DATA

of B is generally larger than 0.8, while its angle is less than 30^{o}. This implies that more than 80% of the scattered power is in phase quadrature with the undeviated signal component, and C_{xy} is finite.

These results readily explain why Rician statistics generally provide a poor fit for scintillation data. The best-fit gaussian PDF in general tends to be more peaked about its mean than either the corresponding Rice, Nakagami, or log-normal PDFs. As a practical engineering matter, the latter PDFs will give more conservative probabilities for a given S_4 index. As an example, we have computed fade margins for a given S_4 index and different PDFs by setting $B = 0.85 \angle 20^{o}$, which seems to a good median value. The results are shown in Figure III-12

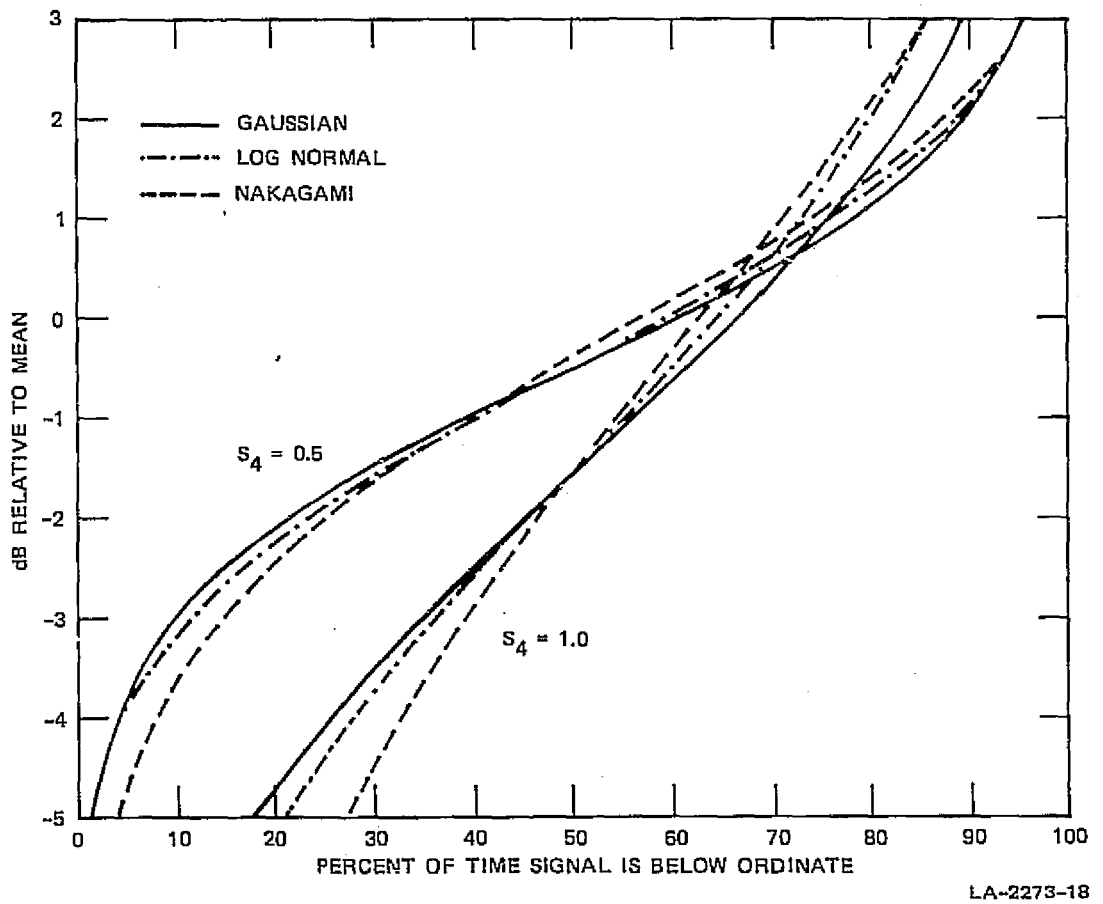

FIGURE III-12 FADE-MARGIN COMPARISON FOR GAUSSIAN, LOG-NORMAL, AND NAKAGAMI PDFs

Finally, we consider the validity of Eq. (III-8). We know from the shape of the intensity power spectrum [see Figure III-7] that a gaussian autocorrelation function is incorrect. Indeed, if one uses e^{-1} point as a measure of spectral width, the gaussian PDF corresponds $\gamma \to \infty$ limit. To see this, consider that $e^{-K^2} = \lim_{N\to\infty} \left(1 + \frac{K^2}{N}\right)^{-N}$.

What we have observed suggests that any diffraction model that gives rise to the appropriate B value for some set of parameters will achieve a near-optimum data fit. It seems unlikely that one could obtain sufficiently accurate data to resolve fine details even if a unique solution did exist.

We shall show in Section IV that independent of the particular spectral-density-function shape, one can always achieve the condition $\sigma_y^2 >> \sigma_x^2$ for sufficiently small Z. The transverse scale parameter can be interpreted as an "outer irregularity scale" following the terminology of turbulence theory. A small value of Z will always be achieved if the outer irregularity scale is sufficiently large. Indeed, for incompressible-fluid turbulence, the outer scale is infinite. Our results are consistent with the assumption of a similar result for magnetohydrodynamic fluids.

In closing this section we note that one possible way to reconcile with theory the result that the field statistics are gaussian rather than log-normal (see Section II) is to reject the Markov assumption. It has been shown that the Markov assumption is sufficient for the validity of the Rytov solution. Tatarski (1971) has discussed the validity of the Markov approximation and shown that it is consistent with iostropic irregularities, but not necessarily with anisotropic-irregularity structures. Since the latter is the case for ionospheric irregularities we have some basis for believing that the Markov assumption is in fact too stringent for radiowave scintillation.

IV THEORETICAL BASIS FOR CHANNEL MODELING

In the introduction to this report we briefly discussed the general problem of channel modeling. In this section we shall present in detail theoretical calculations that form a basis for a scintillation-effects channel model.

A. Introduction

A functional block diagram of an artificial earth satellite communication link is shown in Figure IV-1. For our purposes, the modulation is a complex voltage applied for some period of time--say, T milliseconds. Demodulation is the process of removing the complex envelope from the received signal. If the transionospheric channel were perfect, the demodulated signal would be an exact replica of the modulating waveform.

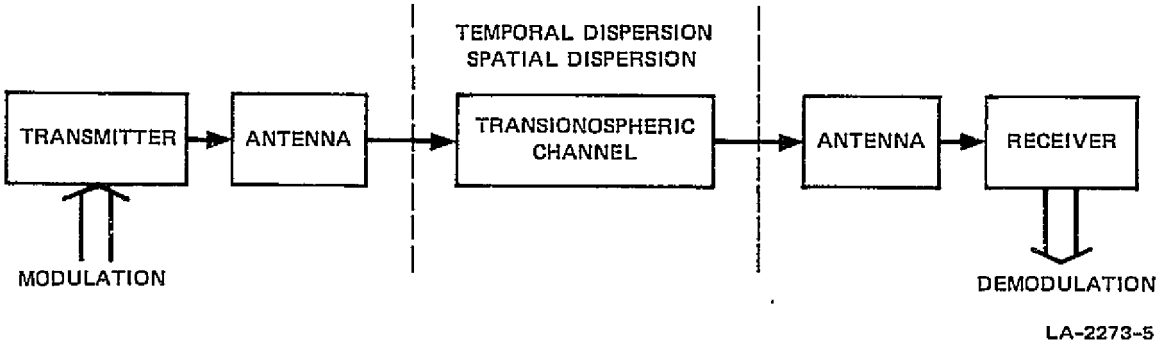

FIGURE IV-1 FUNCTIONAL BLOCK DIAGRAM OF SATELLITE-EARTH COMMUNICATION SYSTEM

We are not concerned here with additive noise or interference, since even in their absence the demodulated signal is not a perfect replica of the modulating signal. A wave packet suffers temporal

dispersion owing to the fact that different frequency components propagate with slightly different velocities. Moreover, raypaths are curved so that a "pencil" of rays suffers spatial dispersion as well.

There are several other effects, such as Faraday rotation and absorption, to name two. These effects are characterized by the fact that they can, in principle, be computed from the deterministic component of the ionospheric index of refraction, which depends explicitly on frequency and position (Lawrence, Little, and Chivers, 1964).

Our interest here is in the effects produced by the irregular departures of the ionospheric index of refraction from its mean value. Thus, we must make a somewhat arbitrary division between the slowly varying (spatially as well as temporally) component, which we shall assume to be deterministic, and the residual, which we assume to be representable by a suitable random function.

For simplicity, we shall ignore the deterministic effects, so that in the absence of index-of-refraction irregularities, the signal free-space-propagates from the transmitting antenna to the receiving antenna. There is no serious loss of generality in neglecting the deterministic effects; some can be eliminated by operating procedures. For example, Faraday-rotation effects can be minimized by using circularly polarized antennas.

For engineering applications we seek a description of the terminal behavior of the system shown in Figure IV-1. Indeed, a fairly well developed theory of signaling in fading dispersive channels exists. One of the most basic measurements is a determination of the system frequency response. For the transionospheric channel, a monochromatic signal emerges with a stochastic component that is slowly varying compared to the frequency of the incident wave.

There are two quantities to be determined--namely, the fraction of the incident energy that is randomized, and the statistical structure of the random component. Our analysis will be restricted to weak scattering, and we shall first calculate the complex second moments of the field. In Section V we shall apply the properties of gaussian fields to calculate intensity statistics.

Following our "black-box" approach to channel modeling, we would calculate the complex second moments of the demodulated voltage $v(t) = \langle v(t) \rangle + \delta v(t)$. The technique has been discussed in detail by Bello (1963). We represent the response of the system shown in Figure IV-1 to a sinusoid of frequency f, as h(t;f), a stochastic function of time t and frequency. Then, the response to an arbitrary signal whose spectrum is $\hat{x}(f)$ can be calculated from the integral

$$v(t) = \int \hat{x}(f) h(t;f) e^{2\pi i f t} df \quad . \qquad \text{(IV-1)}$$

The first important quantity is $\langle |\delta v(t)|^2 \rangle$, which, when compared to $|\langle v(t) \rangle|^2$, is a measure of the intensity of the disturbance. The second-order moments $\langle \delta v(t)\ \delta v^*(t') \rangle$ and $\langle \delta v(t)\ \delta v(t') \rangle$ follow directly from the similar quantities for h(t,f) by applying Eq. (IV-1). We note, however, that from Figure IV-1, h(t,f) includes the effect of the transmitting and receiving antennas, which are spatial filters, and the receiver, which is a temporal filter.

To eliminate these deterministic factors we can compute the response of the transionospheric channel to a single monochromatic plane wave for a time-invariant scattering layer. This is a more fundamental quantity chan h(t,f), and we shall see in Section IV-D that h(t,f) can be readily derived from it. Thus, our problem reduces to one of calculating the second-order complex moments of the random field that results from propagating a plane wave through a weakly scattering irregularity layer.

To formulate that problem, we first consider the equation for wave propagation in an irregular medium--namely,

$$\nabla^2\vec{E} + k^2 \epsilon \vec{E} = -\nabla(\vec{E} \cdot \nabla \log \epsilon) \ . \qquad \text{(IV-2)}$$

The relative permittivity ϵ is a random function parameterized by position and time, although in deriving Eq. (IV-2) we have assumed that the temporal variations of ϵ are slow compared to the propagation time through the medium. We write $\epsilon = \langle\epsilon\rangle + \delta\epsilon$, and restrict ourselves to the class of problems for which $\langle\epsilon\rangle \cong 1$, and $\langle\delta\epsilon^2\rangle^{1/2} << \langle\epsilon\rangle$. (The angular brackets denote ensemble average.) It is then natural to consider a series solution to Eq. (IV-2) with terms $0\left(|\delta\epsilon|^{\ell}\right)$ in magnitude.

The gradient term in Eq. (IV-2), which produces polarization effects (Strohbehn and Clifford, 1967), is usually neglected on the grounds that significant changes in ϵ occur only over large distances compared to a wavelength. For our applications, this is unnecessarily stringent. Following Balser (1957) and Tatarski (1971), we have applied a series solution to Eq. (IV-2) directly. The result is a sequence of "cascading" inhomogeneous vector differential equations.

If the incident field (the zeroth order term) is a plane wave $\vec{E}_o(\vec{r}) = \vec{A}_o \exp\{-i\vec{k} \cdot \vec{r}\}$, it can be shown by repeated application of Green's theorem that the first-order term $\vec{E}_1(\vec{r})$ is given by the integral expression

$$\vec{E}_1(\vec{r}) = \frac{k^2}{4\pi}\left[\vec{A}_o - \left(\hat{a}_r \cdot \vec{A}_o\right)\hat{a}_r\right] \int^{(3)}\delta\epsilon(\vec{r}')\exp\{-i\vec{k} \cdot \vec{r}'\}G(\vec{r},\vec{r}')d\vec{r}'$$

$$+ \text{terms } 0\left(1/r^2\right) \qquad \text{(IV-3)}$$

where

$$G(\vec{r},\vec{r}') = \frac{\exp\{-ik|\vec{r} - \vec{r}'|\}}{|\vec{r} - \vec{r}'|} \qquad \text{(IV-4)}$$

and $\hat{a}_r$ is a unit vector in the direction of $\vec{r}$. We see from Eq. (IV-3) that contributions from the gradient term are ultimately negligible at points well removed from the scattering layer.

We shall consider scattering only in a small cone of angles about $\hat{a}_r$, so that the term in square brackets in Eq. (IV-3) is approximately equal to $\vec{A}_o$. Moreover, for the frequencies of interest, $\delta_e \cong -\frac{4\pi r_e}{k^2}\Delta N_e$, where r_e is the classical electron radius, and ΔN_e is the local departure of the electron density from its mean value. With these simplifications, Eq. (IV-3) becomes

$$\vec{E}_1(\vec{r}) = -r_e \int(3)\int \Delta N_e(\vec{r}')\vec{E}_o(\vec{r}')G(\vec{r},\vec{r}')d\vec{r}' \ . \qquad \text{(IV-5)}$$

We note that Eq. (IV-5) is linear in $\vec{E}_o(\vec{r})$.

The validity of this model depends on the accuracy with which $\vec{E}_1(\vec{r})$ represents the random component of $\vec{E}(\vec{r})$. Clearly, the approximation $\vec{E}(\vec{r}) \cong \vec{E}_o(\vec{r}) + \vec{E}_1(\vec{r})$ is valid only if the condition

$$\langle \vec{E}_1 \cdot E_1^* \rangle << A_o^2 \qquad \text{(IV-6)}$$

is satisfield. It is common experience, however, that the first Born approximation [Eq. (IV-5)] gives an accurate representation of the <u>random</u> component of $\vec{E}$ considerably beyond the few percent limit imposed by Eq. (IV-6). On the other hand, we know from theory and experiment that multiple-scattering effects must ultimately be considered. Nonetheless, our results can still be applied by using Uscinski's (1968) method. In

effect, the weak-scatter results are repeatedly integrated in a multi-layer model.

It remains to assign a statistical structure to ΔN_e and compute appropriate statistical descriptors for $\vec{E}_1$. We have used the transverse spectral decomposition of ΔN_e as was done recently by Lee and Harp (1969). In Appendix A we have compactly summarized the main properties of the spectral decomposition of complex homogeneous fields. The power of this approach is demonstrated by an application to the free-space propagation of random fields.

Before continuing, we note that the major difference between our own analysis and the extensive analyses of deWolf (1972), Tatarski (1971), Lee and Harp (1969), Strohbehn (1968), and others is that we have analyzed the quadrature components of the diffracted field rather than their amplitude and phase. To obtain amplitude and phase statistics we invoke a gaussian signal-statistics hypothesis. It happens that amplitude statistics are simply derived, while phase statistics are quite difficult because the statistics are generally non-Rician (Section V-B).

By comparison, most researchers in computing phase statistics have either accepted the Rytov solution (cf. Tatarski, 1971; Strohbehn, 1968), or they have made the small-phase approximation of equating the signal phase with the phase-quadrature component (cf. Lee and Harp, 1969). When the small-phase approximation is valid, all results agree, including those derived under the gaussian hypothesis.

B. The Transfer Function for a Weakly Scattering Irregularity Layer

Following Lee and Harp (1969) and deWolf (1972) we assume that $\Delta N_e(\vec{r})$ is statistically homogeneous (at least in the wide sense) in any transverse plane z = const. Hence, it admits a spectral decomposition of the form

$$\Delta N_e(\vec{r}) = \int\int \exp\{-i\vec{\kappa} \cdot \vec{\rho}\}\, d\xi(\vec{\kappa}:z) \qquad \text{(IV-7)}$$

where $\vec{r} = \vec{\rho} + \hat{a}_z z$, and $\hat{a}_z \cdot \vec{\rho} = 0$. We shall refer to $\xi(\vec{\kappa};z)$ as the transverse Fourier spectrum of $\Delta N_e(\vec{r})$.

We let $\vec{k} \cdot \vec{r} = \vec{k}_T \cdot \vec{\rho} + k_z z$, and consider a scattering layer of thickness L centered at the origin of coordinates. Substituting Eq. (IV-7) into Eq. (IV-5) and changing the order of integration gives the result

$$\vec{E}_1(\vec{r}) = - r_e \vec{E}_o(\vec{r}) \int\int\int_{-L/2}^{L/2} d\xi(\vec{\kappa};z')\exp\{-i\vec{\kappa} \cdot \vec{\rho}\}$$

$$\times \exp\{ik_z \Delta z\} \int\int_{-\infty}^{\infty} \frac{\exp\left\{-ik\left(\Delta\vec{\rho}^2 + \Delta z^2\right)^{1/2}\right\}}{\left(\Delta\vec{\rho}^2 + \Delta z^2\right)^{1/2}} \exp\{-i[(\vec{\kappa} + \vec{k}_T) \cdot \Delta\rho]\} d\Delta\vec{\rho}\, dz' \qquad \text{(IV-8)}$$

where $\Delta\vec{\rho} = \vec{\rho}' - \vec{\rho}$ and $\Delta z = z' - z$. The integration over $\Delta\vec{\rho}$ has been evaluated by deWolf (1972) as

$$-i\left(\frac{2\pi}{k}\right) \frac{\exp\{-ikg(\vec{\kappa};\vec{k}_T)|\Delta z|\}}{g(\vec{\kappa};\vec{k}_T)} \qquad \text{(IV-9)}$$

where

$$g(\vec{\kappa};\vec{k}_T) = \left[1 - (\vec{\kappa} + \vec{k}_T)^2/k^2\right]^{1/2} \qquad \text{(IV-10)}$$

By using this result, we can write Eq. (IV-4) in the form

$$\vec{E}_1(\vec{r}) = \vec{E}_o(\vec{r})\ \psi_z(\vec{\rho};\vec{k}) \tag{IV-11}$$

where

$$\psi_z(\vec{\rho};\vec{k}) = i\lambda r_e \iint \exp\{-i\vec{\kappa}\cdot\vec{\rho}\}\, d\psi_z(\vec{\kappa};\vec{k}) \tag{IV-12}$$

and

$$d\psi_z(\vec{\kappa};\vec{k}) = \int_{-L/2}^{L/2} d\xi(\vec{\kappa};z')\exp\{ik_z\Delta z\}\ \frac{\exp\{-ik\, g(\vec{\kappa};\vec{k}_T)|\Delta z|\}}{g(\vec{\kappa};\vec{k}_T)}\, dz' \ . \tag{IV-13}$$

We see from Eqs. (IV-11), (IV-12), and (IV-13) that $\vec{E}_1(\vec{r})$ is derived from $\vec{E}_o(\vec{r})$ by scalar multiplication with a complex random function $\psi_z(\vec{\rho};\vec{k})$ that admits a transverse spectral decomposition [Eq. (IV-12)] of the form discussed in Appendix A. It is worth noting here that the only difference between the Born solution and the Rytov solution is that the diffracted field takes the form $\vec{E}(\vec{r}) = E_o(\vec{r})\exp\{\psi_z(\vec{\rho};\vec{k})\}$ for the Rytov solution.

We shall characterize $\vec{E}_1(\vec{r})/\vec{E}_o(\vec{r})$ [Eq. (IV-11)] by the two-frequency correlation functions

$$R_{\psi_z}\left(\vec{\Delta\rho};f^{(\alpha)},f^{(\beta)}\right) \triangleq \left\langle \psi_z\left(\vec{\rho};\vec{k}^{(\alpha)}\right)\psi_z{}^*\left(\vec{\rho};\vec{k}^{(\beta)}\right)\right\rangle \tag{IV-14}$$

and

$$B_{\psi_z}\left(\vec{\Delta\rho};f^{(\alpha)},f^{(\beta)}\right) \triangleq \left\langle \psi_z\left(\vec{\rho};\vec{k}^{(\alpha)}\right)\psi_z\left(\vec{\rho};\vec{k}^{(\beta)}\right)\right\rangle \ . \tag{IV-15}$$

The wave vectors $\vec{k}^{(\alpha)}$ and $\vec{k}^{(\beta)}$ differ only in magnitude ($|\vec{k}| = k = 2\pi f/\lambda$). By using the orthogonal increments property of $d\xi$ (Appendix A), we can easily derive our main result:

$$\begin{Bmatrix} R_{\psi_z} \\ B_{\psi_z} \end{Bmatrix} = \pm\, r_e^2\, \lambda^{(\alpha)} \lambda^{(\beta)} \langle \Delta N_e^2 \rangle \iint \Phi_z \left(\vec{\kappa}; \vec{k}^{(\alpha)}, \vec{k}^{(\beta)} \right) \exp\{-i\vec{\kappa} \cdot \vec{\Delta\rho}\} \frac{d\vec{\kappa}}{(2\pi)^2} \qquad \text{(IV-16)}$$

where

$$\Phi_z\left(\vec{\kappa}; \vec{k}^{(\alpha)}, \vec{k}^{(\beta)} \right) = \int\int_{-L/2}^{L/2} \tilde{\Phi}(\vec{\kappa}; z', z'') \exp\left\{ i \left[k_z^{(\alpha)} \Delta z' \mp k_z^{(\beta)} \Delta z'' \right] \right\}$$

$$\times \frac{\exp\left\{ -i \left[k^{(\alpha)} g\left(\vec{\kappa}; \vec{k}^{(\alpha)} \right) |\Delta z'| \mp k^{(\beta)} g\left(\vec{\kappa}; \vec{k}^{(\beta)} \right) |\Delta z''| \right] \right\}}{g\left(\vec{\kappa}; \vec{k}^{(\alpha)} \right) g\left(\vec{\kappa}; \vec{k}^{(\beta)} \right)} dz' dz'' \qquad \text{(IV-17)}$$

The upper signs in Eqs. (IV-16) and (IV-17) are used for the R_{ψ_z} integral and the lower signs for the B_{ψ_z} integral. In Eq. (IV-17) $\tilde{\Phi}(\vec{\kappa}; z', z'')$ is the "transverse" spectral-density function for the irregularities. When $z' = z''$, $\tilde{\Phi}(\vec{\kappa}; z', z'')$ is purely real, non-negative, and symmetric.

Equation (IV-16) can be simplified by changing variables to $2\chi = z' + z''$ and $\eta = z' - z''$. We assume that

$$\tilde{\Phi}(\vec{\kappa}; z', z'') = \mu(\chi)\, \tilde{\Phi}(\kappa; \eta) \qquad \text{(IV-18)}$$

where

$$\mu(\chi) \cong \begin{cases} \mu(0) & |\chi| \leq L \\ 0 & |\chi| > L \end{cases} . \qquad \text{(IV-19)}$$

The result is

$$\tilde{\Phi}_z\left(\vec{\kappa};\vec{k}^{(\alpha)},\vec{k}^{(\beta)}\right) = \mu(0)\,\frac{\exp\left\{2izH\left(\vec{\kappa};\vec{k}^{(\alpha)},\vec{k}^{(\beta)}\right)\right\}}{g\left(\vec{\kappa};\vec{k}^{(\alpha)}\right)\,g\left(\vec{\kappa};\vec{k}^{(\beta)}\right)}$$

$$\times\left[\int_0^L \tilde{\Phi}(\vec{\kappa};\eta)\exp\left\{-i\eta H^*\left(\vec{\kappa};\vec{k}^{(\alpha)},\vec{k}^{(\beta)}\right)\right\}\operatorname{sinc}\left[\frac{1}{2}(L-\eta)H\left(\vec{\kappa};\vec{k}^{(\alpha)},\vec{k}^{(\beta)}\right)\right](L-\eta)\,d\eta\right.$$

$$\left.+\int_{-L}^{0} \tilde{\Phi}(\vec{\kappa};\eta)\exp\left\{-i\eta H^*\left(\vec{\kappa};\vec{k}^{(\alpha)},\vec{k}^{(\beta)}\right)\right\}\operatorname{sinc}\left[\frac{1}{2}(L+\eta)H\left(\vec{\kappa};\vec{k}^{(\alpha)},k^{(\beta)}\right)\right](L+\eta)\,d\eta\right] \qquad \text{(IV-20)}$$

where

$$H = \left[G^{(\alpha)} \mp G^{(\beta)}\right]/2, \qquad H^* = \left[G^{(\alpha)} \pm G^{(\beta)}\right]/2 \qquad \text{(IV-21), (IV-22)}$$

and

$$G^{(\beta)}_{(\alpha)} = k^{(\beta)}_{(\alpha)} \cos\theta\left[1 - g^{(\beta)}_{(\alpha)}\right] . \qquad \text{(IV-23)}$$

In the coordinate system of Figure IV-2

$$g' = \sec\theta g = \left[1 - \frac{\kappa_x^2 + \kappa_y^2}{(k\cos\theta)^2} - \frac{2\tan\theta(\kappa_x\cos\varphi + \kappa_y\sin\varphi)}{k\cos\theta}\right]^{1/2}. \quad \text{(IV-24)}$$

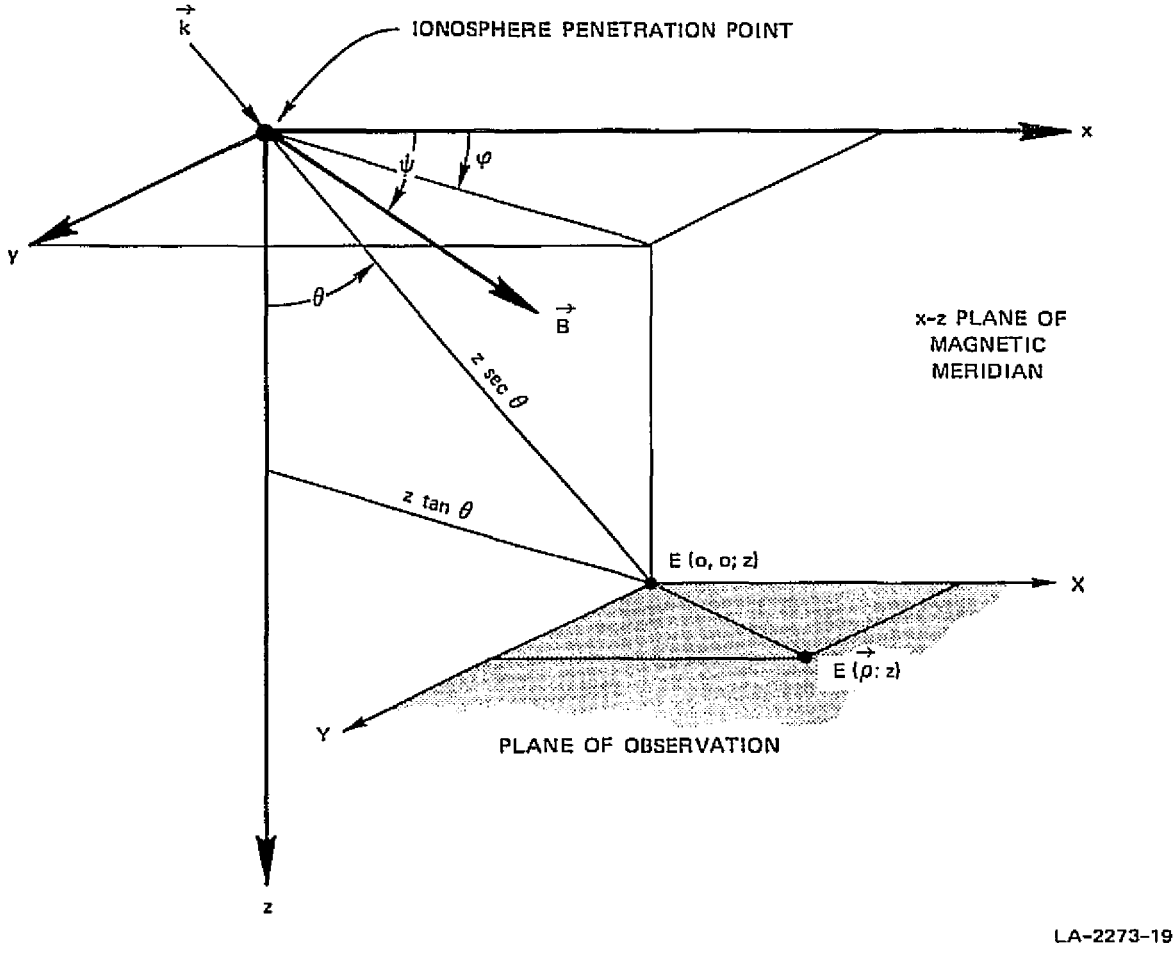

FIGURE IV-2 GEOMETRY FOR LAYERED-MEDIUM SCATTERING CALCULATIONS

A further simplification can be realized when $\underline{\Phi}(\vec{\kappa};\eta) \cong 0$ for $\eta > \eta_{max} << L$. We can then neglect the η-dependence in the sinc-function terms in Eq. (IV-20) and extend the limits of integration to infinity. The integral in Eq. (IV-20) then simplifies to

$$\operatorname{sinc}\left[\frac{L}{2}\,H\left(\vec{\kappa};\vec{k}^{(\alpha)},\vec{k}^{(\beta)}\right)\right] \;\Phi\left[\vec{\kappa},H^{*}\left(\vec{\kappa};\vec{k}^{(\alpha)},\vec{k}^{(\beta)}\right)\right] \qquad \text{(IV-25)}$$

where

$$\bar{\Phi}(\vec{\kappa},\,\kappa_z) = \int_{-\infty}^{\infty} \Phi(\kappa;\eta)\;\; \exp[i\eta\kappa_z]\,d\eta \;. \qquad \text{(IV-26)}$$

We note that in general the entire z dependence is contained in the first term of Eq. (IV-20).

To obtain some feeling for the physical meaning of these results consider the single-frequency case in which $f^{(\alpha)} = f^{(\beta)} = f$. Then, $H \equiv 0$ for the R_{ψ_z} integral, and it is independent of z. This result is expected because of the free-space results of Appendix A. With a suitable normalization, the correlation functions for the in-phase and phase-quadrature components are $\frac{1}{2}\,[\,1 + \mathrm{Re}\{B_{\psi_z}\}]$, respectively. In this formulation there is never a pure phase perturbation because propagation, which takes place continuously, acts to redistribute the phase perturbation as they occur [see Appendix A].

In the next subsection we shall specialize these results by introducing a specific spectral-density function appropriate to the ionosphere. We shall then present some simplifying approximations that are commonly employed and discuss their validity.

C. The Special Case of a Power-Law Spectral-Density Function

Satellite in-situ electron-density measurements reported by Dyson, McClure, and Hanson (1973) show that a power-law spectral-density function is a reasonably accurate analytic form for $\bar{\Phi}$. This is supported by the analysis of radio-star scintillation data by Cronyn (1970) and

Rufenach (1972). We have chosen (after Tatarski, 1971) the analytic form

$$\Phi(S^2) = 8\pi^3 \left(\frac{\Gamma(\gamma + 1/2)}{\sqrt{\pi}\,\Gamma(\gamma - 1)} \right) \alpha^3 a \; \frac{1}{\left[1 + (\alpha S)^2\right]^{\gamma + 1/2}} \qquad \text{(IV-27)}$$

where

$$S^2 = \left(B'(\Psi) \kappa_x^2 + \kappa_y^2 \right) + \kappa_z^2 B(\Psi) - 2\kappa_x \kappa_z C(\Psi) \qquad \text{(IV-28)}$$

$$B'(\Psi) = a^2 \cos \Psi + \sin^2 \Psi \qquad \text{(IV-29)}$$

$$C(\Psi) = (1 - a^2) \cos \Psi \sin \Psi \qquad \text{(IV-30)}$$

and

$$B(\Psi) = \cos^2 \Psi + a^2 \sin^2 \Psi \quad . \qquad \text{(IV-31)}$$

The angle Ψ is the angle to the principal irregularity axis. In the ionosphere it is the geomagnetic dip angle. The parameter a is the axial ratio ($a \geq 1$). The parameters α and γ are the irregularity scale and spectral index respectively. The spectral-density function [Eq. (IV-27)] is normalized so that

$$\int (3) \int \Phi(S^2) \; \frac{d\kappa_x}{2\pi} \; \frac{d\kappa_y}{2\pi} \; \frac{d\kappa_z}{2\pi} = 1 \quad . \qquad \text{(IV-32)}$$

The anisotropy was introduced, following Budden (1965), by performing a coordinate transformation of the isotropic spectral-density function (see Appendix D).

By substituting Eq. (IV-27) into Eqs. (IV-25) and (IV-16) and changing variables to $K_x\alpha$ and $K_y\alpha$ we obtain the result

$$\begin{Bmatrix} R_\psi \\ B_\psi \end{Bmatrix} = \pm \sigma_T^2 \sec\theta \left[8\pi^3 \left(\frac{\Gamma(\gamma + 1/2)}{\sqrt{\pi}\,\Gamma(\gamma - 1)} \right) a \frac{\alpha}{\kappa} \right]$$

$$\times \int\int_{(\vec{K}) \le \rho} \bar{\Phi}_z \left(\vec{K}; \vec{k}^{(\alpha)}, \vec{k}^{(\beta)} \right) \exp\{-\vec{K} \cdot \vec{\Delta\rho}\} \frac{d\vec{K}}{(2\pi)^2} \qquad \text{(IV-33)}$$

where

$$\sigma_T^2 = \mu(0)\, r_e^2\, \lambda^{(\alpha)}\lambda^{(\beta)} (L \sec\theta) \langle \Delta N_e^2 \rangle\, \kappa \qquad \text{(IV-34,}$$

and

$$\bar{\Phi}_z = \exp\left\{ 2iz(k\cos\theta) \left[H - \tan\theta (K_y \cos\varphi + K_y \sin\varphi)/\rho \left(\frac{1 \mp 1}{2} \right) \right] \right\}$$

$$\times \left\{ \frac{\operatorname{sinc}\left(\frac{L}{2} k \cos\theta\, H \right)}{g'^{(\alpha)}\, g'^{(\beta)}} \right\}$$

$$\times \frac{1}{[1 + S^2]^{\gamma + 1/2}} \,. \qquad \text{(IV-35)}$$

In the new coordinates,

$$S^2 = \left(B'(\Psi) K_x^2 + K_y^2 \right) + [H^*\rho]^2\, B(\Psi) - 2K_x H^*\rho C(\Psi) \qquad \text{(IV-36)}$$

and

$$g'^{(\alpha)}_{(\beta)} = \left[1 - \frac{\kappa_x^2 + \kappa_y^2}{\rho^2 (1 \mp \Delta k/k)^2} - 2 \tan\theta \, \frac{(\kappa_x \cos\varphi + \kappa_y \sin\varphi)}{\rho(1 \mp \Delta k/k)} \right]^{1/2} \qquad \text{(IV-37)}$$

where $\rho = \alpha\, k \cos\theta$. The parameters are summarized in Table IV-1.

The normalization factor μ is chosen so that $E_o^2 \sigma_T^2 / 2Z_o$ is the scattered power per unit area crossing a plane perpendicular to z [cf. Rino and Fremouw (1973)]. The linear κ_x, κ_y-term in Eq. (IV-35) was introduced to reference the calculations to the "line-of-sight" intercept in the z plane (see Figure IV-2), which is the natural reference point.

The parameter ρ is the ratio of the scale parameter α to the projected wavelength $\lambda \sec\theta$. If it is sufficiently large, we can apply the so-called Fresnel approximation

$$1 - g'^{(\alpha)}_{(\beta)} \cong \frac{\kappa_x^2 + \kappa_y^2 + \tan^2\theta (\kappa_x \cos\varphi + \kappa_y \sin\varphi)^2}{2\rho^2 (1 \mp \Delta k/k)} + \frac{\tan\theta \, (\kappa_x \cos\varphi + \kappa_y \sin\varphi)}{\rho(1 \mp \Delta k/k)} . \qquad \text{(IV-38)}$$

By using Eq. (IV-38) in Eq. (IV-23) and the equivalence $\Delta k/k = \Delta f/f$, we obtain the approximate forms

Table IV-1

PARAMETERS FOR COMPLEX-CORRELATION-FUNCTION FORMULAS

Parameters	Symbol	Comments
Wavelength(s)	$k; k^{(\alpha)}, k^{(\beta)}$	$k^{(\alpha)} = k - \Delta k$, $k^{(\beta)} = k + \Delta k$ $\left(\text{Note that } \frac{\Delta k}{k} = \frac{\Delta f}{f}.\right)$
RMS electron density	$\langle \Delta N_e^2 \rangle$	
Distance	z	Distance from ionosphere penetration point to receiver, or corrected distance for satellites
Axial ratio	a	Anisotropy parameter ($a \geq 1$)
Magnetic-field angle	Ψ	Geomagnetic dip angle (at ionosphere penetration point)
Scale size to wavelength parameter	ρ	$\rho \triangleq \alpha k \cos\theta$, where α is power-law spectral-density function scale factor
Spectral index	γ	($\gamma > 0$)
Incidence angles	θ, φ	Theta, θ, is the zenith angle at the ionosphere penetration point. Phi, φ, is the azimuth measured from the magnetic-meridian plane.
Layer thickness	L	Centered on origin of coordinates

$$H \cong \begin{cases} \dfrac{\kappa_x^2 + \kappa_y^2 + \tan^2\theta\,(\kappa_x \cos\varphi + \kappa_y \sin\varphi)^2}{2\rho^2} \; \dfrac{\Delta f/f}{1-(\Delta f/f)^2} & \text{for } R_\psi \\ \dfrac{\kappa_x^2 + \kappa_y^2 + \tan^2\theta\,(\kappa_x \cos\varphi + \kappa_y \sin\varphi)^2}{2\rho^2} \; \dfrac{1}{1-(\Delta f/f)^2} & \end{cases} \tag{IV-39}$$

$$+ \tan\theta \left[\frac{\kappa_x \cos\varphi + \kappa_y \sin\varphi}{\rho} \right] \qquad \text{for } B_\psi \; .$$

For H*, the opposite values are used for R_ψ and B_ψ [cf. Eqs. (IV-21) and (IV-22)].

When these approximations are valid, we obtain the "large ρ" form of Eq. (IV-35),

$$\Phi_z \cong \exp\left\{ iZ \left[\frac{\Delta f/f}{1-(\Delta f/f)^2} \; \frac{1}{1-(\Delta f/f)^2} \right] \left[\kappa_x^2 + \kappa_y^2 + \tan^2\theta(\kappa_x \cos\varphi + \kappa_y \sin\varphi)^2 \right] \right\}$$

$$\times \operatorname{sinc}\left[\frac{L}{2} (k \cos\theta) \right] \frac{1}{\left[1 + \left(B'(\Psi)\kappa_x^2 + \kappa_y^2 \right) + (H^*\rho)^2 B(\Psi) - 2\kappa_x (H^*\rho) C(\Psi) \right]^{\gamma + 1/2}} \tag{IV-40}$$

where

$$Z = \frac{\lambda z \sec\theta}{2\pi\, \sigma^2} \; . \tag{IV-41}$$

In Eq. (IV-40) $H^*\rho$ is negligible [see Eq. (IV-39)] for the B_ψ integral, and it is equal to $\tan\theta\,(\kappa_x \cos\varphi + \kappa_y \sin\varphi)$ for the R_ψ integral. The effect of the $H^*\rho$ terms is to distort the angular spectral-density function which, from Eq. (IV-35), is given as $\dfrac{1}{g^2[1 + s^2]^{\gamma + 1/2}}$.

In Figure IV-3 we have plotted $\log [1 + s^2]^{\gamma + 1/2}$ versus $\log (\kappa_x/\rho)$, with $\kappa_y = 0$, and s^2 given by Eq. (IV-36) with $a = 5$ and $\Psi = 45^\circ$. We set $\gamma = 1.5$, which is close to the value inferred from satellite measurements (Section IV-D). The straight lines have a slope of 4, which is the asymptote when the ρ-terms are neglected. We note that for the smaller ρ values, the departure from the asymptote is significant when κ/ρ is large. Numerical calculations show that σ_T^2 is underestimated by approximately 50% when $\rho = 1$, but it is within a few percent of its correct value when $\rho = 10$. Evidently Eq. (IV-40) is valid when ρ is greater than 10. Hence, in the remainder of our calculations the simplified form of Eq. (IV-35) will be used.

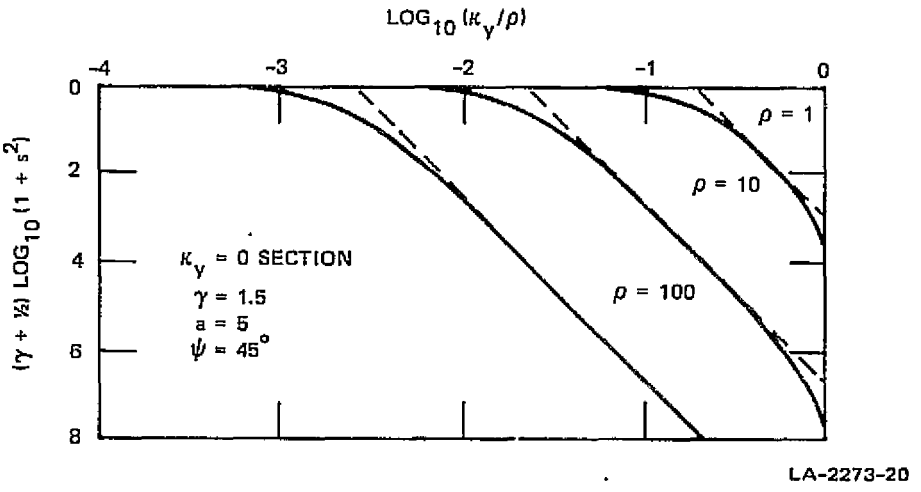

FIGURE IV-3 SPECTRAL-DENSITY-FUNCTION CROSS-SECTION PLOTS SHOWING THE EFFECT OF $H^*\rho$ TERMS IN EQ. (40)

D. Effects of Time-Varying Media

In almost all applications we measure time series that arise because the medium or the source or both are moving relative to the receiver. Moreover, the medium undergoes internal rearrangement, although we can usually neglect this effect. In Appendix B we have derived general formulas for converting two-dimensional spatial results to one-dimensional temporal spectra.

As an example, consider an in-situ measurement with a moving probe such that $v_z = 0$. The power spectrum derived from Eq. (IV-27) is then proportional to

$$\frac{1}{\left[1 + \frac{4\pi^2 \mathcal{I}^2}{v_y^2}\left(1 - \frac{v_x^2}{v_x^2 + B'(\Psi)v_y^2}\right)\right]^{\gamma - 1/2}} \qquad \text{(IV-42)}$$

The effective velocity is

$$v_y \left(1 - \frac{v_x^2}{v_x^2 + B'(\Psi)v_y^2}\right)^{-1/2}$$

which is approximately equal to v_y when $B'(\Psi)v_y^2 >> v_x^2$. However, since $B'(\Psi) >> 1$ for highly elongated irregularities when Ψ os not too large, the condition $B'(\Psi)$ 1 can be satisfied even if v_y and v_x are comparable in magnitude.

In a transmission experiment the potential observable is the complex voltage measured effectively at the antenna terminals. Since the angular width of the field spectrum is typically much narrower than the antenna beamwidth, however, the complex correlation functions are proportional to the $\vec{\Delta\rho} = 0$ terms in Eq. (IV-33) or the $\delta x = \delta y = 0$ terms in Eq. (B-4) of Appendix B. Spaced-receiver measurements then give the $\vec{\Delta\rho}$ dependence directly.

Unfortunately, the corresponding complex power (temporal) spectrum integrals for Eqs. (IV-35) or (IV-40) cannot be evaluated analytically. However, for normal incidence one can show that $\Phi_z(\mathcal{J})$ is proportional to

$$\exp\left\{ iZ \left[\frac{\Delta f/f}{1-(\Delta f/f)^2} \right] \left(\frac{2\pi\mathcal{J}}{v_y} \right)^2 \left(1 - \frac{v_x^2}{v_x^2 + v_y^2} \right) \right\}$$

$$\times \operatorname{sinc}\left[\left(\frac{\lambda L}{2\pi\alpha^2} \right) \left(\frac{2\pi\mathcal{J}}{v_y} \right)^2 \left(1 - \frac{v_x^2}{v_x^2 + v_y^2} \right) \right] \left[\frac{1}{1 + \alpha^2 \left(\frac{2\pi\mathcal{J}}{v_y} \right)^2 \left(1 - \frac{v_x^2}{v_x^2 + B'(\Psi) v_y^2} \right)} \right]^{\gamma}$$

$\times$ correction factor. (IV-43)

In Eqs. (IV-42) and (IV-43) we have used "$\mathcal{J}$" for temporal frequency to avoid confusion with the RF frequency f. The correction factor will exhibit a weak temporal-frequency (f) dependence.

We first note that the effective $\mathcal{J}$-index in Eq. (IV-43) differs by unity from that inferred from Eq. (IV-42) $\left[\mathcal{J}^{-(2\gamma - 1)} \text{ vs. } \mathcal{J}^{-2\gamma} \right]$. This has been pointed out by Cronyn (1970). Dyson et al. (1973) found an $\mathcal{J}^{-1.9}$ frequency dependence from their in-situ measurements. Hence, from Eq. (IV-42), $\gamma = 1.45$, which is one-half the $\mathcal{J}$ index we would observe by Fourier-analyzing the temporal fluctuations of the diffracted signal. One must keep in mind, however, that there is no simple relation such as Eq. (IV-42) for interpreting complex temporal-frequency spectra that include the Z-dependent terms.

On the other hand, the first-order moments are unaffected by the "scan" because they are proportional to integrals over all temporal frequencies. It is easy to see from Eq. (B-4) that the results are identical to those obtained by integrating over all spatial frequencies. Hence, the formulas

$$\sigma_x^2 = \sigma_T^2 \sec\theta \frac{1}{2}\left[1 + \mathrm{Re}\{B_\psi(0;f)\}\right] \tag{IV-44}$$

$$\sigma_y^2 = \sigma_T^2 \sec\theta - \sigma_x^2 \tag{IV-45}$$

and

$$C_{xy} = \frac{1}{2}\sigma_T^2 \sec\theta \, \mathrm{Im}\{B_\psi(0;f)\} \tag{IV-46}$$

which were used in Section III correctly predict the variance of the in-phase and phase quadrature components of the signal and their covariance.

E. Method of Numerical Computation

The results presented in Section IV-C give the spatial and radio-frequency or wavelength dependences of the diffracted field from a weakly irregularity layer. The spatial dependence is derived from a two-dimensional Fourier transform [Eq. (IV-33)]. However, in the remainder of this report we shall consider only the $\vec{\Delta\rho} = 0$ term. In Section IV-C we showed that these integrals are generally adequate for single-receiver measurements.

Hence, the results that we shall be interested in demand an integration of Φ_z [Eq. (IV-35)] over all spatial frequencies for which $g'^{(\alpha)}$ and $g'^{(\beta)}$ [Eq. (IV-37)] is real. Note that, in general, four integrations

must be performed to obtain $\mathrm{Re}\{R_\psi\}$, $\mathcal{Im}\{R_\psi\}$, $\mathrm{Re}\{B_\psi\}$, and $\mathcal{Im}\{B_\psi\}$. Moreover, whenever the Z term is finite (that is, when $H \neq 0$), the integrand oscillates. Indeed, the integrals are of the most difficult type to evaluate.

The large ρ approximations are of some help, but they do not eliminate the oscillation problem. Integrating over the polar coordinates $K_x = K \cos \bar{\Phi}$ and $K_y = K \sin \bar{\Phi}$, however, does simplify the integration considerably. The formulas that we have programmed for machine integration can be summarized as

$$\left\{ \begin{matrix} R_\psi \\ B_\psi \end{matrix} \right\} = \frac{\int_0^{K_m} K F(K) dK}{R_\psi \Big|_{Z=0}} \tag{IV-47}$$

where

$$F(K) = \int_0^{2\pi} \exp\left\{ iZ \begin{bmatrix} F_R \\ F_B \end{bmatrix} K^2 [1 + \tan^2\theta \cos^2(\bar{\Phi} - \phi)] \right\}$$

$$\times \operatorname{sinc}\left\{ \pounds \begin{bmatrix} F_R \\ F_B \end{bmatrix} K^2 [1 + \tan^2\theta \cos^2(\bar{\Phi} - \phi)] + K\left(\frac{L}{2\alpha}\right) \tan\theta \cos(\bar{\Phi} - \phi) \left[\frac{1 \mp 1}{2}\right] \right\}$$

$$\times \left[1 + K^2 \left(B'(\Psi) \cos^2 \bar{\Phi} + \sin^2 \bar{\Phi} \right) + [H*\rho]^2 B(\Psi) - [H*\rho]^2 K \cos\bar{\Phi}\, C(\Psi) \right]^{-(\gamma + 1/2)} d\bar{\Phi} \tag{IV-48}$$

$$\pounds = \frac{\lambda L \sec\theta}{2\pi\alpha^2} \tag{IV-49}$$

$$F_R = \frac{\Delta f/f}{1 - (\Delta f/f)^2} \qquad \text{(IV-50)}$$

$$F_B = \frac{1}{1 - (\Delta f/f)^2} \qquad \text{(IV-51)}$$

$$[H^*\rho] \cong \begin{cases} K \tan\theta \cos(\bar{\varphi} - \phi) & \text{for } R_\psi \\ 0 & \text{for } B_\psi \end{cases} \qquad \text{(IV-52)}$$

No further simplification is justified unless the results are restricted to normal incidence. In that special case both the Z and $\mathcal{L}$-dependent terms in Eq. (IV-48) are $\bar{\varphi}$-independent. Hence, the $\bar{\varphi}$-integration is simplified considerably. The argument is a smooth, slowly varying function of $\bar{\varphi}$, and almost any numerical integration scheme will work. To evaluate the Z-dependent integral it was necessary to use an adaptive Simpson rule (see for example, Lyness, 1970). Basically, the adaptive methods vary the mesh size according to how fast the integrand is changing.

Finally, if the $\mathcal{L}$-dependent term is ignored, and the restriction to normal incidence is retained, it is possible to obtain a series solution involving Legendre functions and eliptic integrals that can be evaluated with sufficient accuracy by approximate formulas. The results, which are easily programmed for machine computations, are summarized in Appendix C.

These results show that the most troublesome factors result from oblique incidence, which, unfortunately, cannot be ignored. Rino and Fremouw (1973) presented a general formula that allowed oblique

incidence. However, in that formula the κ_z term of the spectral density function was set equal to zero. We see from our present results that this is valid only for normal incidence, when the $[H^*\rho]$ terms can be neglected.

However, the error affects only the R_ψ integral [cf. Eq. (IV-52)], so the formula for B given by Rino and Fremouw (1973) is correct. The $[H^*\rho]$ terms affect σ_T^2 through $\varkappa$ in Eq. (IV-34). Hence, the incidence-angle dependence of σ_T^2 is in general somewhat more complicated than a sec θ variation. It could be important, for example, if one were to predict or evaluate the S_4^2 variation for an orbiting satellite.

In the next subsection we present representative results derived by numerically integrating Eq. (IV-47). Some additional calculations will be presented in Section V.

F. Discussion and Examples

To characterize the statistics of a plane-wave field diffracted by a weakly scattering irregularity layer, we have computed the complex covariance functions $R_{\psi_z}\left(\vec{\Delta\rho};f^{(\alpha)},f^{(\beta)}\right)$ and $B_{\psi_z}\left(\vec{\Delta\rho};f^{(\alpha)},f^{(\beta)}\right)$ as defined by Eqs. (IV-14) and (IV-15). The $\Delta\rho$ dependence is given by a two-dimensional Fourier transform [Eq. (IV-16)], and we have considered only the $\vec{\Delta\rho} = 0$ correlations.

The general results depend explicitly on each parameter in Table IV-1. However, the approximate results [Eqs. (IV-40), (IV-41)] show that the ratio of the Fresnel-zone area $\left(\frac{2\lambda z \sec\theta}{\pi}\right)$ to the transverse scale parameter a^2, which we have denoted by Z, is fundamental. Its value determines the degree to which propagation has altered the structure of the field from what it was in the vicinity of the scattering layer.

Indeed, a general characterization of the statistics can be made in terms of Z. Consider that, independent of all other parameters,

$\mathrm{Re}\{B_\psi\}$ is negative and near or equal to its maximum absolute value of unity when Z = o. Moreover, $\mathrm{Im}\{B_\psi\} = \mathrm{Im}\{R_\psi\} = 0$ when Z = 0. Now, as Z increases from zero to infinity, $\mathrm{Re}\{B_\psi\}$ tends to zero, while $\mathrm{Im}\{B_\psi\}$ first becomes more negative and then tends to zero.

The behavior of $\mathrm{Re}\{R_\psi\}$ depends on Δf (we still assume that $\vec{\Delta\rho} = 0$). When $\Delta f = 0$, $\mathrm{Re}(R_\psi\}$ is independent of Z and equal to unity. When Δf is finite, $\mathrm{Re}\{R_\psi\}$ decreases from unity to zero as Z varies from zero to infinity. Similarly, $\mathrm{Im}\{R_\psi\}$ is zero when $\Delta f = 0$, and for finite Δf it varies from zero to a positive maximum and then decays to zero again as Z varies from zero to infinity.

To apply these results, we let the diffracted field at some frequency f be represented by E and E′ at some other frequency f′. It then follows from Eq. (IV-33) that

$$R_{xx} \triangleq \langle XX' \rangle - \langle X \rangle \langle X' \rangle = \frac{1}{2}\sigma_T^2 \sec\theta[\mathrm{Re}\{R_\psi\} + \mathrm{Re}\{B_\psi\}] \qquad \text{(IV-53)}$$

$$R_{yy} \triangleq \langle YY' \rangle - \langle Y \rangle \langle Y' \rangle = \frac{1}{2}\sigma_T^2 \sec\theta[\mathrm{Re}\{R_\psi\} - \mathrm{Re}\{B_\psi\}] \qquad \text{(IV-54)}$$

$$R_{xy} \triangleq \langle XY' \rangle - \langle X \rangle \langle Y' \rangle = \frac{1}{2}\sigma_T^2 \sec\theta[\mathrm{Im}\{R_\psi\} - \mathrm{Im}\{B_\psi\}] \qquad \text{(IV-55)}$$

and

$$R_{yx} \triangleq \langle X'Y \rangle - \langle X' \rangle \langle Y \rangle = -\frac{1}{2}\sigma_T^2 \sec\theta[\mathrm{Im}\{B_\psi\} + \mathrm{Im}\{B_\psi\}] \qquad \text{(IV-56)}$$

where X and Y denote the real and imaginary parts of the field. These formulas are simply generalizations of Eqs. (IV-44), (IV-45), and (IV-46). Indeed, when f = f′, $R_{xx} = \sigma_x^2$, $R_{yy} = \sigma_y^2$, and $R_{xy} = R_{yx} = C_{xy}$.

Now, from the limiting behavior we have just described, it follows that when Z is sufficiently small, $R_{yy} >> R_{xx}$, and both R_{xy} and R_{yx} are near zero. When $f = f'$, this condition becomes $\sigma_y^2 >> \sigma_x^2$; that is, the scattered power is nearly in phase quadrature with the undeviated component. In Rino and Fremouw (1973) this condition characterized the "near zone." When Z is sufficiently large, R_{yy} and R_{xx} are nearly equal, although when Δf is finite the limiting value becomes smaller and smaller as Z increases. When $\Delta f = 0$, $\sigma_x^2 \cong \sigma_y^2 \cong \frac{1}{2}\sigma_T^2 \sec\theta$. This behavior characterized the "far zone" in Rino and Fremouw (1973).

All parameters in our channel model (Table IV-1) that can be varied independently of Z will only affect the rate at which we move from near-zone scattering to far-zone scattering as Z is increased from zero, to infinity. We have illustrated this below by using the equation presented in Section IV-E.

1. Normal-Incidence Computations with $\Delta f = 0$

To evaluate Eq. (IV-48), we must specify the axial ratio a, the dip angle Ψ, a layer thickness parameter $\mathfrak{L}$, the spectral index γ, and the incidence angles θ, φ as well as Δf [Eqs. (IV-47) through (IV-52)]. When θ is finite, it is also necessary to specify the ratio $L/2\alpha$ [Eq. (IV-48)]. However, to start with we shall consider only the normal-incidence single-frequency correlations for which $\Delta f = \theta = \varphi = 0$.

In Figure IV-4 we have illustrated the effect of the "layer-smearing" $\mathfrak{L}$-dependent factor in Eq. (IV-48). The dashed line is for zero layer thickness, and the solid line is for conditions we expect to be typical of ionospheric scattering. The effect of finite layer thickness is confined to the near zone. It acts primarily to make σ_x^2 finite when $Z = 0$.

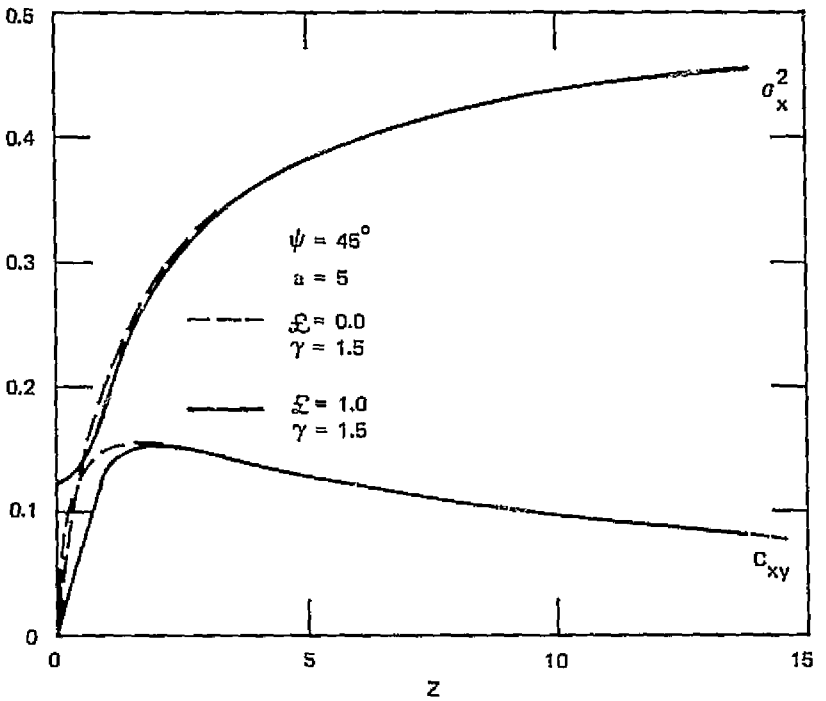

LA-2273-21

FIGURE IV-4 PLOTS OF σ_x^2 AND C_{xy} SHOWING EFFECT OF FINITE LAYER THICKNESS

In Figure IV-5 we show the effect of varying the axial ratio a. We see that as a increases, the convergence to far-zone conditions becomes slower. We expect this, since increasing a effectively compresses the spectrum toward the lower spatial frequencies. Hence, Z must be comparatively larger before propagation can have an impact. Evidently we could produce the same effect by increasing the spectral index γ. This is verified in Figure IV-6, where we have plotted σ_x^2 as a function of Z for different values of the spectral index γ. Varying the incidence angles (θ, φ) has a similar effect, although the details are more complicated. Because of the increased complexity of the computation, however, we have not presented numerical results for oblique incidence.

2. Coherence Bandwidth

If two monochromatic signals at frequencies f and f′ are transmitted through the ionosphere and the received complex signals

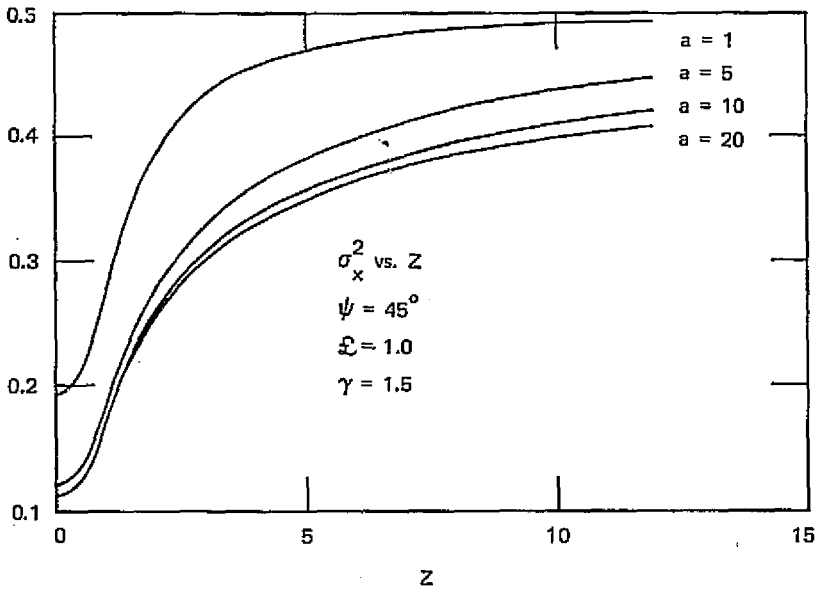

FIGURE IV-5 FAMILY OF σ_x^2 vs. Z CURVES SHOWING EFFECT OF ANISOTROPY

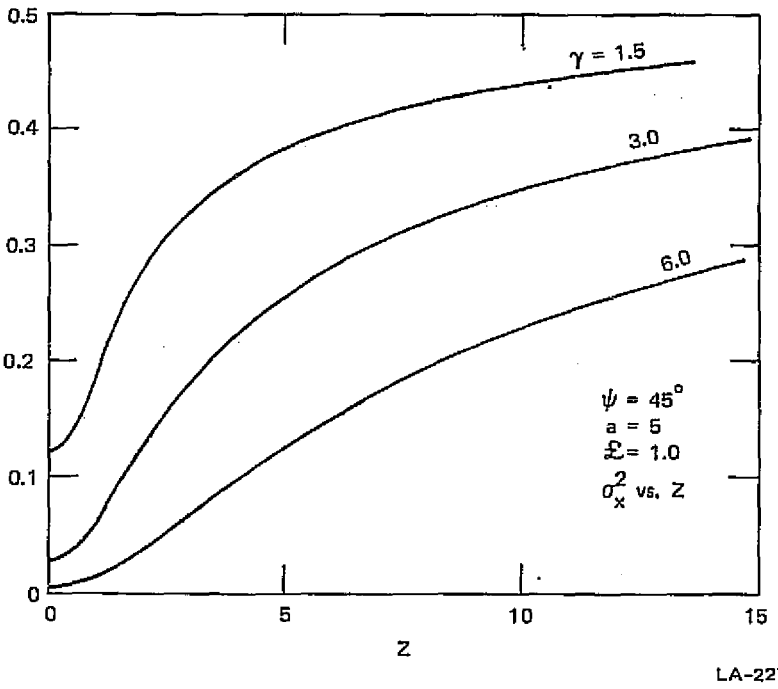

FIGURE IV-6 FAMILY OF σ_x^2 vs. Z CURVES SHOWING EFFECT OF POWER-LAW SPECTRAL INDEX

are cross-correlated, one measure of coherence bandwidth is given by $|\langle E\, E'^{*}\rangle|$. We do not choose to subtract the mean signal values, since one normally processes the complete signal.

From Eq. (IV-33) it follows that

$$\langle E\, E'^{*}\rangle = \langle E\rangle\, \langle E'^{*}\rangle + \sigma_T^2 \sec\theta\, R_{\psi_Z}(\Delta f, f) \quad . \qquad \text{(IV-57)}$$

However, if Δf is not too large, from Eq. (IV-34) it follows that

$$\langle E\, E'^{*}\rangle \cong 1 + \sigma_T^2 \sec\theta \left[R_{\psi_Z}(\Delta f, f) - 1 \right] \quad . \qquad \text{(IV-58)}$$

Hence, we see that coherence bandwidth cannot be specified independent of the scattering intensity.

Nonetheless, the Δf frequency dependence is contained in the covariance function R_{ψ_Z}. In Figure IV-7 we have plotted $|R_{\psi_Z}|$ as a function of $\Delta f/f$ for two different values of Z. As we should expect from the discussion at the beginning of this subsection, the results depend critically on the value of Z. However, since Z itself is frequency-dependent, the curves in Figure IV-7 are not universal. As the center frequency, f, is increased, Z decreases if all other parameters are held constant.

The implication is that for a given value of σ_T^2, the coherence bandwidth will be larger at a higher frequency than at a lower frequency. In Section V we shall calculate the two-frequency correlation function for intensity for comparison.

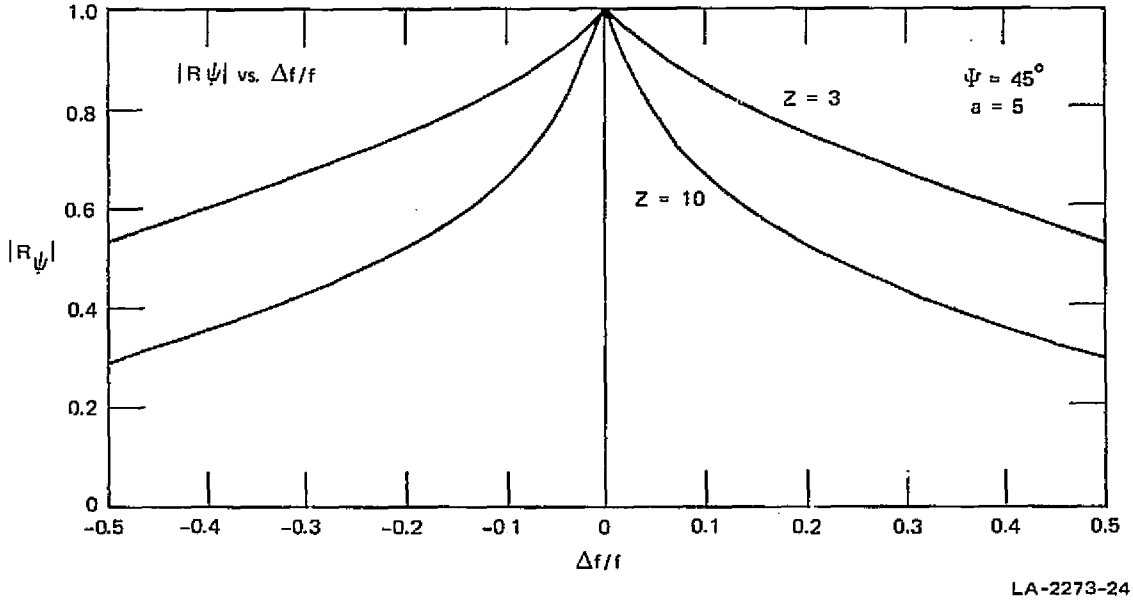

FIGURE IV-7 COHERENCE BANDWIDTH CURVES FOR COMPLEX-FIELD RANDOM COMPONENT

V APPLICATIONS

In Section IV we derived general formulas for the complex correlations that characterize a plane-wave field diffracted by a weakly scattering irregularity layer. We first calculated the time-invariant correlations $\langle E_z(\vec{\rho};f)E_z^*(\vec{\rho};f')\rangle$ and $\langle E_z(\vec{\rho};f)E_z(\vec{\rho}';f')\rangle$. We then considered the generalizations that allow for time variations (see Appendix B).

Hence, the most general observable is a time function with position and frequency dependences--say, $V_t(\vec{\rho};f) = X_t(\vec{\rho};f) + iY_t(\vec{\rho};f)$. For notational simplicity we have suppressed the distance parameter z. The position and frequency dependences can, in principle, be verified by spaced-receiver measurements with multifrequency transmissions. However, in most experiments only amplitude or intensity is available for each independent position-frequency measurement. For this reason, intensity statistics are most important for channel diagnostics.

In this section we shall apply the results of Section IV together with the gaussian signal-statistics hypothesis to derive the second-order moments of intensity. We shall also discuss the method of making a similar computation for phase statistics.

A. Intensity Statistics for Gaussian Fields

The observable of interest here is the intensity of a complex gaussian random field. Note that in the theory of stochastic processes, a random field is simply a function parameterized by one or more variables. The height of an ocean surface is an example. In our case we have a complex function of position, frequency, and time. The power of the gaussian hypothesis lies with the fact that the joint statistics of X and Y

depend only on the complex correlation functions calculated in Section IV or their generalizations derived in Appendix B.

In what follows we assume that the observed field is gaussian and normalized to unity average power. Recall that $\sigma^2 = \sigma_R^2 + \sigma_I^2$ can then be interpreted as the fraction of the incident power that is scattered. We let $I \triangleq VV^*$. A primed dependent variable will imply that it is evaluated with the independent variables $\vec{\rho}'$, f', and t'. In Appendix E we show that

$$\langle II' \rangle - \langle I \rangle^2 = 2\sigma^2(1 - \sigma^2)[\mathrm{Re}\{R\} + |B| \cos 2(\zeta - \phi)] + \sigma^4[|R|^2 + |B|^2] \qquad \text{(V-1)}$$

where R and B are given by Eq. (IV-33) or Eq. (B-4). We have also used the definitions $\tan 2\zeta = \mathrm{Im}\{B\}/\mathrm{Re}\{B\}$ and $\tan \phi = \langle Y \rangle / \langle X \rangle$. We note that for interpreting most experiments, ϕ can be set equal to zero. That is, the coherent component is the phase reference.

When ϕ is equal to zero, the term in square brackets reduces to the correlation of the real part of V, R_{xx} [cf. Eq. (IV-53)]. Hence, when $\sigma^2 \ll 1$, the quadratic terms in σ^2 can be neglected, and Eq. (V-1) reduces to

$$\langle II' \rangle - \langle I \rangle^2 \cong 2\sigma^2 R_{xx} \quad . \qquad \text{(V-2)}$$

This result can be derived directly by equating the amplitude perturbation with the in-phase signal component.

The Fourier transform of Eq. (V-1) or Eq. (V-2) gives (in expectation) the power spectrum of the intensity fluctuation if $I = I'$, or the co-spectrum if spaced receiver and/or two-frequency correlations are employed. The approximate form given in Eq. (V-2) has been used extensively for data

interpretation [see for example, Cronyn (1970) and Rufenach (1972)], although even then the interpretation is not simple [see Section IV-D].

We also note that when $I = I'$, Eq. (V-1) reduces to the formula for the S_4 scintillation index. Indeed, for that special case, $R \equiv 1$, and Eq. (V-1) becomes identical to the formula given in Rino and Fremouw (1973) that was used in Section III [cf. Eq. (III-11)]. In the simplest case, Eq. (V-1) gives the temporal structure of the signal fades whose statistics we analyzed in Section III. The formula is, however, more general since it gives the spatial and frequency dependencies as well.

To summarize, in Section III we discussed the method of computing the first-order amplitude statistics of a complex field. In Section IV we computed the complex second moments of the field. Finally, in this section we have made use of the fundamental property of gaussian fields--namely, that the complete statistical structure of the field can be determined from the complex covariances R and B.

Before presenting some examples derived from Eq. (V-1), we emphasize that in general, R and B depend on $\vec{\Delta\rho} = \vec{\rho} - \vec{\rho}'$, $f = [f + f']/2$, $\Delta f = f - f'$, and $\delta t = t - t'$. In general, there is a more complicated dependence on δt which we have ignored by assuming "frozen fields" [Appendix B]. When $\vec{\Delta\rho} = \Delta f = 0$, the Fourier transform of Eq. (V-1) gives the power spectrum of the intensity fluctuations. The width of this power spectrum is a useful measure of the fading rate, which is fundamental for designing receivers.

Unfortunately, while the statistics of any measurable quantity can in principle be computed from R and B, other results are not as simple as Eq. (V-1). Phase statistics will be discussed in Section V-B.

1. The Wavelength (Frequency) Dependence of S_4

Since the S_4 scintillation index is the most commonly used measure of scintillation activity, its frequency dependence is easily

measured. We first note that $\sigma^2 \propto \lambda^2$. Hence, in the S_4 scintillation-index formula it is convenient to replace σ^2 by $\sigma'^2\lambda^2$ where $\sigma'^2 \triangleq \sigma^2/\lambda^2$. We can think of σ'^2 as the coherence ratio for $\lambda = 1$ m. Recall that for unity incident intensity, σ^2 can be interpreted as the fraction of the incident energy (or power) that is randomized.

Similarly, from Eqs. (IV-41) and (IV-49), we see that Z and $\mathfrak{L}$ are proportional to λ. Hence, they contain the entire wavelength dependence of B_ψ, and therefore, the remaining wavelength dependence of $S_4[R_\psi \equiv 1$ when $\Delta f = 0]$. We define $Z' = Z/\lambda$ and $\mathfrak{L}' = \mathfrak{L}/\lambda$ in a manner analogous to the definition of σ'.

In Figure V-1 we have plotted the logarithm of S_4 against the logarithm of λ for different values of σ'^2 for a power-law spectral-density function with $\gamma = 1.5$. The curves show a decreasing slope with increasing S_4. Moreover, the results show the rate of decrease of the slope to be largest for the largest values of σ^2. Ultimately, the slope becomes negative. However, the theory has not been validated for strong scattering conditions.

Aarons, Allen, and Elkins (1967) define a spectral index for scintillation as

$$\eta = \frac{\log(S_4/S_4')}{\log(\lambda/\lambda')} \quad . \tag{V-3}$$

Actually, their definition is in terms of frequency rather than wavelength, which changes the sign of η. That is, Eq. (V-3) implies a relation of the form $S \propto \lambda^\eta$ or $S \propto f^{-\eta}$ depending on whether frequency or wavelength is used.

Aarons, Allen, and Elkins (1967) report the results of radio-star scintillation observations at four frequencies spaced from HF to UHF. They report that η decreases from ~2 for small index values through zero

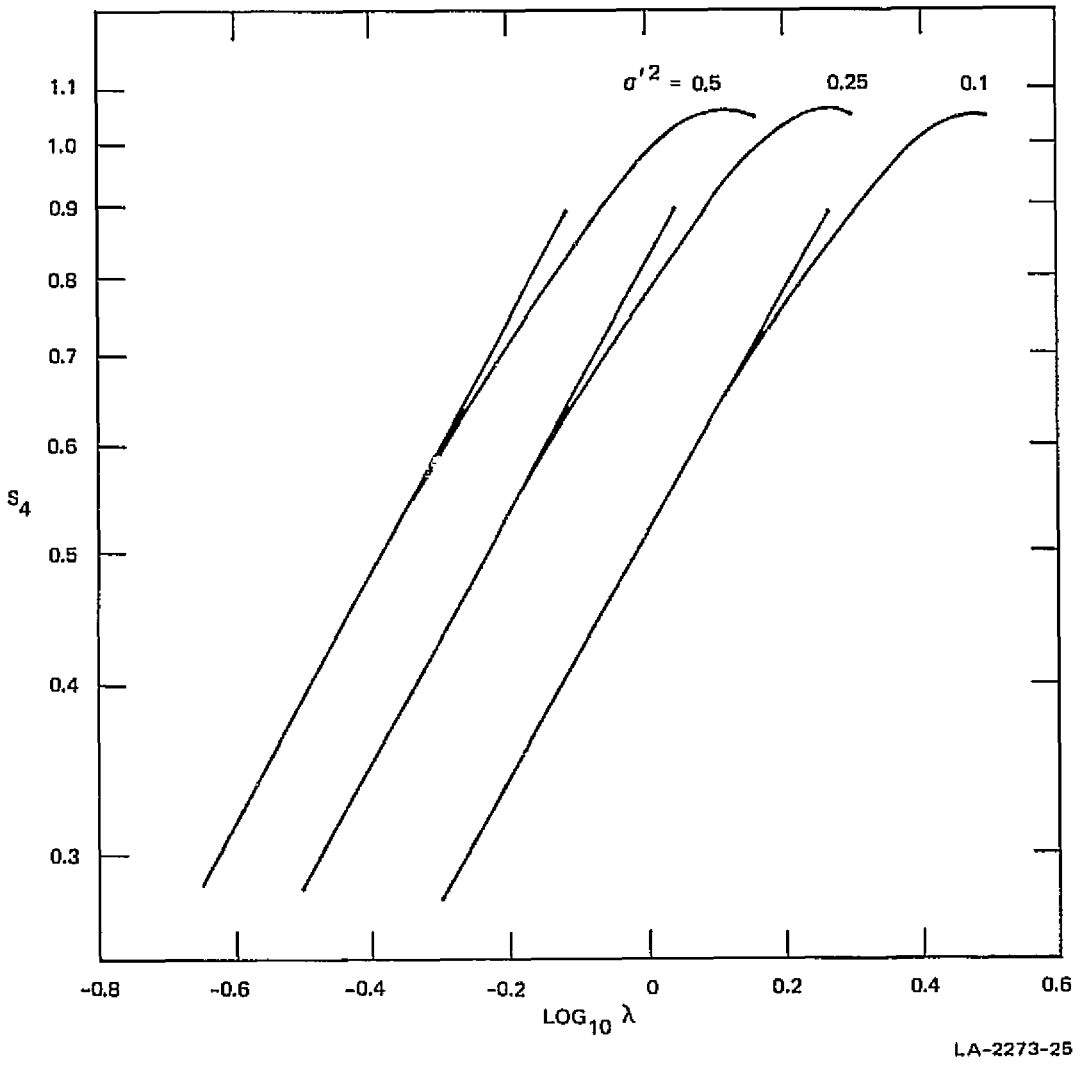

FIGURE V-1 WAVELENGTH DEPENDENCE OF S_4 SCINTILLATION INDEX

for large S_4 values just as the curves in Figure V-1 predict. It should be pointed out, however, that extrapolating the results to L and S bands does not account for the S_4 indices that have been observed at those frequencies. Evidently, the spectral shape deviates from the power-law model in the small-structure region.

2. Two-Frequency Correlation Function for Intensity

As a final example, we have computed from Eq. (V-1) the two-frequency measurement correlation function for intensity. The results are shown in Figures V-2(a) and (b). The curves are normalized to unity at $\Delta f = 0$.

In Figure V-2(a) we show curves corresponding to the parameters used in Figure IV-7. These curves were computed with $\sigma^2 = 0.25$. We see the same general property--namely, that the signals decorrelate faster for larger Z values. Moreover, E decorrelates faster than I. In Figure V-2(b) we have repeated the computation with $\sigma^2 = 0.5$ to show that the intensity decorrelate faster as the level of activity increases.

B. The Method of Computing Phase Statistics

To conclude this section, we discuss the method of computing phase statistics. Consider a complex gaussian random process evaluated at two "points" giving $\underset{\sim}{X} = (X, Y, X', Y')$ as a data vector. The covariance matrix for $\underset{\sim}{X}$ is

$$\Lambda \triangleq \left\langle \left(\underset{\sim}{X}^T - \langle \underset{\sim}{X}^T \rangle \right) \left(\underset{\sim}{X} - \langle \underset{\sim}{X} \rangle \right) \right\rangle = \begin{bmatrix} \sigma_x^2 & C_{xy} & R_{xx} & R_{xy} \\ C_{xy} & \sigma_x^2 & R_{yx} & R_{yy} \\ R_{xx} & R_{xy} & \sigma_y^2 & C_{xy} \\ R_{xy} & R_{yy} & C_{xy} & \sigma_y^2 \end{bmatrix} \qquad \text{(V-4)}$$

where T denotes transpose. The joint probability-density function for X, Y, X′, and Y′ can be written as

$$P_{\underset{\sim}{X}}(X,Y,X',Y') = \frac{1}{4\pi^2 |\Lambda|^{1/2}} \exp\left\{ - \left(\tilde{\underset{\sim}{X}}^T - \langle \tilde{\underset{\sim}{X}}^T \rangle \right) \Lambda^{-1} \left(\tilde{\underset{\sim}{X}} - \langle \tilde{\underset{\sim}{X}} \rangle \right) \right\} \quad . \qquad \text{(V-5)}$$

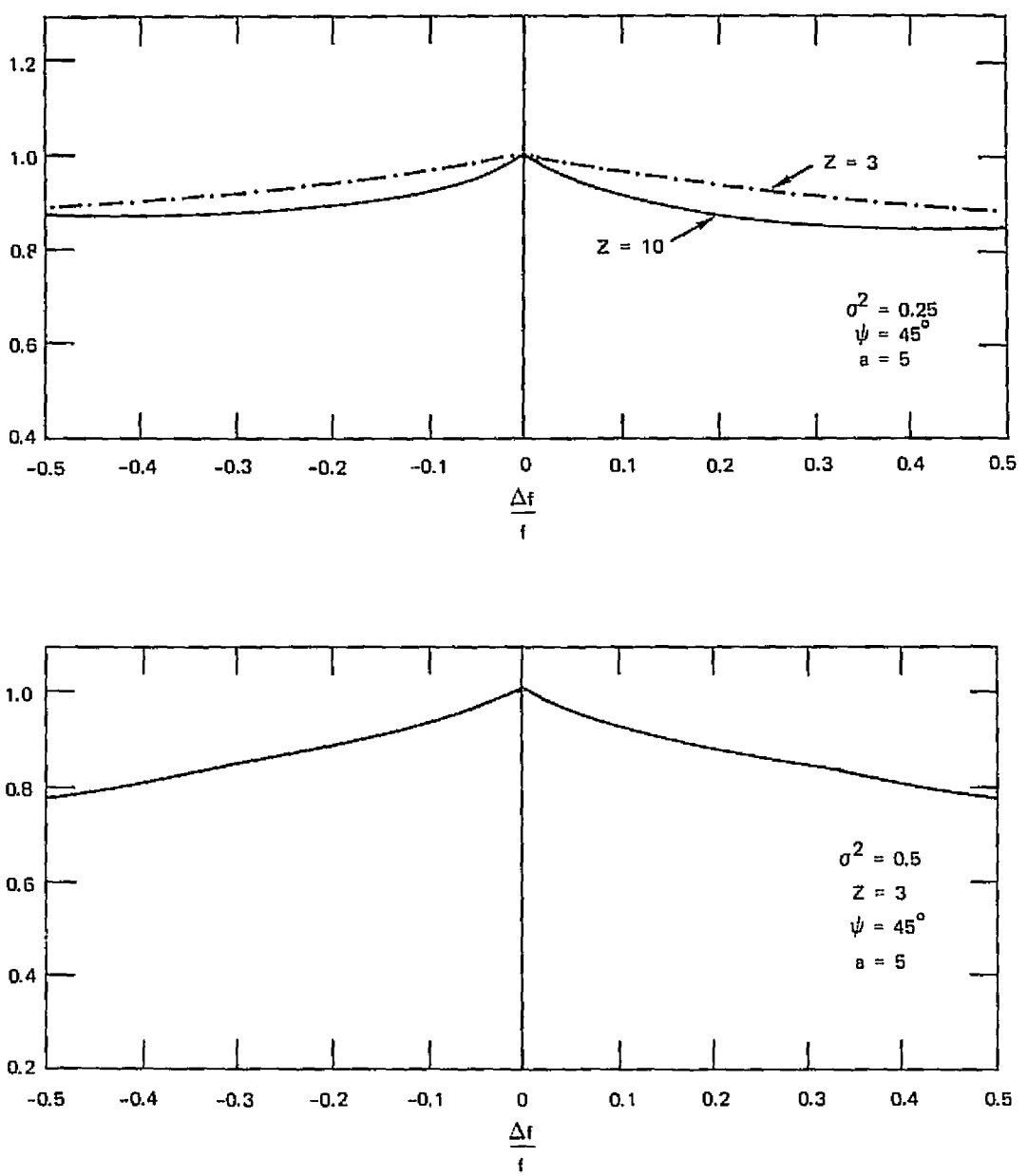

FIGURE V-2 TWO-FREQUENCY CORRELATION FUNCTION FOR INTENSITY

These results are well known; they are discussed in any basic statistics textbook. By a simple change of variables, it is easy to show that

$$P(A,\phi,A',\phi') = A\,A'\,P_{\underset{\sim}{X}}(A\cos\phi,\ A\sin\phi,\ A'\cos\phi',A'\sin\phi') \ . \quad \text{(V-6)}$$

The joint probability-density function for ϕ and ϕ' is then given formally as

$$P(\phi,\phi') = \int_0^\infty \int_0^\infty P(A,\phi,A',\phi')\,dA\,dA' \quad . \quad \text{(V-7)}$$

Finally, from Eq. (V-7) it follows that

$$\langle \phi\ \phi' \rangle = \iint \phi\ \phi' P(\phi,\phi')\,d\phi\,d\phi' \quad . \quad \text{(V-8)}$$

For the special case of Rician statistics, it is possible to obtain an analytic form for $P(\phi,\phi')$. [See, for example, Davenport and Root, 1958, pp. 161-165.] However, we have shown that one cannot assume that the quadrature signal components are of equal intensity and uncorrelated. At the present time it is not known whether similar results can be obtained for general gaussian statistics. The formal results are presented here mainly to illustrate further the technique of combining the gaussian-statistics hypothesis with the results of Section V to calculate various measurable quantities.

VI SUMMARY, DISCUSSION, AND RECOMMENDATIONS

Through the research conducted under this contract we have (1) evaluated a gaussian signal-statistics hypothesis for ionospheric scintillation, (2) reformulated the diffraction theory in terms of quantities that can be employed directly in the analysis of linear systems, and (3) presented examples that illustrate the characteristics of the transionospheric channel.

A. Gaussian Signal Statistics

The main thrust of our work has been to characterize the structure of the complex random field that results when a wave propagates through a randomly irregular medium. The most natural and useful a-priori assumption is that the quadrature components of the complex field have jointly gaussian statistics. Historically, gaussian signal statistics were indeed the first to be postulated (Section II).

Since only amplitude or intensity data are available in most experiments, however, it is usually not possible to test the gaussian hypothesis directly. In Section III we presented a formula for the second central moment of intensity and showed that it depended on quantities that could not be unambiguously determined from intensity data alone. This problem does not arise for the special cases of Rayleigh and Rice statistics.

However, researchers in radio astronomy and optics have consistently observed that Rayleigh and Rice statistics do not correspond to measured intensity histograms. This fact alone is not sufficient for rejecting gaussian statistics, but there is a considerable amount of theoretical and experimental evidence supporting the competitive log-normal hypothesis.

According to the latter hypothesis, the logarithm of the complex field has jointly gaussian statistics for its quadrature components rather than the complex field itself.

Because of our earlier work [summarized in Rino and Fremouw (1973)] and the work of Armstrong, Coles, and Rickett (1972), we believed that the differences between scintillation-data histograms for gaussian and log-normal statistics would be subtle and difficult to ascertain. Thus, one of the main tasks was to carefully evaluate intensity histograms.

The results presented in Section IV-D show that with the one exception out of 10 cases, the best-fit gaussian PDF achieved a lower value for its chi-square-fit parameter than did the corresponding log-normal PDF. The exceptional data set can possibly be discounted because of its inconsistency with simultaneous data taken with a separate receiver (Section III-D-2). In addition, for a given scintillation intensity, as measured by S_4, for example, interplanetary and ionospheric scintillation data show a striking degree of similarity in their intensity histograms.

Unfortunately, the data base is not as large as we had originally planned, as explained in Sections III-D-1 and III-D-2. Nonetheless, the available data do support the following conclusions:

- Scintillation-intensity probability-density functions derived under the assumption of joint gaussian statistics for the quadrature-field components achieve a better data fit than the corresponding log-normal probability-density function.

- The signal structure is characterized by the fact that, independent of the scintillation level (e.g., S_4), more than 80 percent of the random signal component is in phase quadrature with the steady or coherent component. An equivalent statement is that the equiprobability ellipses characterizing the random component of the signal have their semi-major axes more than ten times as large as their semi-minor axes, and their orientation is within 10° of perpendicularity to the coherent signal component.

- The log-normal probability-density function tends to achieve a smaller rise time than the measured histograms and it underestimates the peak. In the tail region, the differences are not significant.

- The signal structure that we have described is independent of incidence angles and the detailed shape of the spectral-density function that characterizes the irregularity medium, provided that it is smooth. However, structure comparable to the Fresnel-zone area must be present.

These results must be qualified by the fact that no reliable data were processed with S_4 indices greater than 0.55. The limitations imposed by the implicit first Born assumption will be discussed in detail in Section VI-D below.

B. The Nakagami Distribution

Because the Nakagami distribution has been used extensively in ionospheric scintillation studies, its applicability needs to be discussed. It is usually described as an approximation to a general gaussian probability-density function for amplitude or intensity if the appropriate variable change is made. It is convenient in that it depends on the single parameter $m = S_4^{-2}$.

We have pointed out, however, that the exact relationship between the Nakagami distribution and the more general gaussian family of distributions is not established. For example, one cannot specify the joint statistics for the quadrature signal components that will give rise to a Nakagami amplitude distribution. Because of this uncertainty, the Nakagami distribution should be viewed simply as a convenient distribution that can be easily applied to scintillation data.

As such, its applicability depends mainly on how well it works for the intended application. We showed in Section III-E that, like the log-normal distribution, it tends to be broader than the correct gaussian

distribution. We have made direct comparisons for fade-margin determination (Section III-E) to show that the Nakagami distribution gives a conservative bound for the fade margin.

For systems planning, a conservative margin is probably desirable. Moreover, the differences are small enough (less than 1 dB at the 90 percent margin for $S_4 \leq 0.5$) to be of no practical consequence. We suspect that a similar conclusion would hold for scintillation-index conversion, at least for the smaller values of S_4.

C. Complex Second Moments for Ionospheric Transfer Function Characterization

Basic to any channel-modeling effort is a means of calculating the diffracted field for an elementary incident wave. We first considered a stationary time-invariant medium and then generalized the results. We have chosen to compute the complex second moments of the diffracted field, which are most convenient for systems analysis. Indeed, for a gaussian field these quantities are sufficient for a complete statistical characterization.

Our most general results for a specific spectral-density function--namely, a power-law form--are given by Eqs. (III-33) through (III-37). They admit arbitrary incidence angles and a simple anisotropy, and no a-priori Fresnel approximation was made in deriving them. The results depend explicitly on the parameter $\rho = \alpha k \cos \theta$, where α is effectively the "outer" irregularity scale.

When ρ is sufficiently large, a considerable simplification of the formulas can be realized. Note that ρ large is implied by the condition $\alpha \gg \lambda$, which is expected to be valid even at HF frequencies. However, the effect of the large ρ terms depends on the spectral index γ. We have found that when $\gamma > 1.5$, $\rho > 10$ is generally sufficient to justify the Fresnel approximation (Section III-E).

When the Fresnel approximation is valid a general channel characterization is possible in terms of a single parameter $Z = (\lambda z \sec\theta)/2\pi\alpha^2$. That is, independent of all other parameters, the limiting behavior for large and small Z can be specified. For small Z, the phase-quadrature signal component is much larger than the in-phase component. For large Z, the in-phase and phase-quadrature components are nearly equal.

We have characterized these two behavior regions as the near and far zones respectively. The rate at which one proceeds from the near to the far zones as Z is increased from zero to infinity and the detailed behavior of the various quantities depend on the parameter values.

For numerical computations we have used Eqs. (III-47) and (III-48) with the parameters defined by Eqs. (III-49) through (III-52). The quantities that are evaluated depend on the parameters listed in Table VI-1 below. The simplified formulas are valid whenever ρ is sufficiently large to justify the Fresnel approximation.

The effects of the various parameters can be summarized as follows:

- Ratio of Fresnel-zone area to scale parameter squared, Z. The value of Z determines to what extend free-space propagation has redistributed the scattered power from what it was in the vicinity of the scattering layer. When Z is sufficiently small the scattered power is nearly in phase quadrature with the coherent-signal component. When Z is sufficiently large the scattered power is nearly equally distributed between the in-phase and phase-quadrature components.

- Layer thickness parameters, $\mathcal{L}$[$(L/2\alpha)$ contributes when θ is finite]. The layer-thickness factor $\mathcal{L}$ imposes a spatial filtering that suppresses spatial frequencies beyond $\pi/\mathcal{L}$. Hence, its primary effect is for small Z. For example, it acts to keep σ_x^2 finite when $Z \cong 0$ (Figure IV-4).

- Two-frequency correlations $\Delta f/f$. The primary effect of finite $\Delta f/f$ is to make R_ψ Z-dependent. Indeed, the functional dependence of R_ψ on Z and $\Delta f/f$ is nearly identical to that of B_ψ with Z replaced by $Z\,\Delta f/f$ [Eq. (IV-48)]. It follows that

Table VI-1

PARAMETERS FOR MACHINE COMPUTATION

Parameter	Symbol	Comments
Scattering cross section	$\sigma^2 \triangleq \sigma_T^2 \sec\theta$	In Eq. (IV-47) σ^2 is set equal to unity for convenience.
Ratio of Fresnel zone area to scale parameter squared	Z	$Z \triangleq \frac{\lambda z \sec\theta}{2\pi\alpha^2}$
Fractional frequency separation	$\Delta f/f$	For two-frequency correlations. Note that $\lvert\Delta f/f\rvert < 1$.
Layer thickness parameters	$\mathfrak{L}$	$\mathfrak{L} \triangleq \frac{\lambda L \sec\theta}{2\pi\alpha^2}$
Ratio of layer thickness to scale parameter	$(L/2\alpha)$	Only necessary for oblique incidence
Axial ratio and magnetic dip angle	a, Ψ	Enters Eq. (IV-48) as $(a\cos\Psi + \sin\Psi)$
Spectral index	γ	
Incidence angles	θ, φ	Theta is zenith angle. Phi is magnetic azimuth.

the decorrelation of two frequencies is very slow for small Z; hence, the large coherence bandwidths that are characteristic of ionospheric scintillation.

- Anisotropy, a, Ψ. The anisotropy acts through $\beta \triangleq (a\cos^2\Psi + \sin^2\Psi)^{1/2}$ to reduce the rate of convergence to far-zone conditions as β increases from unity. For isotropic irregularities one observes the most rapid convergence.

- Spectral index γ. The spectral index acts effectively in the same way as the anisotropy. When γ is large the spectrum has a sharp cutoff. Thus, the transition from near- to far-zone behavior is abrupt. When γ is small (near unity), as it is generally observed to be, the transition is much slower.

- Oblique incidence, θ, φ. The dependences on incidence angles are generally quite complicated. For example, the scattering cross section will exhibit a more complicated zenith-angle dependence than sec θ. The main impact is that for ionospheric modeling one can make large errors if proper account for incidence angles is not taken.

We have noted that for gaussian fields, the complex covariances suffice to completely define the statistics. We have made use of this fact to calculate the intensity autocorrelation function. The results were applied to evaluate the wavelength dependence of the S_4 scintillation index and the two-frequency intensity correlations. We also outlined the method of computing phase statistics.

The major limitation of our calculations stems from the restriction to weak scattering. We shall consider this limitation in detail below. However, we cannot expect a power-law spectral-density function with a constant spectral index to be accurate over an indefinite range. Indeed, the calculated wavelength dependence of the scintillation index cannot account for the unexpectedly large scintillation observed at L-band and higher frequencies.

D. Consequences of the Weak-Scattering Restriction

The most obvious problem with the first Born approximation is that it does not account for "extinction." That is, it gives no direct information about the coherent field component. We have compensated for this deficiency in our calculations by reducing the incident field amplitude by the factor $\sqrt{1 - \sigma^2}$ so that energy is conserved.

Having done this, we observed no obvious breakdown of our intensity-statistics procedures as the S_4 index became large ($\sim$0.6). However, our data base was limited. Nonetheless, the results do suggest that the general near-zone structure of the field $\left(\sigma_y^2 \gg \sigma_x^2\right)$ is likely to hold true for strong scattering. At the present time we cannot be certain of this.

We do know that we must ultimately account for the spectral broadening that accompanies multiple scattering and assess its effects as well as properly accounting for extinction. Unfortunately, there is no completely satisfactory method of proceeding.

The parabolic-equation approach combined with the Markov approximation is currently gaining acceptance. The parabolic equation is valid for narrow-angle scattering, which is probably an acceptable restriction. However, the Markov approximation demands that the medium be "delta-function"-correlated along the propagation direction.

DeWolf (1972) has analyzed the full Born series summation with various approximations. His results show that the correlation terms that are neglected in the Markov approximation can change the nature of the solution considerably. Moreover, anisotropy combined with the generally smaller ratio of the small-scale structure to wavelength for radio waves as compared to optical waves, works to invalidate the Markov approximation.

We believe that the fact that the first-order intensity statistics are most accurately reproduced by probability-density functions derived under the gaussian hypothesis is evidence that the Markov approximation is invalid for radio-wave scintillation. If it were valid, one would observe log-normal statistics for weak scattering.

To relax the Markov approximation it appears that a direct summation of the Born series is required. One can achieve this indirectly by applying the weak-scattering results as an operator acting on an arbitrary incident field. The scattering medium is divided into slabs that are large compared to the axial correlation distance. Then, the weak-scattering operator can be applied successively to each layer. This is essentially the method described by Uscinski (1968).

One would not expect the results to be analytically tractable. However, the method is amenable to machine computation. The necessary

integrations are similar to those that we have performed in deriving the numerical results presented in this report. The disadvantages that result from not having an analytic solution are largely offset by the fact that there are very few restrictions.

E. Data Restrictions

Scintillation data that are analyzed for intensity statistics are limited by non-stationarity and noise contamination. Hence, for weakly scintillating signals one cannot obtain accurate statistics. The non-stationarity limits the length of the data interval that can be represented by a single histogram. For analyzing higher-order statistics the problem is even more difficult.

Diffraction effects complicate the interpretation of scintillation data, as we have discussed in Section III-D. However, even when this is not the case, sample rates and noise limit our ability to analyze small-scale structure. The ultimate breakdown of the assumption of statistical homogeneity limits our ability to accurately determine the large-scale structure. At the present time the spatial wavenumber spectrum is not well defined below 1 km nor above 50 km.

The small-scale region is probably important in explaining the scintillation that is being reported at L band and at 6 GHz. Thus, before an accurate channel model can be constructed, a considerable amount of careful data analysis will be required.

To conclude, we reiterate our main result--namely, that a gaussian signal structure most accurately reproduces observed intensity histograms. This fact to our knowlege has not previously been demonstrated. Moreover, it is in conflict with the predictions of a large body of random-media propagation theory.

Appendix A

THE SPECTRAL REPRESENTATION OF HOMOGENEOUS COMPLEX RANDOM FIELDS WITH APPLICATIONS TO FREE-SPACE PROPAGATION

Appendix A

THE SPECTRAL REPRESENTATION OF HOMOGENEOUS COMPLEX RANDOM FIELDS WITH APPLICATIONS TO FREE-SPACE PROPAGATION

1. General Results

In Section III of this report the fundamental quantity is a scalar complex random field

$$E(x,y,z) = E_R(x,y,z) + iE_I(x,y,z) \quad . \tag{A-1}$$

For simplicity of notation we let $E' = E(x',y',z')$ and $E'' = E(x'',y'',z'')$. Clearly, there are at least three spatial autocorrelation functions that characterize E--viz., $\langle E_R'E_R''\rangle$, $\langle E_I E_I'\rangle$, and $\langle E_R E_I'\rangle$. Because of the layered model that we have used, E is homogeneous in any transverse plane. Hence, the correlations depend only on $\delta x = x' - x''$, and $\delta y = y' - y''$. In general, the z-dependence will involve both z' and z''.

Consider E_R. It admits a spectral representation of the form

$$E_R(x,y,z_o) = \iint \exp\{i(\kappa_x x + \kappa_y y)\} d\mathcal{S}_R(\kappa_x,\kappa_y;z_o) \quad . \tag{A-2}$$

Since E_R is real, we must have

$$d\mathcal{S}_R(\kappa_x,\kappa_y;z_o) = d\mathcal{S}_R^*(\kappa_x,\kappa_y;z_o) \quad . \tag{A-3}$$

Now, $\mathcal{S}_R$ has orthogonal (k_x,k_y) increments. In a purely formal notation, we can write

$$\langle d\mathcal{S}_R' d\mathcal{S}_R''^* \rangle = \delta(\kappa_x' - \kappa_x'')\delta(\kappa_y' - \kappa_y'')\varphi_R(\kappa_x,\kappa_y;z',z'') \frac{d\kappa_x}{2\pi}\frac{d\kappa_y}{2\pi} \quad . \tag{A-4}$$

We exclude any discrete spectral components. Because of Eq. (A-3), however, we can also write

$$\langle d\mathcal{S}'_R d\mathcal{S}''_R \rangle = \delta(\kappa'_x + \kappa''_x)\delta(\kappa'_y + \kappa''_y)\varphi_R(\kappa_x,\kappa_y;z',z'') \frac{d\kappa_x}{2\pi}\frac{d\kappa_y}{2\pi} \quad . \tag{A-5}$$

We have a similar set of relations for E_I and $d\mathcal{S}_I$, as well as for the cross-correlations $\langle d\mathcal{S}'_R d\mathcal{S}''^*_I \rangle$ and $\langle d\mathcal{S}'_R d\mathcal{S}''_I \rangle$. By combining these results we can deduce the properties of the "transverse" spectral decomposition of E,

$$E(x,y,z_o) = \iint \exp[i(\kappa_x x + \kappa_y y)] d\mathcal{S}(\kappa_x,\kappa_y;z_o) \tag{A-6}$$

where

$$d\mathcal{S} = d\mathcal{S}_R + i d\mathcal{S}_I \quad . \tag{A-7}$$

We can write

$$\langle d\mathcal{S}' d\mathcal{S}''^* \rangle = \delta(\kappa'_x - \kappa''_x)\delta(\kappa'_y - \kappa''_y)\varphi_{R_E}(\kappa_x,\kappa_y;z_o) \frac{d\kappa_x}{2\pi}\frac{d\kappa_y}{2\pi} \tag{A-8}$$

and

$$\langle d\mathcal{S}' d\mathcal{S}'' \rangle = \delta(\kappa'_x + \kappa''_x)\delta(\kappa'_y + \kappa''_y)\varphi_{B_E}(\kappa_x,\kappa_y;z_o) \frac{d\kappa_x}{2\pi}\frac{d\kappa_y}{2\pi} \tag{A-9}$$

where

$$\varphi_{R_E} = \varphi_R + \varphi_I + i(\varphi_{RI} - \varphi_{IR}) \tag{A-10}$$

is the Fourier transform of $R_E = \langle E' E''^* \rangle$, and

$$\varphi_{B_E} = \varphi_R - \varphi_I + i(\varphi_{RI} + \varphi_{IR}) \tag{A-11}$$

is the Fourier transform of $B_E = \langle E' E'' \rangle$.

The quantity φ_{R_E} is the ordinary angular spectral-density function. Indeed, since $\varphi_{RI} = \varphi_{IR}^*$, the angular spectral-density function is purely real. Moreover, since $\langle E^2 \rangle \geq 0$, it is also non-negative, although not necessarily symmetric. From the angular spectral-density alone, we cannot separate φ_R and φ_I. The additional quantity φ_{B_E} provides the necessary information. As an example, we shall consider free-space propagation.

2. Application to Free-Space Propagation

A plane wave propagating from z_o to z has its phase advanced $\overline{k_z}(z - z_o)$ radians, where

$$\overline{k_z} = \left(k^2 - k_x^2 - k_y^2\right)^{1/2} \quad . \tag{A-12}$$

It follows that

$$E(x,y,z) = \iint \exp\{i[\kappa_x x + \kappa_y y + \overline{k_z}(z - z_o)]\} d\delta(\kappa_x \kappa_y; z_o) \quad . \tag{A-13}$$

By using Eq. (A-8), we can immediately deduce the well-known result that

$$R_E(\delta x, \delta y, z) = R_E(\delta x, \delta y; z_o) \quad . \tag{A-14}$$

However, φ_R, φ_I, and φ_{RI} do depend on z. Indeed, by applying Eq. (A-9), we have

$$\varphi_{B_E}(\kappa_x, \kappa_y; z) = \varphi_{B_E}(\kappa_x, \kappa_y; z_o) \exp\{2i\overline{k_z}(z - z_o)\} \quad . \tag{A-15}$$

It follows that with an obvious notation simplification,

$$\varphi_R(z) = \varphi_R(z_o)\cos^2[\overline{k_z}(z - z_o)]$$

$$+ \varphi_I(z_o)\sin^2[\overline{k_z}(z - z_o)]$$

$$- \mathrm{Re}\{\varphi_{RI}(z_o)\}\sin[2k_z(z - z_o)] \qquad \text{(A-16)}$$

$$\varphi_I(z) = \varphi_R(z_o)\sin^2[\overline{k_z}(z - z_o)]$$

$$+ \varphi_I(z_o)\cos^2[\overline{k_z}(z - z_o)]$$

$$- \mathrm{Re}\{\varphi_{RI}(z_o)\}\sin[2\overline{k_z}(z - z_o)] \qquad \text{(A-17)}$$

and

$$\varphi_{RI}(x) = [\varphi_R(z_o) - \varphi_I(z_o)]\sin[2\overline{k_z}(z - z_o)]$$

$$+ \mathrm{Re}[\varphi_{RI}(z_o)]\cos[2\overline{k_z}(z - z_o)]$$

$$+ i\,\mathrm{Im}[\varphi_{RI}(z_o)] \quad . \qquad \text{(A-18)}$$

In the special case in which $\varphi_R = \varphi_{RI} = 0$ at $z = z_o$, the results reduce to

$$\varphi_R(z) = \varphi_I(z_o)\sin^2[\overline{k_z}(z - z_o)] \qquad \text{(A-19)}$$

$$\varphi_I(z) = \varphi_I(z_o)\cos^2[\overline{k_z}(z - z_o)] \qquad \text{(A-20)}$$

$$\varphi_{RI}(z) = -\varphi_I(z_o)\,\frac{1}{2}\,\sin[2\overline{k_z}(z - z_o)] \qquad \text{(A-21)}$$

This special case was originally derived by Bowhill (1957). The results derived in Section III take this form when the layer thickness L is zero. This is the so-called "phase-changing" screen approximation, although "phase-quadrature" changing screen would be a more nearly correct description. A true phase-changing screen has been analyzed by Mercier (1962).

Appendix B

THE TEMPORAL STRUCTURE OF THE SCATTERED FIELD

Appendix B

THE TEMPORAL STRUCTURE OF THE SCATTERED FIELD

The time variation of the scattered field arises from the relative motion of the medium and the frame of reference as well as from temporal changes in the medium itself. Hence, in the measurement frame,

$$E_t(x,y;z) = \iint \exp\{-i[\kappa_x(x - v_x t) + \kappa_y(y - v_y t)]\} d\tilde{s}_t(\kappa_x,\kappa_y;z) \quad . \tag{B-1}$$

By appling Eqs. (A-8) and (A-9) we can derive the results

$$\begin{Bmatrix} R_E \\ B_E \end{Bmatrix} = \iint \exp\{-i[\kappa_x(\delta x - v_x \delta t) + \kappa_y(\delta y - v_y \delta t)]\} \bar{o}_z(\kappa_x,\kappa_y;\delta t) \frac{d\kappa_x}{2\pi} \frac{d\kappa_y}{2\pi} \quad . \tag{B-2}$$

In deriving Eq. (B-2) we assumed stationarity of the temporal variations. We introduce the temporal frequency variable

$$2\pi\mathcal{F} = \kappa_x v_x + \kappa_y v_y \quad . \tag{B-3}$$

Changing variables in Eq. (B-2) gives the result

$$\begin{Bmatrix} R_E \\ B_E \end{Bmatrix} = \int_{-\infty}^{\infty} \exp\{2\pi i \mathcal{J} \delta t\}$$

$$\times \frac{1}{v_y} \int_{-\infty}^{\infty} \bar{\Phi}\left(\kappa_x, \frac{2\pi\mathcal{J} - \kappa_x v_x}{v_y}; \delta t\right) e^{-i\kappa_x\left(\delta x - \frac{v_x}{v_y}\delta y\right)} \frac{d\kappa_x}{2\pi} \exp\left\{2\pi i \mathcal{J} \frac{\delta y}{v_y}\right\} d\mathcal{J}$$

or

$$\times \frac{1}{v_x} \int_{-\infty}^{\infty} \bar{\Phi}\left(\frac{2\pi\mathcal{J} - \kappa_y v_y}{v_x} \kappa_y; \delta t\right) e^{-i\kappa_y\left(\delta y - \frac{v_y}{v_x}\delta x\right)} \frac{d\kappa_y}{2\pi} \exp\left\{2\pi i \mathcal{J} \frac{\delta x}{v_x}\right\} d\mathcal{J} \; .$$

(B-4)

The form of Eq. (B-4) would be greatly simplified if $\bar{\Phi}(\kappa_x, \kappa_y; \delta t)$ had the form $\bar{\Phi}(\kappa_x, \kappa_y)R(\delta t)$. It seems unlikely, however, that the decay mechanism is independent of spatial frequency or, equivalently, scale size.

On the other hand, it is generally true that the lifetime of the irregularity structure is long compared to the transit time---that is, the irregularity structure is "frozen." Then, the integrals over κ_x or κ_y are effectively δt-independent, and they can be interpreted as the temporal spectral densities (power spectrum in the case of R_E) of the field fluctuations.

Appendix C

POWER-LAW SPECTRAL-DENSITY-FUNCTION FORMULAS FOR NORMAL INCIDENCE

Appendix C

POWER-LAW SPECTRAL-DENSITY-FUNCTION FORMULAS FOR NORMAL INCIDENCE

In this appendix we consider evaluating the integral of Eq. (IV-40) for normal incidence with L = 0. By using hypergeometric series, it is possible to obtain the following formulas for $\mathrm{Re}\{B\}$ and $\mathcal{I}\mathrm{m}\{B\}$:

$$1 + \mathrm{Re}\{B\} = \sum_{n=1}^{\infty} D_n + (-1)^{\gamma/2} C_\gamma \sum_{n=0}^{\infty} [A_n + B_n] \tag{C-1}$$

$$-\mathcal{I}\mathrm{m}\{B\} = \sum_{n=1}^{\infty} E_n + (-1)^{\gamma/2} C_\gamma \sum_{n=0}^{\infty} [A_n - B_n] \tag{C-2}$$

for γ and even integer, and

$$1 + \mathrm{Re}\{B\} = \sum_{n=1}^{\infty} D_n + (-1)^{(\gamma-1)/2} C_\gamma \sum_{n=0}^{\infty} [A_n - B_n] \tag{C-3}$$

$$-\mathcal{I}\mathrm{m}\{B\} = \sum_{n=1}^{\infty} E_n + (-1)^{(\gamma-1)/2} C_\gamma \sum_{n=0}^{\infty} [A_n + B_n] \tag{C-4}$$

for γ an odd integer.

The quantities D_n, E_n, A_n, B_n, and C_γ can be evaluated as

$$D_n = \frac{(-1)^{n+1}(Z)^{2n}\beta^{-2n}P_{2n}\left(\frac{\beta^2+1}{2\beta}\right)}{(-\gamma+3/2)(-\gamma+5/2)\ldots(-\gamma+1/2+2n)} \qquad \text{(C-5)}$$

$$E_n = \frac{(-1)^{n+1}(z)^{2n+1}\beta^{-(2n-1)}P_{2n-1}\left(\frac{\beta^2+1}{2\beta}\right)}{(-\gamma+3/2)(-\gamma+5/2)\ldots(-\gamma-1/2+2n)} \qquad \text{(C-6)}$$

$$A_n = \frac{(-1)^n(z)^{2n}P_{2n+\gamma-1/2}\left(\frac{\beta^2+1}{2\beta}\right)}{(2n)!\beta^{(2n+\gamma-1/2)}} \qquad \text{(C-7)}$$

$$B_n = \frac{(-1)^n z^{2n+1}P_{2n+\gamma+1/2}\left(\frac{\beta^2+1}{2\beta}\right)}{(2n+1)!\beta^{2n+\gamma+1/2}} \qquad \text{(C-8)}$$

and

$$C_\gamma = \sqrt{\frac{\pi}{2}}\,\frac{2^{\gamma-1}(z)^{\gamma-1/2}}{1\cdot 3\cdot 5\ldots(2\gamma-3)} \qquad \text{(C-9)}$$

where $P_\alpha(x)$ is the α^{th} Legendre polynomical when α is an integer or the appropriate Legendre function when α is non-integral.

In formulas (C-7) and (C-8), the relations

$$P_{-1/2}\left(\frac{\beta^2+1}{2\beta}\right) = \frac{4\sqrt{\beta}}{\pi(\beta+1)}\,K\left[\left(\frac{\beta-1}{\beta+1}\right)^{1/2}\right] \qquad \text{(C-10)}$$

and

$$P_{+1/2}\left(\frac{\beta^2+1}{2\beta}\right) = \frac{2\sqrt{\beta}}{\pi}\,E\left[\left(\frac{\beta^2-1}{\beta}\right)^{1/2}\right] \qquad \text{(C-11)}$$

where K and E are standard elliptic integrals, can be used together with the recurrence relations for P_n to evaluate the successive terms in the series.

The series in Eqs. (C-1), (C-2), (C-3), and (C-4) converge quite rapidly for small Z when γ is not too large (say less than 6), and more slowly as Z is increased. Hence, they are most effective in the near zone.

Appendix D

SPECTRAL-DENSITY FUNCTIONS FOR "SIMPLY" ANISOTROPIC MEDIA

Appendix D

SPECTRAL-DENSITY FUNCTIONS FOR "SIMPLY" ANISOTROPIC MEDIA

In general, the three-dimenstional spectral-density function is

$$\Phi(\vec{k}) = \int(3)\int R(\delta\vec{r})\exp\{i\vec{k}\cdot\delta\vec{r}\}d\delta\vec{r} \qquad \text{(D-1)}$$

where $R(\delta\vec{r})$ is the spatial autocorrelation function. The z-axis is taken downward, with the x-z plane containing a unit vector $\hat{u}_B$ along the earth's magnetic field.

Consider a rotation about y into a new coordinate system (u_1,u_2,u_3) with u_3 along $\hat{u}_B$, the elongation direction. In standard matrix notation we have

$$\vec{u} = M_1\delta\vec{r} \qquad \text{(D-2)}$$

where

$$M_1 = \begin{pmatrix} \cos\psi & 0 & -\sin\psi \\ 0 & 1 & 0 \\ \sin\psi & 0 & \cos\psi \end{pmatrix} . \qquad \text{(D-3)}$$

The angle ψ is measured from z to $\hat{u}_B$.

A second coordinate transformation to elongate the coordinate along the u_3 direction produces a coordinate system with spherical symmetry for the simple anisotropy we are considering--viz., elongation of the irregularities along a single direction. In the new system,

$$\vec{\mu} = M_2\vec{u} \qquad \text{(D-4)}$$

where

$$M_2 = \begin{pmatrix} 1 & 0 & 0 \\ 0 & 1 & 0 \\ 0 & 0 & b \end{pmatrix} \qquad \text{(D-5)}$$

Now, changing coordinates in Eq. (D-1) gives

$$\Phi\left(\left|\vec{S}\right|^2\right) = a\int(3)\int R(\delta\vec{r})e^{i\vec{k}\cdot M_1^{-1}M_2^{-1}\vec{\mu}}\,d\vec{\mu} \qquad \text{(D-6)}$$

where $a = b^{-1}$ is the axial ratio. Let

$$\begin{aligned}\vec{S}\cdot\vec{\mu} &= \vec{k}\cdot\delta\vec{r} \\ &= \left(M_1^{-1}M_2^{-1}\right)^T\vec{k}\cdot\vec{\mu} \\ &= \vec{k}^T M_1^{-1}M_2^{-1}\vec{\mu} \quad . \end{aligned} \qquad \text{(D-7)}$$

It follows that

$$S_1 = k_1\cos\psi - k_3\sin\psi \qquad \text{(D-8)}$$

$$S_2 = k_2 \qquad \text{(D-9)}$$

$$S_3 = +k_1 a\sin\psi + k_3 a\cos\psi \quad . \qquad \text{(D-10)}$$

Hence,

$$\begin{aligned}\left|\vec{S}\right|^2 = \vec{S}\cdot\vec{S} &= k_1^2\cos^2\psi + k_3^2\sin^2\psi - 2k_1k_3\cos\psi\sin\psi \\ &\quad + k_2^2 \\ &\quad + k_1^2 a^2\sin^2\psi + k_3^2 a^2\cos^2\psi + 2k_1k_3a^2\cos\psi\sin\psi \\ &= B(\psi)\left(k_1\frac{C(\psi)}{B(\psi)} - k_3\right)^2 + k_1^2\frac{a^2}{B(\psi)} + k_2^2 \end{aligned} \qquad \text{(D-11)}$$

where

$$B(\psi) = \sin^2\psi + a^2 \cos^2\psi \qquad \text{(D-12)}$$

and

$$C(\psi) = (1 - a^2) \cos\psi \sin\psi \quad . \qquad \text{(D-13)}$$

We now note that $\Phi(|\vec{S}|^2)$ is a real symmetric function. The quantity of interest is

$$\Phi(k_1,k_2;\delta z) = \int \Phi\left(|\vec{S}|^2\right) \exp\left\{-ik_3\delta z\right\}\frac{dk_3}{2\pi}$$

$$= \exp\left\{ik_3\delta z\,\frac{C(\psi)}{B(\psi)}\right\} \int \Phi\left(k_3^2 B(\psi) + k_1^2\,\frac{a^2}{B(\psi)} + k_2^2\right) \exp\left\{-ik_3\delta z\right\}\frac{dk_3}{2\pi} \qquad \text{(D-14)}$$

The integral in Eq. (D-14) is purely real, as is the additional integral

$$\int_{-\infty}^{\infty} \Phi(k_1,k_2;\delta z)d\delta z = \Phi(k_1,k_2,k_3)\,\big|_{k_3 = 0} \quad . \qquad \text{(D-15)}$$

Appendix E

INTENSITY CORRELATIONS FOR COMPLEX GAUSSIAN FIELDS

Appendix E

INTENSITY CORRELATIONS FOR COMPLEX GAUSSIAN FIELDS

In Section V we considered a general complex field of the form $V = X + iY$, where X and Y are jointly gaussian real fields. To make the deterministic components explicit, we write

$$X = \tilde{X} + \eta_x \quad , \tag{E-1}$$

$$Y = \tilde{Y} + \eta_y \quad , \tag{E-2}$$

where $\tilde{X}$ and $\tilde{Y}$ have zero means. Note that we have not assumed statistical homogeneity. That is, η_x and η_y can vary with position and/or time as well as the moments of $\tilde{X}$ and $\tilde{Y}$.

We let

$$R_{xx} \triangleq \langle \tilde{X}\tilde{X}' \rangle \quad , \tag{E-3}$$

$$R_{yy} \triangleq \langle \tilde{Y}\tilde{Y}' \rangle \quad , \tag{E-4}$$

and

$$R_{xy} \triangleq \langle \tilde{X}\tilde{Y}' \rangle \quad , \tag{E-5}$$

$$R_{yx} \triangleq \langle \tilde{X}'\tilde{Y} \rangle \quad . \tag{E-6}$$

When $\tilde{X} = \tilde{X}'$ and $\tilde{Y} = \tilde{Y}'$, we shall use the notation

$$\sigma_x^2 \triangleq \langle \tilde{X}^2 \rangle \tag{E-7}$$

$$\sigma_y^2 \triangleq \langle \tilde{Y}^2 \rangle \tag{E-8}$$

$$C_{xy} \triangleq \langle \tilde{X}\tilde{Y} \rangle \tag{E-9}$$

and

$$\sigma^2 = \sigma_x^2 + \sigma_y^2 \quad . \tag{E-10}$$

Finally, we shall employ the auxiliary definitions

$$R \triangleq \langle VV^* \rangle = R_{xx} + R_{yy} + i(C_{xy} - C_{yx}) \tag{E-11}$$

$$B \triangleq \langle VV \rangle = R_{xx} - R_{yy} + i(C_{xy} + C_{yx}) \quad . \tag{E-12}$$

To proceed, we first note that

$$\langle I \rangle = \langle X^2 + Y^2 \rangle = \sigma^2 + \eta_x^2 + \eta_y^2 \quad . \tag{E-13}$$

The quantitiy that we shall compute is the second central moment of intensity $\langle II' \rangle - \langle I \rangle^2$. By direct computation we have

$$\langle II' \rangle - \langle I \rangle^2 = 4\left[R_{xx}\eta_x^2 + R_{yy}\eta_y^2 + (R_{xy} + R_{yx})\eta_x\eta_y\right] + \langle X^2X'^2 \rangle + \langle Y^2Y'^2 \rangle + \langle X^2Y'^2 \rangle + \langle X'^2Y^2 \rangle \quad . \tag{E-14}$$

For gaussian processes it is easily shown that (see, for example, Papoulis, 1965, pp. 481-482),

$$\langle X^2X'^2 \rangle = (\sigma_x^2)^2 + 2R_{xx}^2 \tag{E-15}$$

$$\langle X^2Y'^2 \rangle = \sigma_x^2\sigma_y^2 + 2R_{xy}^2 \tag{E-16}$$

with similar results for $\langle Y^2Y'^2 \rangle$ and $\langle X'^2Y^2 \rangle$. Hence, the intensity correlation can be written in terms of R_{xx}, R_{yy}, R_{xy}, R_{yx}, and the first moments η_x and η_y.

The final form can be simplified if we write B and $\langle V \rangle$ in polar form with

$$\tan 2\zeta \triangleq \frac{\mathrm{Im}\{B\}}{\mathrm{Re}\{B\}} \tag{E-17}$$

and

$$\tan \phi \triangleq \frac{\eta_y}{\eta_x} \quad . \tag{E-18}$$

After some algebraic manipulations, we have the desired result,

$$\langle II' \rangle - \langle I \rangle^2 = 2\sigma^2\left(\langle I \rangle - \sigma^2\right)\left[\frac{\mathrm{Re}\{R\}}{\sigma^2} + \frac{|B|}{\sigma^2}\cos 2(\zeta - \phi)\right]$$

$$+ \sigma^4\left[\frac{|R|^2}{\sigma^4} + \frac{|B|^2}{\sigma^4}\right] \quad . \tag{E-19}$$

We note that both R and B are proportional to σ^2. Hence, Eq. (E-19) is a quadratic equation in σ^2.

REFERENCES

Aarons, J., R. Allen and T. Elkins, "Frequency Dependence of Radio Star Scintillation," J. Geophys. Res., Vol. 72, No. 11, pp. 2891-2902 (1967).

Armstrong, J. W., W. A. Coles, and B. J. Rickett, "Observations of Strong Interplanetary Scintillation at 74 MHz," J. Geophys. Res., Vol. 77, No. 16, pp. 2739-2743 (1972).

Balser, M., "Some Observations on Scattering by Turbulent Inhomogeneities," IRE Trans. on Antennas and Propagation, pp. 383-390 (October 1957).

Barabanenkov, N., A. Kravstov, S. M. Rytov, and V. I. Tamarskii, "Status of the Theory of Propagation of Waves in a Randomly Inhomogeneous Medium," Soviet Phys., Vol. 13, No. 5, pp. 551-680 (March-April 1971).

Bello, P. A., "Characterization of Randomly Time-Variant Linear Channels," IEEE Trans. on Communication Systems, Vol. CS-11, pp. 360-393 (December 1963)

Bischoff, K., and B. Chytil, "A Note on Scintillation Indices," Planet. Space Sci., Vol. 17, pp. 1059-1066 (1969).

Blank, H. A., and T. S. Golden, "Analysis of the Frequency Dependence and the Polarization Properties of Ionospheric Scintillation in the Equatorial Region," paper presented at URSI Meeting, Boulder, Colorado, September 1973.

Booker, H. G., J. A. Ratcliffe and D. H. Shinn, "Diffraction from an Irregular Screen with Applications to Ionospheric Problems," Phil. Trans. Roy. Soc. A, Vol. 242, pp. 579-607 (September 12, 1950).

Bowhill, S. A., "Ionospheric Irregularities Causing Random Fading of Very Low Frequencies," J. Atmos. Terr. Phys., Vol. 11, pp. 91-101 (1957).

Bowhill, S. A., "Statistics of a Radio Wave Diffracted by a Random Ionosphere," Res. Nat. Bu. Std.--Radio Propagation, Vol. 65D, No. 3, pp. 275-292 (May-June 1961).

Bowker, A. H., and G. J. Liberman, Engineering Statistics (Prentice-Hall, Englewood Cliffs, N. J., 1959).

Briggs, B. H., and I. A. Parkin, "On the Variation of Radio Star and Satellite Scintillations with Zenith Angle," J. Atmos. Terr. Phys., Vol. 25, No. 6, pp. 339-366 (1963).

Briggs, B. H., and G. H. Phillips, "A Study of the Horizontal Irregularities of the Ionosphere," Proc. Phys. Soc. B, Vol. 63, p. 907 (1950).

Brown, W. P., Jr., "Validity of the Rytov Approximation in Optical Propagation Calculations," J. Opt. Soc. Am., Vol. 56, No. 8, pp. 1045-1052 (August 1966).

Budden, K. G., "The Amplitude Fluctuations of the Radio Wave Scattered from a Thick Ionospheric Layer with Weak Irregularities," J. Atmos. Terr. Phys., Vol. 27, pp. 155-172 (1965).

Chandrasekhar, S., "A Statistical Basis for the Theory of Stellar Scintillation," Monthly Notices Roy. Astron. Soc., Vol. 112, p. 475 (1952).

Chernov, L. A., Wave Propagation in a Random Medium, translated from Russian by R. A. Silverman (McGraw-Hill Book Co., Inc., N.Y., N.Y. 1960).

Cronyn, W. M., "The Analysis of Radio Scattering and Space-Probe Observations of Small-Scale Structure in the Interplanetary Medium," Astrophys. J., Vol. 161, p. 755 (1970).

Davenport, W. B., and W. L. Root, An Introduction to the Theory of Random Signals and Noise (McGraw-Hill Book Co., Inc., N.Y., N.Y. 1958).

deWolf, D. A., "Strong Amplitude Fluctuations of Wave Fields Propagating through Turbulent Media," TR-72-51, Rome Air Development Command, Griffiss Air Force Base, N.Y. (1972).

Dyson, P. L., J. P. McClure, and W. B. Hanson, "In-situ Measurements of Amplitude and Scale Size Characteristics of Ionospheric Irregularities," University of Texas at Dallas, Dallas, Tex. (1973).

Fejer, J. A., "The Diffraction of Waves in Passing through an Irregular Refracting Medium," Proc. Roy. Soc., Vol. 220 A, pp. 455-471 (1953).

Fremouw, E. J., and C. L. Rino, "Development of a Worldwide Model for F-Layer-Produced Scintillation," Final Report, Contract NAS5-21551, SRI Project 1079, Stanford Research Institute, Menlo Park, California (November 1971).

Fremouw, E. J., and C. L. Rino, "An Empirical Model for Average F-Layer Scintillation at VHF/UHF," Radio Science, Vol. 8, No. 3, pp. 213-222 (1972).

Golden, T. S., and E. A. Wolf, eds., "Scintillation Advisory Panel Workshop Report," NASA Goddard Space Flight Center, Greenbelt, Md. (June 15, 1973).

Hewish, A., "The Diffraction of Galactic Radio Waves as a Method of Investigating the Irregular Structure of the Ionosphere," Proc. Roy. Soc. London, Vol. 214, pp. 494-514 (1952).

Lawrence, R. S., C. G. Little and H. J. A. Chivers, "A Survey of Ionospheric Effects upon Earth-Space Radio Propagation," IEEE Scintillation Effects Survey, pp. 4-27 (January 1964).

Lee, R. W., and J. C. Harp, "Weak Scattering in Random Media, with Applications to Remote Probing," IEEE Proc., Vol. 57, No. 4, pp. 375-406 (April 1969).

Lyness, J. N., "Algorithm 379," Communications of the ACM, Vol. 13, No. 4, pp. 260-263 (1970).

Mercier, R. P., "Diffraction by a Screen Causing Large Random Phase Fluctuations," Proc. Camb. Phil. Soc., Vol. 62, pp. 382-400 (1962).

Mood, A. M., Introduction to the Theory of Statistics, (McGraw-Hill Book Co., Inc., N.Y., N.Y. 1950).

Ochs, G. R., and R. S. Lawrence, "Saturation of Laser Beam Scintillation under Conditions of Strong Atmospheric Turbulence," J. Opt. Soc. Am., Vol. 59, pp. 226-227 (1969).

Papoulis, A., Probability,Random Variables, and Stochastic Processes (McGraw-Hill Book Co., Inc., N.Y., N.Y. 1965).

Ratcliffe, J. A., "Some Aspects of Diffraction Theory and Their Application to the Ionosphere," Roy. Physc. Soc. Progress in Physics, Vol. 19, pp. 188-266 (1956).

Ratcliffe, J. A., and J. L. Pawsey, "A Study of the Intensity of Downcoming Wireless Waves," Proc. Camb. Philos. Soc., Vol. 29, p. 301 (1933).

Rice, S. O., "Mathematical Analysis of Random Noise," Bell Syst. Tech. J., Vol. 23, p. 282 (1944); Ibid., Vol. 24, p. 46 (1945).

Rino, C. L. and E. J. Fremouw, "Statistics for Ionospherically Diffracted VHF/UHF Signals," Radio Sci., Vol. 8, No. 3, pp. 223-233 (1973).

Rufenach, C. L., "A Power-Law Wavenumber Spectrum Deduced from Ionospheric Scintillation Observations," J. Geophys. Res., Space Physics, Vol. 77, No. 25, pp. 4761-4772 (1972).

Strohbehn, J. W., "Line-of-Sight Wave Propagation through the Turbulent Atmosphere," Proc. IEEE, Vol. 56, No. 8, pp. 1301-1318 (August 1968).

Strohbehn, J. W., and S. F. Clifford, "Polarization and Angle-of-Arrival Fluctuations for a Plane Wave Propagated through a Turbulent Medium," IEEE Trans. on Antennas and Propagation, Vol. AP-15, No. 3, pp. 416-421 (May 1967).

Tatarski, V. I., "The Effects of the Turbulent Atmosphere on Wave Propagation," TT-68-50464, National Technical Information Service, Washington, D. C. (1971).

Tatarski, V. I., Wave Propagation in a Turbulent Medium, translated from Russian by R. A. Silverman (Dover Publications, N.Y., N.Y. 1961).

Uscinski, B. J., "The Multiple Scattering of Waves in Irregular Media," Roy. Soc. London Phil. Trans., Ser. A. Math. and Phys. Sc., Vol. 262, No. 1133, pp. 609-643 (March 14, 1968).

Wernik, A. W., and L. Liszka, "On the Amplitude Distribution of Scintillating Radio Signals from Artificial Satellites," Arkiv. Geofysik., 5(34), pp. 501-514 (1969).

Whitney, H. E., J. Aarons, R. S. Allen, and D. R. Seemann, "Estimation of the Cumulative Amplitude Probability Distribution Function of Ionospheric Scintillations," Radio Science, Vol 7, No. 12, pp. 1095-1104 (1972).

Whitney, H. E., J. Aarons, and C. Malik, "A Proposed Index for Measuring Ionospheric Scintillations," Planet. Space Sci., Vol. 17, pp. 1069-1073 (1969).